KATHERINE ALLISE MALMGREN

COASTAL GROUNDWATER RESPONSE TO CLIMATE VARIABILITY COUPLING IN CALIFORNIA AND PORTUGAL

UNIVERSIDADE DO ALGARVE

FACULDADE DE CIÊNCIAS E TECNOLOGIA

2020

KATHERINE ALLISE MALMGREN

COASTAL GROUNDWATER RESPONSE TO CLIMATE VARIABILITY COUPLING IN CALIFORNIA AND PORTUGAL

Master in Marine and Coastal Systems

Work performed under the supervision of:

Maria da Conceição Lopes Videira Louro Neves (UAlg, IDL)

Jason Gurdak (Santa Clara Valley Water District)

UNIVERSIDADE DO ALGARVE

FACULDADE DE CIÊNCIAS E TECNOLOGIA

2020

Declaração de autoria de trabalho / Declaration of Authorship of work

COASTAL GROUNDWATER RESPONSE
TO CLIMATE VARIABILITY COUPLING
IN CALIFORNIA AND PORTUGAL

Declaro ser o(a) autor(a) deste trabalho, que é original e inédito. Autores e trabalhos consultados estão devidamente citados no texto e constam da listagem de referências incluída.

I declare to be the author of this work, which is original and unpublished. Authors and works consulted are duly cited in the text and are included in the list of references.

X

Katherine Allise Malmgren

Faro, 9th of October 2020

Copyright

ACKNOWLEGEMENTS

Paramountly, I would like to thank my thesis advisor, Maria da Conceição Lopes Videira Louro Neves for her guidance, encouragement, and calm throughout the development of this thesis. Her intelligence, inquisitiveness and professionalism were evident from my first classes with her at the start of this master's program. As a successful woman of science, she has been an exceptional mentor and colleague. It was an honor to collaborate with her on this research project. Secondly, I would like to express my sincere gratitude to Luis Costa (PhD candidate at UAlg) for his utter generosity, positivity, integrity, and particularities. I have gained a depth of hydrogeological knowledge, pursued, and attained research scholarship funding, and developed proficiency in groundwater monitoring field methods thanks to Luis. I look forward to a continual exchange of project ideas in L36 in the months to come. I would also like to thank my co-supervisor Jason Gurdak for sharing his expertise on sustainable groundwater management in California, Óscar Ferreira for his responsiveness and tenure as the former Director of the MaCS master's program, László Varga for helping me settle into a new life in Portugal, and my dear friends and fellow colleagues Amelie Prince, Jasmine Haskell, Camila Cotrim and Lara Mills for the laughter, strength building and emotional support. Finally, I am eternally grateful for my loving and supportive family, Laurie, Daniel, Lee, and my revered grandmother Gwen.

ABSTRACT

Aquifers are a fundamental source of freshwater, yet they are particularly vulnerable in coastal Mediterranean regions due to climate and anthropogenic pressures. This comparative study examines the interrelationships between ocean-atmosphere teleconnections, groundwater levels and precipitation in coastal aquifers of California and Portugal, deepening the understanding of climate variability coupling behaviors across mirrored Mediterranean climates. Piezometric and precipitation records (1982-2019) are analyzed using singular spectral analysis, wavelet transform and lag correlation methods. Additionally, the development of a groundwater sustainability index (GSI) exposes vulnerability to drought and provides useful insights for future groundwater management and security. Singular spectral analysis identify signals consistent with the six dominant climate patterns, the Pacific Decadal Oscillation (PDO), the El Niño-Southern Oscillation (ENSO), and the Pacific/North American Oscillation (PNA) in California, and the North Atlantic Oscillation (NAO), the Eastern Atlantic Oscillation (EA) and the Scandinavian Pattern (SCAND) in Portugal. Lower frequency oscillations have a greater influence on hydrologic patterns, with PDO (52.75%) and NAO (46.25%) accounting for the largest amount of groundwater level variability. Wavelet coherences show non-stationary covariability between climate patterns and groundwater levels in distinct period bands; 4-8 years for PDO, 2-4 years for ENSO, 1-2 years for PNA, 5-8 years for NAO, 2-4 years for EA and 2-8 years for SCAND, presenting some dispersion of the low frequency signals. Wavelet coherence patterns also show that coupled climate patterns (NAO+ EA- and paired PDO and ENSO phases) are associated with major drought periods in both regions. Finally, the GSI classify highly vulnerable and low sustainability aquifers in southern California and in northern Portugal, warranting further policy and mitigation measures in these at-risk areas. The current work shows how pairing hydro-climatological knowledge with a GSI can provide insightful knowledge, which can be used to enrich and inform effective sustainable groundwater management policies.

Keywords: Groundwater, climate variability, coastal aquifers, Mediterranean, sustainability

RESUMO

Os aquíferos são uma fonte fundamental de água doce, mas são particularmente vulneráveis nas regiões costeiras do Mediterrâneo devido a pressões climáticas e antropogénicas. Este estudo comparativo examina as inter-relações entre as teleconexões oceano-atmosfera, os níveis de água subterrânea e a precipitação, em aquíferos costeiros da Califórnia e Portugal. Desta forma visa contribuir para a compreensão acerca dos sinais acoplados de variabilidade climática em climas mediterrâneos. Foram analisados registos piezométricos e de precipitação (1982-2019) utilizando métodos de análise espectral singular, transformada *wavelet e correlações*. Adicionalmente, calculou-se um índice de sustentabilidade da água subterrânea (GSI) que avalia a vulnerabilidade à seca e fornece informações úteis para a futura gestão e segurança das águas subterrâneas. A análise espectral singular identifica sinais consistentes com os seis padrões climáticos dominantes, a Oscilação Decadal do Pacífico (PDO), Oscilação Meridional – El Ninho (ENSO) e a Oscilação do Pacífico / América do Norte (PNA) na Califórnia e a Oscilação do Atlântico Norte (NAO), a Oscilação do Atlântico Este (EA) e o Padrão Escandinavo (SCAND) em Portugal. As oscilações de baixa frequência apresentam maior influência nos padrões hidrológicos, com PDO (52,75%) e NAO (46,25%) sendo responsáveis pela maior parte da variabilidade do nível de água subterrânea. As coerências wavelet mostram relações não estacionárias com covariabilidade entre os padrões climáticos e o os níveis piezométricos em bandas de período distintas; 4-8 anos para PDO, 2-4 anos para ENSO, 1-2 anos para PNA, 5-8 anos para NAO, 2-4 anos para EA e 2-8 anos para SCAND, apresentando alguma dispersão na influência dos padrões de baixa frequência. Os padrões de coerência *wavelet* também mostram que os padrões climáticos acoplados (NAO+ EA- e fases PDO e ENSO conjuntas) estão associados a períodos de seca severos em ambas as regiões. Finalmente, o GSI permite classificar os aquíferos no sul da Califórnia e no norte de Portugal como altamente vulneráveis e com baixa sustentabilidade, alertando para a importância de políticas e medidas de mitigação nestas áreas de risco. O trabalho desenvolvido demonstra como a junção do conhecimento hidro-climatológico com um GSI pode fornecer informação importante para enriquecer e delinear políticas eficazes para a gestão sustentável de águas subterrâneas.

Palavras-chave: Água subterrânea, variabilidade climática, aquíferos costeiros, Mediterrâneo, sustentabilidade

RESUMO ALARGADO

Alterações climáticas antropogénicas e variabilidade climática são questões proeminentes deste milénio que irão moldar a segurança da água doce no futuro. O *nexus* hidrológico entre os sistemas de água doce e marinho em áreas costeiras é complexo, dinâmico e sensível à variabilidade climática global e regional. A água subterrânea, um recurso vital de água doce, pode ser afectada por vários mecanismos de alterações climáticas que induzem a ocorrência de secas. Os eventos periódicos de seca podem ser exacerbados por um lado pela variabilidade climática interanual a multidecadal, através de flutuações anómalas de precipitação ou, por outro lado, por pressões humanas, como extracção de água, irrigação intensiva para agricultura e alterações de uso do solo. Adicionalmente, os aquíferos costeiros nas regiões mediterrâneas e semiáridas são particularmente vulneráveis às alterações climáticas e ao excesso de extracção de água. Neste estudo comparativo, analisa-se o impacto que os eventos de acoplamento da variabilidade climática têm nas oscilações do nível de água subterrânea, em dois sistemas de aquíferos costeiros na Califórnia e em Portugal, uma vez que ambos apresentam clima mediterrânico e propensão para secas recorrentes. A quantificação da vulnerabilidade de aquíferos à seca é posteriormente analisada através do desenvolvimento de um índice de sustentabilidade das águas subterrâneas (GSI), que pode fornecer informações úteis para a gestão e segurança das águas subterrâneas no futuro.

A variabilidade climática refere-se a desvios naturais do estado médio do clima que ocorrem em várias escalas temporais e espaciais. As flutuações do nível piezométrico podem ser influenciadas por padrões de variabilidade climática, também conhecidos como teleconexões. As teleconexões mais importantes associadas a tais flutuações são a Oscilação Decadal do Pacífico (PDO), El Niño-Oscilação Sul (ENSO) e Oscilação Pacífico / América do Norte (PNA) na Califórnia, e Oscilação do Atlântico Norte (NAO), o Oscilação do Atlântico Este (EA) e o Padrão Escandinavo (SCAND) em Portugal. Nesta tese, analizam-se registos piezométricos e de precipitação (1982-2019) através de análise espectral singular (SSA), transformada *wavelet* e métodos de correlação para estudar as ligações entre os padrões climáticos, os níveis piezométricos e eventos hidrológicos extremos. Uma análise GSI é usada para complementar as estratégias de gestão de recursos hídricos, identificando aquíferos com baixa confiabilidade, baixa resiliência, alta vulnerabilidade e baixa

sustentabilidade. Classificar a sustentabilidade de um sistema aquífero é útil para identificar condições de alto risco, fornecendo informações importantes aos decisores políticos para definir medidas para a gestão sustentável das águas subterrâneas.
Este estudo é aplicado aos aquíferos costeiros da bacia da California e vários sistemas aquíferos costeiros de Portugal. Em ambas as regiões, cerca de metade da precipitação anual ocorre no período de três meses de dezembro a fevereiro. Os aquíferos da bacia da Califórnia são predominantemente compostos de sedimentos marinhos e aluviais com alguns depósitos vulcânicos. Os aquíferos costeiros de Portugal são multicamadas com litologias variadas de norte a sul. Os aquíferos na zona de estudo do norte são geralmente sedimentares compostos de aluviões e argilas arenosas. No Algarve, no sul de Portugal, os aquíferos são predominantemente de composição calcária.

Através da SSA foram identificados os períodos de variabilidade significativa nos níveis de água subterrânea. Todas as séries temporais de nível de água subterrânea possuem oscilações estatisticamente significativas, potencialmente relacionadas com as periodicidades PDO (15-30 anos), ENSO (2-7 anos) e PNA (<1-4 anos), NAO (6-10 anos) e EA / SCAND (2-6 anos) . As oscilações de baixa frequência têm uma maior influência nos padrões hidrológicos, com o PDO (52,75%) e o NAO (46,25%) sendo responsáveis pela maior quantidade de variabilidade nos níveis de água subterrânea. As frequências altas (sinais de curto prazo) também representam uma quantidade significativa de variabilidade. Os padrões ENSO e PNA são responsáveis por até 63% da variabilidade associada aos níveis de água subterrânea na Califórnia. Em Portugal, até 54% das flutuações do nível piezométrico estão associadas a frequências do tipo EA / SCAND. Esses padrões também apresentam impactos espaciais variáveis. Em Portugal, a variância associada aos sinais de maior frequência (EA e SCAND) é de 33,25% em média para os aquíferos situados na zona de estudo a norte e de 13,25% em média para o sul. O NAO é o principal motor da variabilidade hidrológica, mas a sua influência é mais forte no sul de Portugal. No sul da Califórnia, a concentração de sinais ENSO é mais evidente.

A transformada *wavelet* contínua (CWT) permite visualizar com eficácia a ocorrência e a evolução de eventos meteorológicos significativos nos registos piezométricos. Eventos hidrológicos anómalos, como os anos de forte precipitação de 1998 e 2007, coincidem com o sinal ENSO (El Niño) na Califórnia. Em Portugal, a ocorrência e o impacto da seca verifica-se com mais intensidade nos anos 2004-05.

Os eventos de acoplamento climático e as associações com a ocorrência de seca são posteriormente identificados por meio da coerência *wavelet*. A covariabilidade entre os padrões climáticos e os níveis piezométricos é mais forte nos seguintes períodos dominantes: 4-8 anos para PDO, 2-4 anos para ENSO, 1-2 anos para PNA, 5-8 anos para NAO, 2-4 anos para EA e 2-8 anos para SCAND. As frequências associadas ao EA e SCAND encontram-se amiúde acopladas às frequências do sinal NAO. As combinações de modos climáticos (acoplamentos) estão associadas a anomalias de nível de água subterrânea, por exemplo, o NAO+ EA- aos períodos de seca, e NAO- EA + SCAND + a forte precipitação em Portugal, e na Califórnia fases acopladas PDO e ENSO associadas tanto a condições húmidas no sul como condições secas no norte. Correlações entre a precipitação e o nível de água subterrânea foram também realizadas, assumindo a precipitação como a variável independente (causal) e o nível dde água subterrânea a variável dependente (responsiva). Os resultados mostram que o setor sul tanto na Califórnia quanto em Portugal apresentam as correlações cruzadas mais fortes. Os resultados de SSA e *wavelet* também permitiram identificar a conexão entre os padrões El Niño (ENSO+) e NAO- e o aumento de precipitação nas zonas mais a sul da Califórnia e de Portugal, respetivamente. Isto mostra que a resposta das águas subterrâneas à recarga direta é mais intensa no sul da Califórnia e no Algarve do que a norte.

Finalmente, a sensibilidade destes sistemas a ocorrência de seca é analisada através do desenvolvimento de um Índice de Sustentabilidade de Águas Subterrâneas (GSI). O GSI é calculado a partir dos registos de nível de água subterrânea para definir indicadores de desempenho, incluindo confiabilidade, resiliência, vulnerabilidade e sustentabilidade. O GSI permitiu classificar aquíferos muito vulneráveis e de muito baixa sustentabilidade no sul da Califórnia e no norte de Portugal. Apesar de se esperar uma maior vulnerabilidade para os aquíferos no Algarve, esta classificação pode ser um importante sinal de alerta para decisores políticos, fomentando novas políticas e medidas de mitigação nas áreas de maior risco.

Os impactos dos modos de variabilidade climática são bastante semelhantes entre os sistemas aquíferos costeiros da Califórnia e de Portugal. Caracteristicamente, ambos têm clima mediterrâneo, são propensos a secas e são influenciados por padrões de baixa e alta frequência de variabilidade climática. Uma característica distinta é a diferença na extensão da seca, durando até 5-6 anos na Califórnia,

enquanto as secas em Portugal duram no máximo 1-2 anos. As diferenças na distribuição espacial dos índices de sustentabilidade entre Portugal e a Califórnia devem-se a fatores locais, nomeadamente às propriedades hidrogeológicas específicas dos aquíferos, e não podem ser consideradas como uma característica geral.

Em suma, esta pesquisa apresenta uma abordagem multifacetada que combina o conhecimento hidro-climatológico com um GSI, a qual permite apoiar e informar políticas sustentáveis de gestão de águas subterrâneas de forma a prioritizar a sua acção em função do risco associado às massas de água subterrânea.

TABLE OF CONTENTS

LIST OF FIGURES

LIST OF TABLES

LIST OF EQUATIONS

LIST OF ACRONYMS

AMO	Atlantic Multidecadal Oscillation
CA	California
CWT	Continuous wavelet transform
EA	Eastern Atlantic Oscillation
ENSO	El Niño Southern Oscillation
GSAs	Groundwater sustainability agencies
GSI	Groundwater sustainability index
GSPs	Groundwater sustainability plans
HydroClimATe	USGS Hydrologic and Climatic Analysis Toolkit
MAR	Managed aquifer recharge
MEIv2	Multivariate ENSO Index v2
NAO	North Atlantic Oscillation
NOAA	National Oceanic and Atmospheric Administration
NWIS	National Water Inventory System
PA	Principal Aquifer
PDO	Pacific Decadal Oscillation
PNA	Pacific/North American Oscillation
PT	Portugal
RBMP	Water Framework Directive's River Basin Management Plan
RCs	Reconstructed components
REL	Reliability
RES	Resilience
SCAND	Scandinavian Pattern
SGMA	California Sustainable Groundwater Management Act
SLPs	Sea level pressures
SNIRH	Sistema Nacional de Informação de Recursos Hídricos
SSA	Singular Spectrum Analysis
SSTs	Sea surface temperatures
USGS	United States Geological Survey
VUL	Vulnerability
WTC	Wavelet coherence

1 INTRODUCTION

Water resources are increasingly threatened in the Anthropocene (Van Loon et al., 2016) as rising drying trends catalyze droughts (Dai, 2013), spark frequent wildfires (Jolly et al., 2015; Liu et al., 2010) and deplete groundwater reserves (Famiglietti, 2014; Ferguson & Gleeson, 2012), posing further urgency around global water security. Groundwater is a subsurface freshwater resource that acts as an essential buffer to meet domestic and irrigation demands during periods of drought and could be overexploited if not managed sustainably (Gurdak, 2017; Russo & Lall, 2017). Globally, over 2 billion people rely on groundwater as their primary source of water (Gurdak, 2017) and 1.7 billion live in water-stressed areas (Gleeson et al., 2012). Systematic groundwater scarcity has lasting socio-economic implications and consequently generates tension between stakeholders (UN-Water, 2006) when sustainability and resilience measures are not mandated.

Aquifers in semi-arid regions including the Mediterranean (Giorgi, 2006; Stigter et al., 2014), southwestern U.S. (Barco et al., 2010; Manna et al., 2019), northeastern Brazil, and southwestern Africa (Döll, 2009) are particularly vulnerable to climate change (Navarra & Tubiana, 2013) and natural climate variability (Taylor et al., 2013). Two thirds of the world's population inhabit coastal areas (UN Atlas of the Oceans, http://www.oceansatlas.org/) making coastal aquifers in semi-arid areas susceptible to excessive anthropogenic activities such as over abstraction and population inflation from tourism.

Interannual to multidecadal ocean-atmosphere oscillation patterns, also known as teleconnections are associated with fluctuations of precipitation, streamflow, snowmelt, groundwater recharge, and temperature directly alter hydrological budgets (Beebee & Manga, 2004; Brabets & Walvoord, 2009; Hanson et al., 2004; Mantua et al., 1997; McCabe et al., 2004; Ropelewski & Halpert, 1986; Vicente-Serrano et al., 2011). Individual teleconnections, such as the El Niño-Southern Oscillation (ENSO) have been repeatedly correlated with drought occurrence and medieval megadroughts in the U.S. (Steiger et al., 2019) and the North Atlantic Oscillation (NAO) is suggested as a proxy to forecast groundwater recharge around the Mediterranean (De Vita et al., 2012). In Portugal, dominant climate patterns drive most (80%) of groundwater variability (Neves et al., 2019b) and over 80% in the California Coastal Basins aquifers that are not directly influenced by anthropogenic stresses, such as pumping or managed aquifer recharge (Velasco et al., 2017). While links between climate

variability and groundwater levels have been identified in several parts of the world, little is known about the implications of complex couplings among modes, and their connection to droughts, which is pertinent to understanding future recharge and groundwater availability.

Groundwater level fluctuations are linked to climate variability, and stored groundwater volumes are intrinsically tied to water security (Thomas et al., 2017), which become more relevant during extreme hydrological droughts. The development of groundwater sustainability index (GSI) can inform resource management decisions (Thomas, 2019) and may effectively compliment base knowledge regarding hydro-climatological behaviors. Such a groundwater sustainability framework is currently underway in California, through the California Sustainable Groundwater Management Act (SGMA – legislative bill package AB1739, SB 1168 and SB 1319), requiring agencies to halt overdraft and re-stabilize groundwater resources (California Department of Water Resources, 2020b) and in Europe through the Water Framework Directive's River Basin Management Plan (RBMP) ensuring groundwater and surface waters achieve "Good" status. The computation of localized groundwater sustainability indicators is also politically relevant, especially when paired with existing water stress indices. Combining these science and policy tools can offer a wholistic approach to water resource management and ecosystem health. A deeper understanding of aquifer response to human and climate driven stressors will be essential for the future of sustainable groundwater resources.

This comparative study examines the implications of coupling climate variability modes on groundwater levels in coastal aquifers of California (U.S. west coast) and Portugal (Iberian west coast). These climate variability modes are exhibited as indices and include the Pacific Decadal Oscillation (PDO), the ENSO, and the Pacific/North American Oscillation (PNA) in California and the NAO, the Eastern Atlantic Oscillation (EA) and the Scandinavian Pattern (SCAND) in Portugal. Each mode of climate variability has a quasi-periodic cycle, and negative and positive phasing.

1.1 Objectives

Previous works, assessing the global depletion of groundwater resources examine abstraction and recharge (Famiglietti, 2014; Wada et al., 2010), but miss the contributions climate variability modes can have on groundwater storage and drought occurrence. Furthermore, water resources in Mediterranean and semi-arid climate

zones are particularly vulnerable to climate change (Döll, 2009; Giorgi, 2006; Navarra & Tubiana, 2013). Here, the impact of large-scale ocean-atmosphere oscillation systems on coastal aquifers are examined in California and Portugal, due to their Mediterranean climate classification, mirrored north-to-south precipitation regimes, and propensity for hydrological drought. This work aims to address the following research questions: Are extreme groundwater level fluctuations in coastal aquifers of California and Portugal driven by coupling of climate modes? What is the connection between mode couplings and drought? How can this information be leveraged to foster groundwater sustainability? This thesis is the first to provide a comparative statistical and analytical analysis of climate mode coupling effects on coastal aquifers of California and Portugal, offering insights for coastal aquifers in vulnerable regions around the world. It also advances the current understanding of hydro-climatological behaviors needed for effective sustainable water resource management under increasing climate uncertainty.

1.2 Climate Variability

Climate variability refers to the natural variation from the mean state of climate, which occur on various spatio-temporal scales, surpassing that of individual weather events. Indices that integrate variables including sea-level pressures (SLPs), sea surface temperatures (SSTs), pressure heights, wind speed, and orbital variations (Ghil, 2002) are often used to define ocean-atmosphere behaviors. Natural climate variability is represented by anomalous climate conditions, resulting from the difference between the current state and the mean climate in key locations (Hurrell et al., 2003). Depending on their phase (positive, negative, and neutral), different weather circulation patterns and conditions of precipitation and air temperature develop. Positive and negative phases are associated with extreme weather events in particular parts of the world, resulting in flooding for some areas and drought in other areas (Table 1). Aquifers are inherently connected to modes of climate variability through precipitation and hydrological cycling.

Table 1. Synthesis of the hydrological implications of the positive phase of six climate patterns pertinent to climate variability in California and Portugal: PDO, ENSO, PNA, NAO, EA and SCAND. The negative phase has inverse effects. CA represents California, EU represents Europe.

Climate Pattern	Hydrological impact
PDO +	↑ precipitation in S CA ↓ precipitation in N CA
ENSO +	↑ precipitation in S CA ↓ precipitation in N CA
PNA +	↓ precipitation in N CA
NAO +	↑ precipitation in N EU ↓ precipitation in S EU
EA +	↑ precipitation in N EU ↓ precipitation in S EU
SCAND +	↓ precipitation in S EU

1.3 Climate patterns of coastal California (West Coast U.S.)

The leading climate patterns affecting the west coast of North America (Figure 1) are the Pacific Decadal Oscillation (PDO), the El Niño-Southern Oscillation (ENSO), and the Pacific/North American Oscillation (PNA) (Ghil, 2002; McCabe et al., 2004; Velasco et al., 2017). While the Atlantic Multidecadal Oscillation (AMO) does affect climatic phenomenon in North America as well (Enfield et al., 2001; Feng et al., 2011; McCabe et al., 2004; Sutton & Hodson, 2005), its 50 to 80 year periodicity exceeds the scope of this study, therefore it may be mentioned but it’s impact on groundwater levels are not analyzed here.

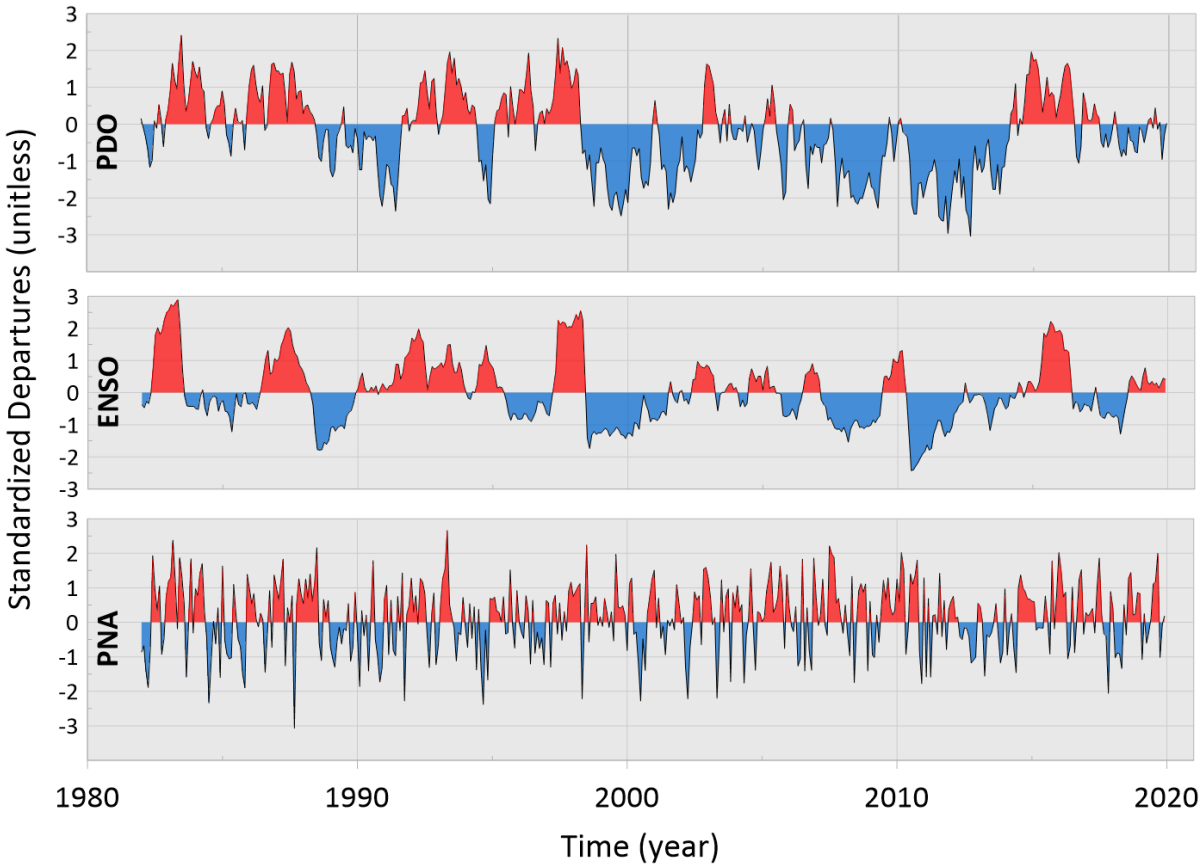

Figure 1. Time series of teleconnection indices pertinent to coastal California. The Pacific Decadal Oscillation has a 15-30 year cycle, the El Niño-Southern Oscillation has a 2-7 year cycle, and the Pacific/North American Oscillation has a <1-4 year cycle. Red signifies a positive phase and blue signifies a negative phase.

1.3.1 The Pacific Decadal Oscillation (PDO)

The PDO index is calculated using detrended monthly SST anomalies of the northern Pacific ocean, poleward from 20° north latitude (Zhang et al., 1997). The PDO periodicity occurs every 15-30 years, yet a second phenomenon from 50-70 years has emerged in the 20th century (Figure 1) (Hanson et al., 2006; Mantua & Hare, 2002; Mantua et al., 1997). Positive phases of the PDO are marked by decreased winter precipitation associated with warm dry periods and sustained droughts in the Pacific Northwest and cool wet periods in the southwestern United States (Higgins et al., 2007; Mantua & Hare, 2002; Mantua et al., 1997). Precipitation conditions are reversed during the negative PDO phase. These shifts are triggered by cooler than normal SSTs in the central North Pacific during the positive phase, and warmer than normal SSTs adjacent to the west coast of North America. Phasing of the PDO is known to influence the dipole signature of ENSO winter precipitation in the western

U.S. (Brown & Comrie, 2004). The PDO was in a positive phase during the periods 1925 to 1946 and from 1977 through the late 1990s, and again with a shorter period from 2002 to 2005, followed by a neutral phase until 2007. The PDO's last positive phase shift was in 2014. Negative phases occurred from 1890 to 1924, 1947 to 1976, and remain largely in a negative phase since 1999 (Mantua & Hare, 2002; McCabe et al., 2004). A more evident negative signal was expressed from 2007 to 2013.

1.3.2 The El Niño-Southern Oscillation (ENSO)

The ENSO is a 2-7 year quasiperiodic fluctuation of SSTs and SLPs anomalies occurring in the equatorial Pacific (NOAA, 2020b). ENSO is regarded as the most important interannual climate pattern globally (Palmer & Anderson, 1994), is the largest signal driving North American climate (Gershunou et al., 1999) and has consequential environmental and socio-economic impacts around the world (Bove et al., 1998; IPCC, 2001; N. J. Mantua et al., 1997; Poveda et al., 2001). While many ENSO indices are available, the Multivariate ENSO Index (MEI.v2) (Figure 1) is used here due to its comprehensiveness, combining SLP, SST, zonal and meridional winds, air temperature and total cloudiness of the tropical Pacific (Wolter & Timlin, 1993, 1998, 2011). For the period between 1979 and 2018, the ICOADS-based MEI and MEI.v2 are correlated at 0.95. (NOAA, 2020d). As with other indices, MEI.v2 signs reflect ENSO phases. Positive MEI.v2 is related to positive ENSO (El Niño) and negative MEI.v2 reflects negative ENSO (La Niña). During the positive ENSO phase (El Niño), unusually low SLPs in the eastern equatorial Pacific and high SLPs in the western equatorial Pacific enable warm western waters to migrate eastward. These warm SSTs in the eastern-central Pacific generate height and pressure anomalies in the mid-upper troposphere in the subtropics, therefore strengthening and shifting the polar jet stream southward delivering storms across the southern U.S. from coastal California to Florida. This altered storm track is responsible for increased above-average precipitation in southern California, and below-average precipitation in northern California (Huang & Ullrich, 2017; Jong et al., 2016; O'Brien et al., 2019). Conversely, during the negative phase (La Niña) a reversal of the SLPs results in cooler SSTs in the eastern equatorial Pacific and shifts a subdued polar jet stream northward, creating drier conditions in southern California and wetter conditions in northern California. Although ENSO is strongly correlated with precipitation in the southwest and central U.S., it forces fluctuations of precipitation from coast-to-coast.

The most extreme El Niño events occurred in the periods 1877–1878, 1982–1983, and 1997–1998 and 2015-2016 (Wolter & Timlin, 2011). These particularly strong El Niño events have immediate socio-economic repercussions resulting from catastrophic flooding, landslides, tornadoes, droughts, and forest fires. When compared to other climate variability modes, the ENSO is the most reliable climate oscillation in terms of prediction (Cayan et al., 1999) and is well tracked by climate prediction centers.

1.3.3 The Pacific/North American Oscillation (PNA)

The PNA is an index with a periodicity of <1-4 years, which is based on recurrent quadripole pressure center fluctuations of 500 millibar heights above sea level over the central Pacific and North American continent (Figure 1) (NOAA, 2020b). The PNA is one of the most prominent low-frequency climate variability modes in the extratropics of the Northern Hemisphere. During its positive phase, the PNA expresses above average geopotential heights near Hawaii and the intermountain region of North America, and below average geopotential heights located south of the Aleutian Islands and in the southeastern U.S. The inverse is true during its negative phase. The PNA pattern is closely tied to fluctuations in the strength and position of the East Asian jet stream, which is enhanced and shifted eastward towards the western U.S. during the positive phase. In contrast, the negative phase is associated with a retraction of the jet towards East Asia (Wallace & Gutzler, 1981). The positive PNA phase is associated with anomalously high temperatures in western Canada and the western limits of the U.S. and anomalously low temperatures in the south-central and southeastern U.S. During its positive phase, winter precipitation is below average in the Pacific Northwest and along the eastern half of the conterminous U.S. (Dahlman, 2009). The PNA pattern, although it is a natural internal mode of variability, is often synchronized with ENSO phase shifts. Winter PNA values are also associated with the PDO SST anomalies and warm El Niño phases (Rodionov & Assel, 2001).

1.4 Climate patterns of coastal Portugal (West Iberian Peninsula)

The dominant climate patterns affecting coastal Portugal (Figure 2) are the North Atlantic Oscillation (NAO), the East Atlantic Oscillation (EA), and the Scandinavian Pattern (SCAND). Cumulatively, these climate variability patterns are responsible for 80% of the total variance of groundwater levels in Portugal (Neves et al., 2019b).

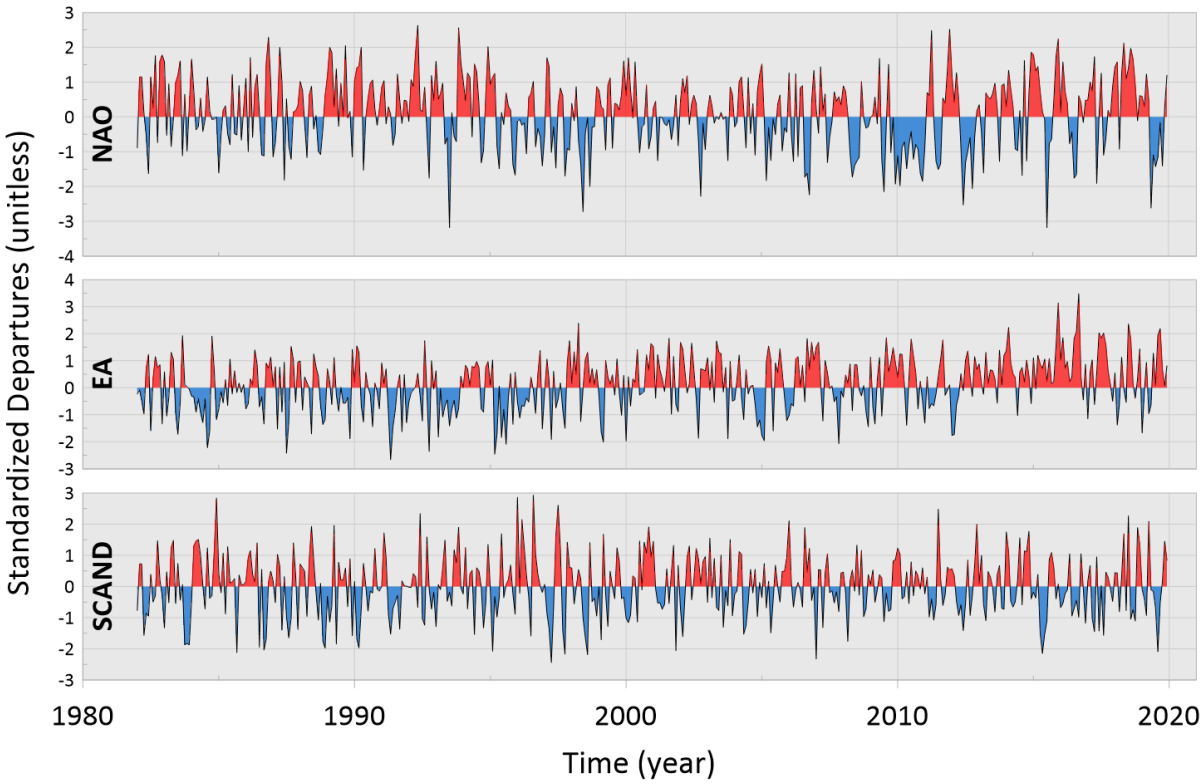

Figure 2. Time series of teleconnection indices pertinent to coastal Portugal. The North Atlantic Oscillation has a 6-10 year cycle, and the East Atlantic Oscillation and Scandinavian Pattern have a 2-6 year oscillation. Red signifies a positive phase and blue signifies a negative phase.

1.4.1 The North Atlantic Oscillation (NAO)

The NAO is an index comprised of a meridional dipole of pressure anomalies over southern Greenland (Icelandic Low) and the Azores (Azores High), spanning latitudes between 35° and 40° in the North Atlantic (Hurrell, 1995) (Figure 2). The dominant periodicity of the NAO is 3-6 years, with a second less significant oscillation of 8-10 years (Hurrell et al., 2003). A 6-10 year frequency is most relevant to coastal Portugal (Neves et al., 2019a; Neves et al., 2019b) and is therefore referenced in the analysis conducted in this study. Considerable inter-annual and decadal oscillations are determined by the sign and strength of the NAO (Hurrell & Van Loon, 1997). The positive NAO phase is characterized by high pressures over the Azores and low pressures over Iceland, transporting warm moist air over Europe and the eastern U.S., thus promoting wet winters across northern Europe and drier conditions in southern Europe. During the negative NAO phase, surface westerlies are shifted southward driving precipitation over southern Europe. In western Iberia, the NAO has been known

to dictate winter rainfall, river flow and surface storage (García-Herrera et al., 2007; S. Jerez et al., 2013; Trigo et al., 2004).

1.4.2 The East Atlantic Oscillation (EA)

The EA is a prominent low-frequency variability pattern that is structurally similar to the NAO, but is oriented to the southeast aligning with nodal lines of the NAO (NOAA, 2020b) (Figure 2). Consequently, the EA is often interpreted as a southward semblance of the NAO pattern, yet a lower-latitude subtropical link helps distinguish it from the NAO. In its positive phase, low pressure centers of EA are located over the north Atlantic, west of the United Kingdom (Barnston & Livezey, 1987) and is associated with anomalously high precipitation over northern Europe and Scandinavia, and below-average precipitation along southern Europe (NOAA, 2020b). A negative EA phase occurred from 1950-1976 and was followed by a positive phase from 1977-2004, of which 1997-2004 held a particularly strong EA signal.

1.4.3 The Scandinavian Pattern (SCAND)

The SCAND index is comprised of monthly pressure anomalies of 700 millibar heights (m) with a primary center of action over the Scandinavian Peninsula and ancillary centers over the northeastern Atlantic and central Siberia (Bueha & Nakamurab, 2007) (Figure 2). The positive SCAND phase is associated with anticyclonic pressure anomalies, below-average precipitation throughout southern Europe and dry conditions in Scandinavia (NOAA, 2012). The EA and SCAND patterns impact on precipitation regimes across Europe vary spatially and are inconsistent, whereas the NAO's influence is much more predictable (Trigo et al., 2008).

1.5 Coupling of Climate Variability Modes

Recent studies have presented results on teleconnection interactions across various domains, including groundwater level fluctuations (Corona et al., 2018; Neves et al., 2019a; Neves et al., 2019b; Velasco et al., 2017) wildfire fire regimes, drought extent (Jolly et al., 2015; Liu et al., 2010; Norman & Taylor, 2003), carbon sequestration (Bastos et al., 2016), and renewable energy potential (Correia et al., 2017; Jerez & Trigo, 2013). The coupling of climate variability modes can have either constructive (enhancing) or destructive (reducing) variability effects. For example, the

combined effects of NAO+ and EA- phases has extended drought severity and period in Portugal (Neves, et al., 2019; Trigo et al, 2013) (Figure 3). Synchronized NAO, EA, SCAND and EA/WR (East Atlantic/West Russian pattern) patterns can determine heat transfer, surface water and groundwater flows in across Europe (Holman et al., 2011; Kalimeris et al., 2017; Steirou et al., 2017). PDO can enhance the effect of ENSO when both modes are synchronized. A positive PDO phase can intensify El Niño, driving a more robust pattern of wetter winters in the southern U.S. (Gershunov & Barnett, 1998). Moreover, La Niña events are more frequent during PDO-, whereas El Niño events occur more often when PDO is in its positive phase (Gutzler et al., 2002; Lapp et al., 2013). Coupling events can also modify the placement of climate variability patterns spatially, constraining effects at a smaller regional scale. McCabe et al. (2004) found that drought frequency increased in the southwest U.S during the positive phase of the AMO and PDO- but shifted to the northern U.S. during AMO+ and PDO+. While comprehensive knowledge of how the three dominant climate variability patterns in California and Portugal affect each other is not fully understood, it is nonetheless important to acknowledge the modifications that can occur to expected hydro-climatic systems when different modes of climate variability are coupled.

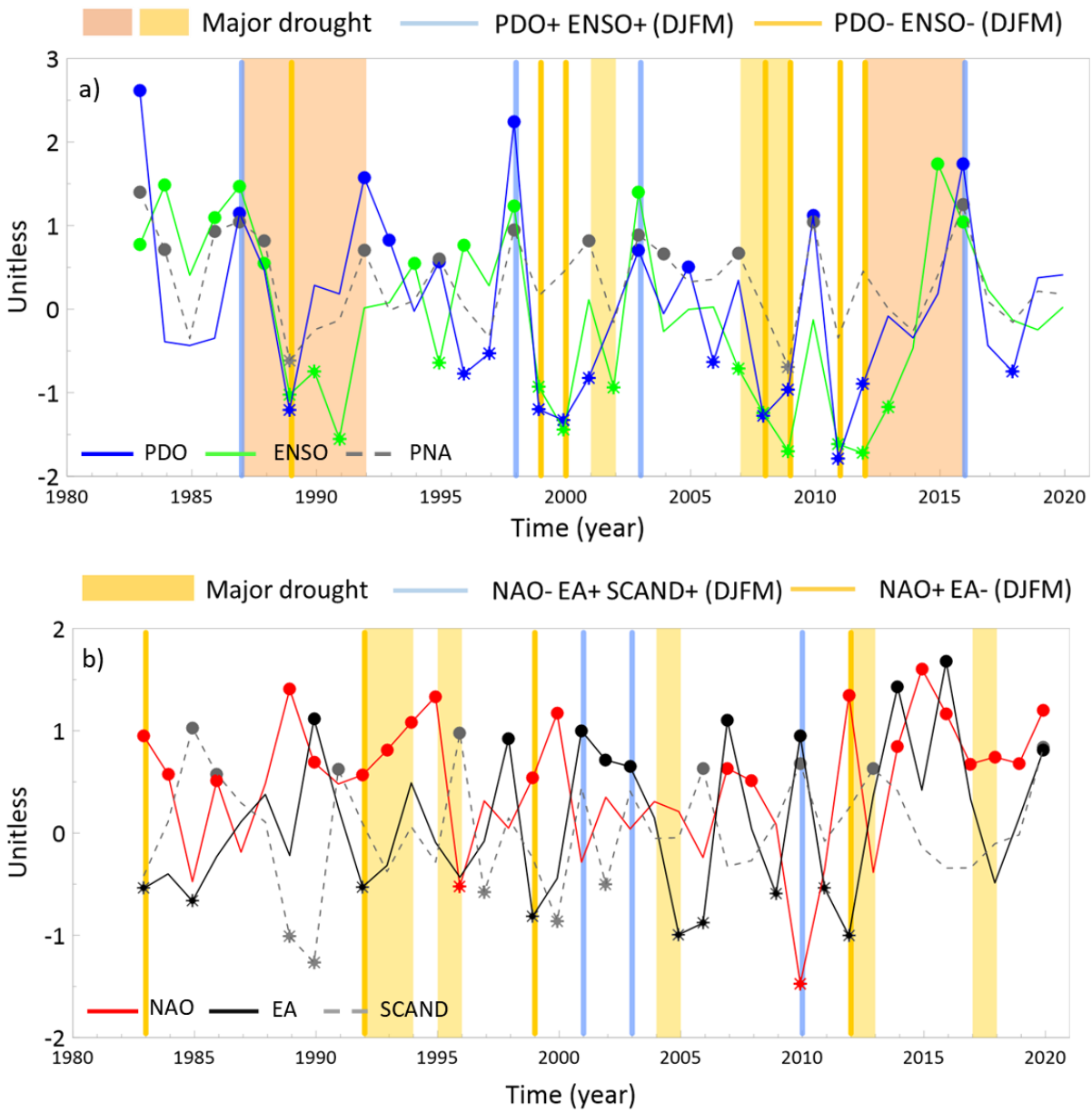

Figure 3. Time series of the winter composites (December-March) of the climate indices in a) California and b) Portugal. Positive and negative phases of each indices are defined by winter index values above 0.5 and below -0.5, respectively and are marked by circle and asterisk symbols. Color bars indicate major droughts and anomalous wet winters associated to phase couplings.

1.6 Groundwater Use in California and Portugal

Groundwater is a valuable component to California's water supply, providing about one-third of the water used in average years and more than one-half of the water used during drought years (California Department of Water Resources, 2020b). Irrigation and food production account for the largest demand on groundwater resources (Maupin & Barber, 2005). Overdrafts, resulting from unsustainable yields of

groundwater have catalyzed water quality degradation, seawater intrusion, land subsidence, damage to infrastructure and impacts to the function of groundwater dependent ecosystems across aquifers in California.

In Portugal, domestic water supply was largely dependent on groundwater prior to the switch (in the Algarve) in 1999, to a regional surface reservoir system. A network of 62 dam-backed storage reservoirs are located within the main river basins throughout the country (APA, 2019). Once the surface water supply system was operational, public supply wells were deactivated and held as emergency reserves. Today, groundwater is primarily used for agricultural purposes. However, the fragility of this single source supply scheme was magnified during the severe drought of 2004-05 leading to advocacy around an integrated water resource management approach (Stigter et al., 2009).

1.7 Sustainable Groundwater Management

Groundwater is predominantly a renewable freshwater resource, when managed properly. It can ensure a long-term supply for human use and ecosystem function even amidst increasing demands and anticipated effects of global climate change. However, aquifers are strongly influenced by climate variability, and recharge rates vary across aquifer systems, further highlighting the importance of regulations to ensure sustainable groundwater use. Van Loon et al. (2016) also argue that the human influence on drought is as integral as natural climate variability. Here, two foundational sustainable groundwater management legislative acts are presented for each study area offering context for the further advancement of sustainable groundwater management.

1.7.1 Sustainable Groundwater Management Act – California

After a long history of overdraft and many years of providing legislative authority for local agencies to manage groundwater on a voluntary basis, in 2014 the Governor of California enacted the Sustainable Groundwater Management Act (SGMA). As stated in the act, "It is the policy of the state that groundwater resources be managed sustainably for long-term reliability and multiple economic, social, and environmental benefits for current and future beneficial uses" (AB 1739 (Dickinson), SB 1168 (Pavley), and SB 1319 (Pavley), dated 16th September 2014). SGMA requires local agencies overseeing designated groundwater basins to take affirmative steps to

manage basin resources for long-term sustainability. California's Department of Water Resources (DWR) and the State Water Resources Control Board administer various parts of the legislation, including the DWR's development and promulgation of groundwater sustainability plan regulations. One early milestone for SGMA implementation was reached in mid-2017, with the formation of groundwater sustainability agencies (GSAs) for the basins. Under SGMA, GSAs are required to develop groundwater sustainability plans (GSPs) with local stakeholder engagement that will be implemented by 2040.

1.7.2 River Basin Management Plan – Portugal

In Europe, a major driver to improve groundwater and surface water status is the European Union (EU) Water Framework Directive (2000/60/EC, dated 23rd October 2000), which requires EU member states to achieve “Good” status for groundwater and surface water bodies by 2027. This includes measures for groundwater quality and quantity, and surface water quality, quantity, and ecology and hydromorphology. This is managed by individual member states through the River Basin Management Plan (RBMP) process, which define groundwater and surface water bodies, identify their current status, identify the significant issues or pressures in each water body, and define and deliver specific improvements in order to meet “Good” status by 2027. Two RBMP’s have been produced already, and the third will cover the period 2022-2027. Regional Hydrographic Management Plans pertinent to this study are RH4, encompassing Regiao Hidrografica do Vouga, and Mondego e Lis and RH8, which includes Ribeiras do Algarve (APA, 2019).

1.8 Site descriptions

This study evaluates the California Coastal Basins aquifers (CA) and several coastal aquifer systems of Portugal (PT). Climatically, these coastal landmasses are classified as Mediterranean, with similar zonation from north to south. In both Portugal and California, about half of the annual precipitation arrives in the three-month period from December through February (Miranda et al., 2002), and in California 90% of the annual precipitation falls between October 1st and April 30th. Consequently, precipitation during wet winters determine the availability of water resources in the months that follow. Northwest Iberia and northern California are classified (Köppen-Geiger) as type Csb, temperate with dry and mild summers (Kottek et al., 2006). In

northern Portugal, the monthly average temperature ranges between 10 and 20 °C and the total annual rainfall is approximately 1000 mm/year. In northern California, the monthly average temperature ranges between 8 and 16 °C and the total annual rainfall is approximately 1024 mm/year. The Algarve region, in southern Portugal (SW Iberia) and central California are classified as type Csa, temperate with dry and hot summers, while southern California is arid to semi-arid, Bwk. In the Algarve, the monthly average temperature ranges between 12 and 24 °C and the total annual rainfall is about 500 mm/year (IPMA, 2017). In southern California, the monthly average temperature ranges between 13 and 22 °C and the total annual rainfall is about 470 mm/year (NOAA, 2020a). To make regional comparisons across the two prevailing climate zones, aquifer systems in each country were separated according to their location. The boundary of the aquifer system and the selected groundwater observation points are illustrated in Figures 4 and 5, while Tables 2 and 3 detail the descriptive attributes of each groundwater level record. Aquifers that are considered to reside in the northern sector are sites 01-04 in Portugal and 01-03 in California. Aquifers considered to be in central California are site 04. Finally, aquifers considered to be in the southern sector of the region are 05-08 in Portugal and 05-08 in California.

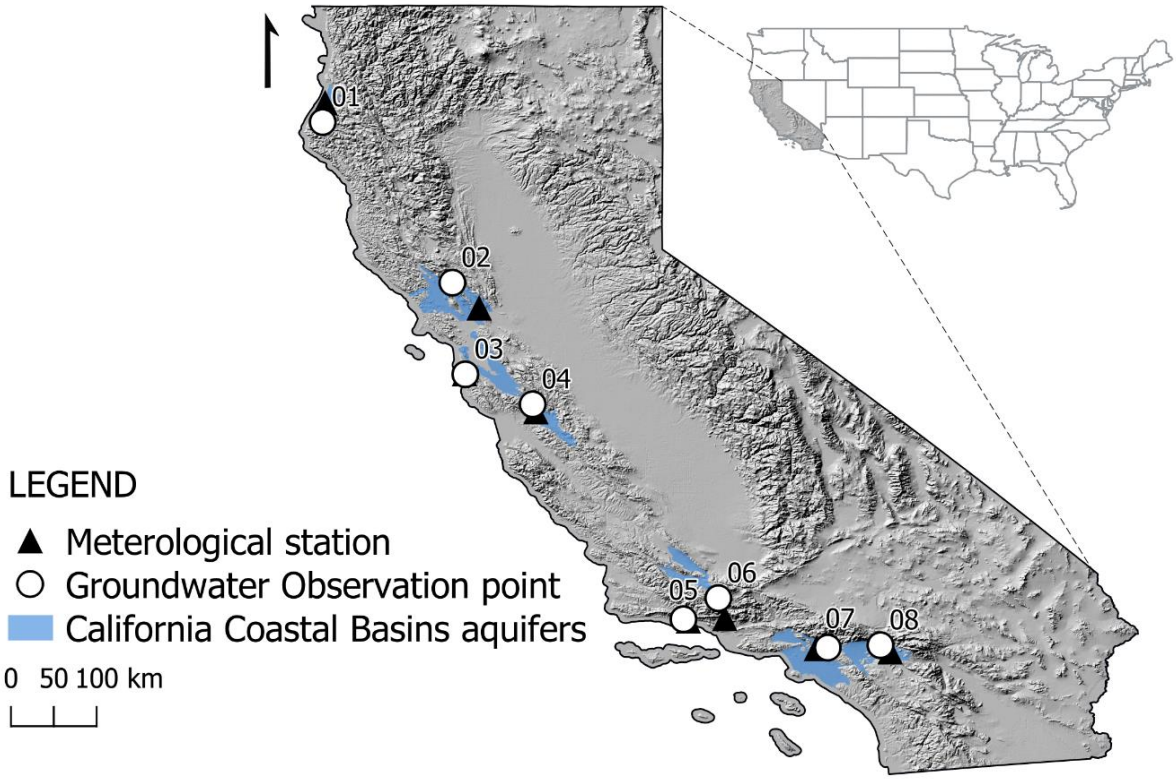

Figure 4. Map showing the location of precipitation and groundwater observation points in the California Coastal Basins aquifer system.

Table 2. Descriptive attributes for the location of groundwater observation points in the California Coastal Basins aquifer system. The Site ID identifies the aquifer name (CA), the site type (GW for groundwater), and the location (01–08 from northwest to southeast).

Site ID	Location	Site Number	Latitude	Longitude
CA GW 01	Humboldt	405702N1241874W001	40.5702	-124.1874
CA GW 02	Napa	385926N1225938W001	38.5926	-122.5938
CA GW 03	Half Moon Bay	374643N1224317W001	37.4643	-122.4317
CA GW 04	San Martin	370881N1216003W001	37.08806	-121.60031
CA GW 05	Santa Barbara	342630119442301	34.4419	-119.7402
CA GW 06	Ventura	344156119184801	34.6985	-119.3136
CA GW 07	Los Angeles	340535117573501	34.0930	-117.9597
CA GW 08	San Bernardino	340655117184006	34.1151	-117.3116

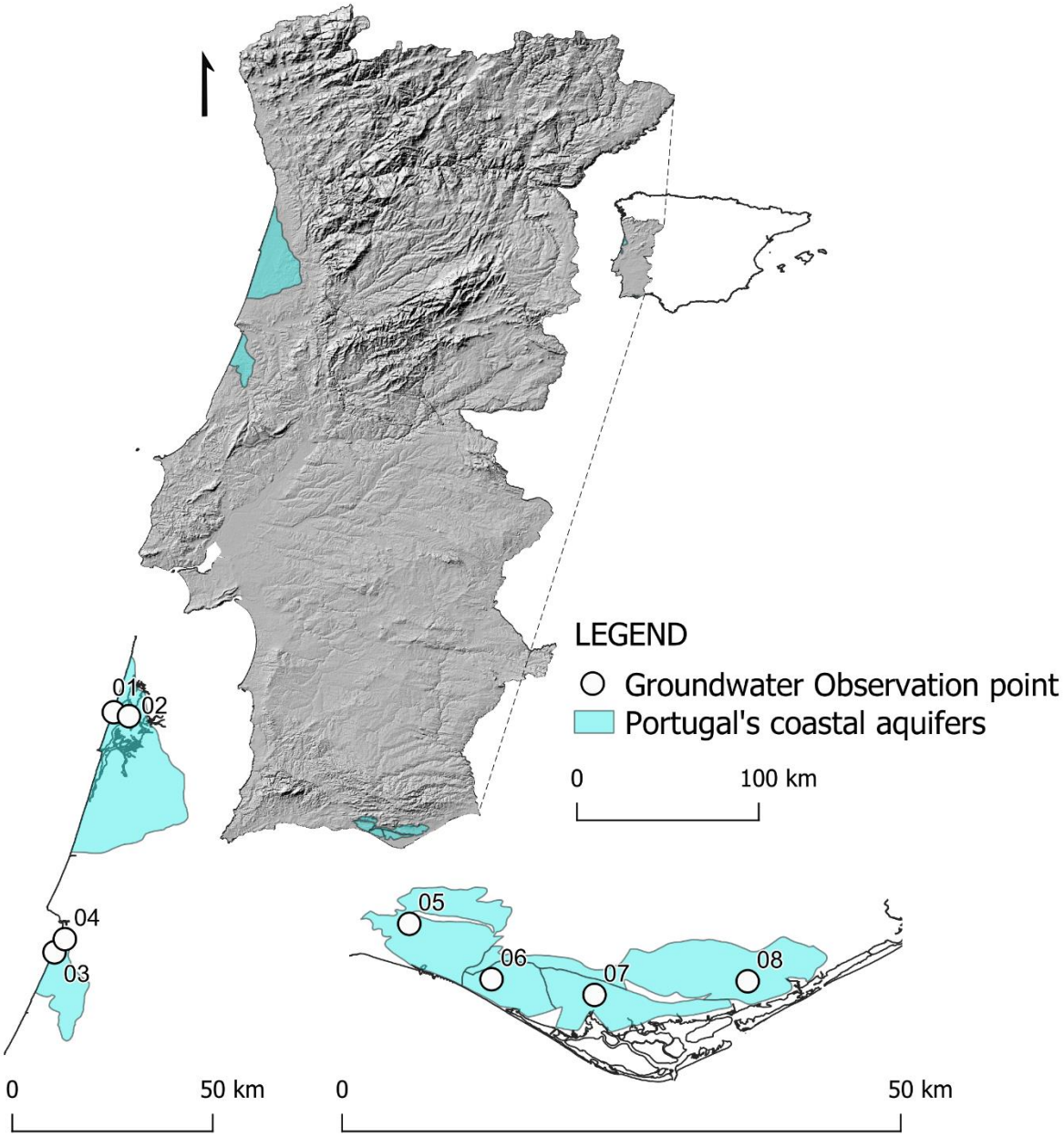

Figure 5. Map showing the location of groundwater observation points in Portugal's coastal aquifer system. Precipitation records and piezometers share the same coordinates and are therefore not displayed.

Table 3. Descriptive attributes for the location of groundwater observation points in Portugal's coastal aquifer system. The Site ID identifies the aquifer name (PT), the site type (GW for groundwater), and the location (01–08 from northwest to southeast).

Site ID	Location	Site Number	Latitude	Longitude
PT GW 01	Cretacico de Aveiro (O2)	162A/9	-8.7118256	40.753993
PT GW 02	Cretacico de Aveiro (O2)	174/2	-8.6676507	40.742662
PT GW 03	Leirosa – Monte Real (O10)	249/4	-8.8843293	40.055807
PT GW 04	Leirosa – Monte Real (O10)	261/117	-8.854263	40.094272
PT GW 05	Quarteira (M7)	605/303	-8.1342549	37.12038
PT GW 06	Campina de Faro (M12)	606/647	-8.0515888	37.064728
PT GW 07	Campina de Faro (M12)	611/230	-7.9481014	37.048967
PT GW 08	São João da Venda-Quelfes (M10)	607/484	-7.7941745	37.06265

1.8.1 Hydrogeologic description of the California Coastal Basin aquifers

The U.S. Geological Survey (USGS) classifies the California Coastal Basins system as a Principal Aquifer (PA) of the United States. PAs are generally unconfined and are formed from unconsolidated to semi-consolidated sand and gravel material, with characteristically moderate to high hydraulic conductivity (USGS, 2015). The California Coastal Basins aquifers, located along the coast of California are comprised of over 100 basin-fill aquifers predominantly composed of marine and alluvial sediments with some volcanic deposits (Planert & Williams, 1995). In the subsequent sections, the details on each aquifer within the California Coastal Basins are derived primarily from the USGS Ground Water Atlas of the United States (Segment 1, Hydrologic Investigations Atlas 730-B), which is a publication that describes the location, extent, geographic, geologic and hydrologic characteristics of the major aquifers of the U.S. The online version of the atlas is available at http://pubs.usgs.gov/ha/ha730/ gwa.html.

1.8.1.1 Eureka Area Basins

The Eureka area aquifers are composed of primarily alluvial deposits from the Pliocene or younger. Unconsolidated deposits of sand, gravel, silt, and clay interdigitate with estuarine sediments at the coast and are locally underlain by marine sediments. The primary groundwater body is in the Eel River Valley, where unconfined conditions make fresh groundwater available nearly everywhere at depths of 9 meters or less.

1.8.1.2 North San Francisco Bay Area Valley Basin

The main water-yielding materials of the North Bay Valleys are unconsolidated and semi-consolidated marine and continental sediments and unwelded tuffaceous beds in volcanic rocks. Underlying consolidated rocks of Cretaceous and Jurassic age with low permeability establish boundaries within the groundwater flow system. This valley basin system contains a collection of connected and isolated aquifers. This is due to lenticular confining units, unconfining units and faulting. Historic over withdrawal has induced saltwater intrusion at the discharge area of San Pablo Bay.

1.8.1.3 Santa Clara Valley Basin

The Santa Clara Valley is nestled between the Santa Cruz Mountains in the southwest and the Diablo Range on the northeast, generating a structural trough in which the aquifer system is located. The Valley is also flanked by two major faults of the San Francisco Bay area: The San Andreas fault in the southwest and the Hayward fault in the northeast. Deposits are generally impermeable consolidated rocks at the base of the two surrounding mountain ranges, and groundwater is primarily contained in lenticular coarse-grained sand and gravel beds. Due to the early expansion of irrigated agriculture, and domestic and industrial development in the Santa Clara Valley the reliance on groundwater supply and over withdrawals have resulted in land subsidence particularly in the heavily urbanized areas. Due to groundwater management activities by Santa Clara Valley Water District, subsidence has essentially been halted since the 1970s (SCVWD, 2020). Groundwater pumping in the basin is used to support municipal and domestic supply, as well as industrial uses and irrigated agriculture in the southern areas of the basin. Other areas of groundwater discharge are local streams and the San Francisco Bay. Although precipitation supports natural recharge to the basin, Santa Clara Valley Water District operates a large managed aquifer recharge (MAR) program that supplies the vast majority of recharge to the basin, particularly in the northern areas of the basin. However, in the southern areas of the basin, natural recharge and managed recharge are approximately equal in most years.

1.8.1.4 Santa Barbara and Foothill Basins

The Santa Barbara basin is dominated by faulting that has uplifted and overturned many sedimentary rock layers of mostly marine origin. In the groundwater

basin, tertiary sedimentary rocks are overlain by unconsolidated to partially consolidated deposits. Marine and non-marine unconsolidated and partially consolidated deposits from the late Pliocene and Pleistocene and Holocene alluvium overlay the consolidated units (Freckleton et al., 1998; Paulinski et al., 2018). The study area, within the Foothill Basin is divided by a fault generating two sub-basins and acts as partial barriers to groundwater flow (Freckleton et al., 1998).

1.8.1.5 The Central Los Angeles Basin

The Central Los Angeles basin is bounded by the San Gabriel Mountains and the Puente Hills in the north and the Dominguez Hills in the southeast. Several fault zones trend NW to WNW, and the Newport-Inglewood Uplift separates the Central basin from the western basin. The Central Los Angeles basin is a multilayer system composed of upper Miocene to lower Pleistocene of nonmarine fluvial and lagoonal deposits and upper Pleistocene to Holocene units, deposited in canyons incised into the Pleistocene deposits during sea-level low stands (Reichard et al., 2003). Dense urban development around the larger Los Angeles area has decreased the potential for direct recharge to the aquifer. The Los Angeles Coastal Plain aquifer system has already experienced saltwater intrusion since the 1930s although mitigation measures to slow or cease sea water intrusion have been implemented in recent years.

1.8.2 Hydrogeologic description of Portugal's aquifers

The four large morphostructural and corresponding hydrogeologic units of Portugal, as defined by the Instituto da Água (INAG) are the Hespéric Massif, the West and Southern Meso-Cenozoic Basins and Tejo-Sado Tertiary Basin. A compilation of seminal hydrogeological knowledge for the aquifer systems of Mainland Portugal are contained in a report trilogy authored by Almeida et al (2000). In the following sections, a hydrogeologic overview of Portugal's coastal aquifer systems are largely drawn from the Almeida et al. (2000) dossiers.

1.8.2.1 Creticico de Aveiro

The Aveiro aquifer (O2) is located within the lower Vouga River Basin, known for a shallow coastal lagoon, the 'Ria de Aveiro' of both marine and estuarine composition. The area of the system is 894 km² (SNIRH, 2020). Groundwater bearing deposits of the Aveiro aquifer (O2) have a discontinuous stratigraphic sequence from

late Triassic to Holocene (Condesso & Marques Da Silva, 2008). Deposits of alluvial sediments and fine sand dunes are overlaid by beach deposits and fluvial terraces. The Quaternary deposits unconformably overlie consolidated Cretaceous units of limestones deposited in fluvial, deltaic or shallow marine environments. Both the Quaternary and the Cretaceous units form multilayer aquifer systems which produce substantial volumes of freshwater (Condesso & Marques Da Silva, 2008).

1.8.2.2 Leirosa – Monte Real

The Leirosa-Monte Real aquifer (O10) is a highly productive porous multilayered system formed by Plio-Pleistocene, pre-Miocene sandy clays and Mesozoic calcareous loams with an area of 218 km² (SNIRH, 2020). Groundwater flow is directed to the Atlantic and in morphologically depressed areas, during high water the phrenic surface emerges giving rise to ephemeral pools. This system's piezometric levels are unusual, in that they have not suffered declines from over-abstraction over the last decades (Ribeiro & Cunha Da, 2010).

1.8.2.3 Quarteira

The Quarteira (M7) basin is composed of mostly productive Miocene and Jurassic lithologies, with occasional Cretaceous formations overlaid with a low permeability Plio-Quarternary layer and has an area of 81 km² (SNIRH, 2020). This is a multi-layered aquifer system where groundwater is primarily contained by detrital-carbonate deposits from the Miocene and limestones from the Upper Jurassic which can be in direct contact or separated by a Cretaceous aquitard. Low permeability Plio-quaternary formations overlay the Miocene aquifer, confining the aquifer in some locations which are evinced by artesian wells near the city of Quarteira. Boundaries of the aquifer system are drawn by three major tectonic features, the Algibre flexure to the north, the NE-SW S.Bras de Alportel – Loule – Quarteira fault in the east, and the S.Marcos da Serra-Quarteira fault to the west, which drains the aquifer towards the Ribeira de Quarteira and the sea, to the south, where main discharge of the aquifer occurs.

1.8.2.4 Campina de Faro

The Campina de Faro aquifer (M12) is a three-unit multilayered system where the deepest layer is formed by marls and Cretaceous limestones and spans over an area of 86.4 km^2 (SNIRH, 2020; Tibor Yvan Stigter, 2005). The second aquifer is

comprised of a Miocene fossil-rich sandy limestone deposits, with an irregular topography. Sands, clayey sandstones, gravels, and conglomerates of the Plio-Quaternary overlay the Miocene deposits. The third system is formed by fine Miocene sands and Plio-Quaternary sand and gravels. Although this aquifer is partly covered by Holocenic deposits, it is phreatic due to the thin depositional layer. The general direction of groundwater flow runs N-S (Tibor Yvan Stigter, 2005). The third (Plio-Quaternary) and the second (Miocene) aquifers are the most important in terms of groundwater abstraction, supporting water abstraction for the intensive agriculture area in the system. The aquifer boundary is set to the north by the Cretaceous less permeable formation and to the south by the sea and the coastal lagoon of Ria Formosa, where the main discharge of the system occurs. To the west, the aquifer limits are defined by the contact with M7, whereas to the east the aquifer limit is defined by the São João da Venda-Quelfes (M10) aquifer system.

1.8.2.5 São João da Venda-Quelfes

The São João da Venda-Quelfes (M10) aquifer system is formed by Lower Cretaceous deposits, of detritic material at the base overlaid by a thick carbonate unit of marls and marly limestones from the Upper Cretaceous (Almeida et al., 2000). The aquifer area is 113 km^2 (SNIRH, 2020). The Faro fault running NNE-SSW crosses the entire aquifer system. The São João da Venda-Quelfes connects to several aquifers systems: Quarteira in the west, Campina de Faro and Chão de Cevada-Quinta de João de Ourém in the south, and the adjacent Luz-Tavira system. The multilayer system is divided into two sub-units which likely function independently and have varying hydrologic productivity.

2 METHODOLOGY

2.1 Data Selection

The time series evaluated here include previously described climate indices (ENSO, PDO, PNA, NAO, EA and SCAND), groundwater level, and precipitation. Climate indices were obtained from NOAA's Climate Prediction Center for EA and SCAND, the National Center for Environmental Information (NCEI) for PDO, PNA and NAO, and the Physical Sciences Laboratory (PSL) for ENSO, which published the most contemporary bi-monthly Multivariate ENSO index (MEI.v2).

Groundwater level time series, spanning the years of 1982 to 2019, were obtained from monitoring wells in the California Statewide Groundwater Elevation Monitoring (CASGEM) program's online public portal (https://www.casgem.water.ca.gov/), the USGS National Water Information System (NWIS) (http://nwis.waterdata.usgs.gov/usa/nwis/gwlevels), and the Portuguese National System for Water Resources Information (SNIRH) (https://snirh.apambiente.pt/). Pertinent hydrogeologic details of each groundwater time series are provided in Tables 4 and 5. Monitoring wells within each aquifer system were selected based on criteria including the length and completeness of the record and contemporariness. A continuous record length of 30 years is assessed to capture interannual to interdecadal climate variability, including signals up to the PDO periodicity (15-30 years), with at least a quarterly temporal resolution. While groundwater records for Portugal all have the same time span (1989-2018), records in California have a mixed range (Table 4) as it was not possible to find a common and complete 30-year recording. Monitoring wells within the California Coastal Basins aquifers and Portugal's coastal aquifer system are selected to represent a range of hydrogeological conditions.

Table 4. Descriptive attributes for the groundwater record and hydrology in the California Coastal Basins aquifers system. The Hydrologic Soil Group categories are: A for sandy and gravelly textures, B for loamy sand or sandy loam textures, C for loamy and silty textures, and D for clayey textures. N/A = information not available.

Site ID	Starting Year	Ending Year	Length of Record (years)	Sampling rate	Hydrologic Soil Group	Well use	Mean Piezometric Level (meters)
CA GW 01	1990	2019	30	Q	B	Residential	6.32
CA GW 02	1990	2019	30	Q	B	Residential	113.40
CA GW 03	1990	2019	30	Q	B	Irrigation	14.39
CA GW 04	1990	2019	30	M	B	Observation	75.21
CA GW 05	1990	2019	30	M	B	Observation	35.72
CA GW 06	1982	2011	30	Q	B	Observation	1125.33
CA GW 07	1984	2013	30	M	N/A	Observation	69.83
CA GW 08	1990	2019	30	M	A	Observation	286.29
						Aquifer Average:	215.81

Table 5. Descriptive attributes for the groundwater record and hydrology of groundwater wells in Portugal's coastal aquifer system. The Hydrologic Soil Group categories are: Cambissolos cromicos calcarios (BCA), Cambissolos humicos rochas sedimentares (Bh), Fluvissolos eutricos (Je), Podzois orticos (Po), and Solonchaks gleizados (Zg).

Site ID	Starting Year	Ending Year	Length of Record (years)	Sampling rate	Hydrologic Soil Group	Well use	Mean Piezometric Level (meters)
PT GW 01	1989	2018	30	M	Zg, Bh, Je	Observation	-0.10
PT GW 02	1989	2018	30	M	Zg, Bh, Je	Observation	-10.86
PT GW 03	1989	2018	30	M	Po	Observation	23.03
PT GW 04	1989	2018	30	M	Po	Observation	50.40
PT GW 05	1989	2018	30	M	BCA	Observation	12.12
PT GW 06	1989	2018	30	M	BCA, Po	Observation	-2.85
PT GW 07	1989	2018	30	M	BCA, Po	Observation	3.23
PT GW 08	1989	2018	30	M	BCA	Observation	6.56
						Aquifer Average:	10.19

Precipitation data for California were obtained from meteorological stations within NOAA's Global Historical Climatology Network (NOAA, 2020c) as seen in Appendix IV. These data were downloaded from NOAA's National Climatic Data Center, Climate Data Online (CDO) portal. For Portugal, ERA5-Land data (Copernicus

Climate Change Service (C3S), 2019) was accessed through the European Center for Medium-Range Weather Forecasts (ECMWF) as provided in Appendix V. Total precipitation data was downloaded from the Copernicus Climate Change Service (C3S) Climate Data Store. Reanalysis data from ERA5-Land provides a spatial resolution of ¬9 km and is validated by ground observations, offering a robust time series when compared to dispersed meteorological station records in Portugal. Precipitation data was downloaded as daily measurements thus, monthly sums were computed to maintain consistency with the frequency of climate indices and groundwater level measurements from SNIRH and NOAA.

Each groundwater well and precipitation record was given a site ID that includes the following details: the aquifer name (CA, California Coastal Basins; PT, Portugal's coastal aquifer system), the type of record (GW, groundwater; PR, precipitation), and relative location in the form of an ordinal number representing its position in a west to east or north to south ordering of sites across the aquifer system. The location number also indicates which sites are in close proximation. For example, CA GW 01 and CA PR 01 are both the northernmost sites in the CA aquifer, whereas CA GW 08 and CA PR 08 are sites that are the furthest south in the aquifer system.

2.2 Time Series Analysis

After pre-processing, analysis of the various time series is conducted using the USGS Hydrologic and Climatic Analysis Toolkit (HydroClimATe) and MATLAB. HydroClimATe is a computer program which automates the use of several objective methods for assessing relations among hydrologic and climatic time series with spatial-temporal variability (Dickinson et al., 2014). Some of the functions in HydroClimATe include data pre-processing, Singular Spectrum Analysis (SSA), time series regression and correlation. Here, HydroClimATe is used to perform the SSA, and calculate lag correlations.

2.3 Pre-processing

Standard pre-processing steps such as treating outliers, interpolating missing values were carried out with a custom script in Python, while detrending and normalization were conducted in HydroClimATe before the analysis.

To have consistent monthly observations of piezometric level, the original time series were resampled to a monthly value and interpolated using quadratic

interpolation. Quadratic interpolation is preferred over linear interpolation here as its approximation is more appropriate for variables with larger variations. Outliers were identified with a z-score and were replaced with a rolling average of six months. Any remaining data gaps were filled with a rolling average of six months. For some records (CA GW 01, 02, 03 and 06) the same methods were applied at a quarterly sampling rate due to gaps exceeding 6 months, which could have produced synthetic records if interpolated at a monthly value. Precipitation time series were converted into a cumulative departure series using a monthly mean, to allow comparison with groundwater level which is a cumulative departure. To maintain low frequency signals, such as PDO a linear curve fit was subtracted from the time series to obtain the residuals of the interpolated time series. Lastly, the detrended time series were standardized by the historic mean to form normalized departures (unitless) which allows for statistical comparisons among various data types.

2.4 Singular spectrum analysis

SSA is a form of principal component analysis used to examine long-term variations in noisy time series, and is often applied to hydrologic time series (Enfield et al., 2001; Gurdak et al., 2007; Hanson et al., 2006; Kuss & Gurdak, 2014; McCabe et al., 2004). Dominant frequencies representing the maximum possible amount of covariance are determined in a lagged covariance matrix by employing eigenanalysis (Broomhead & King, 1986; Vautard et al., 1992). These frequencies are often called the temporal empirical orthogonal functions (T-EOFs) and the way in which the T-EOFs change through time is described by the temporal principal components (T-PCs) (Dickinson et al., 2014). When combined linearly, the T-EOFs and the T-PCs form reconstructed components (RCs) which refashion oscillatory modes, noise, and phase information in hydrologic time series. Significant components contribute more variance than that from noise background and are listed in order of decreasing variance and are labeled with a sequential number starting at 1 (Ghil, 2002; Vautard et al., 1992). Typically the first 10 RCs (1 through 10) are assessed with hydrologic time series because they often account for nearly 100% of the variability in the original time series (Hanson et al., 2004).

HydroClimATe is used to compute SSA of the normalized departure time series of groundwater level and precipitation datasets in this study. To determine which RCs are statistically significant against a red-noise null hypothesis, a Ghil and Mo

significance test is applied (Ghil & Mo, 1991). Significance can also be determined by visual inspection of the spectrum and error bars. For the groundwater time series, composite RCs were created by taking only the statistically significant RCs and grouping and summing them together according to the climate variability period ranges of interest: 15-30 years (PDO-like), 6-10 years (NAO-like), 2-7 years (ENSO-like), 2-6 years (EA/SCAND-like) and <1-4 years (PNA-like).

2.5 Continuous wavelet transform

The continuous wavelet transform (CWT) is useful to analyze non-stationary signals with variability in both amplitude and frequency, as it exposes dominant modes of variability with time evolving frequencies. CWT is well suited to detect localized or sporadic events. As defined by Daubechies (1990), CWT is the convolution of the signal with a scaled and translated version of the wavelet function. Here, the method is implemented in MATLAB using the Morlet wavelet described in Torrence & Compo (1998). The Morlet wavelet is advantageous due to the equivalence between scale and the equivalent Fourier period (Sang, 2013). Once computed, the CWT spectrum illustrates the temporal distribution of the power (variance) as a function of the period (scale), over the 30 years of analysis. The spectrum is normalized by $1/\sigma 2$, where $\sigma 2$ is the variance of the time series. The 5% significant levels, indicated by white contours, are computed using a Chi-square test against a red noise spectrum as the null hypothesis. The cone of influence indicated by black lines delimits the regions where results are less dependable.

2.6 Wavelet coherence

The wavelet coherence (WTC) is a powerful method used to identify common time-localized oscillatory behaviors in two time series. Some applications involve identifying and characterizing similar patterns in two time series, of which one time series can drive or influence the other, or an unobserved mechanism can influence both time series. For nonstationary time series analysis, where the frequency content changes over time, a correlation of coherence in the time-frequency plane is measured. WTC is similar to a localized correlation coefficient between two continuous wavelet transforms (CWT) (Torrence & Webster, 1998). The algorithm described by Grinsted et al., (2004) is used to compute a 95% confidence level of the WTC. Phase relationships are shown by arrows in the regions of high coherence. Orientation of the

arrows, illustrating the phase of the wavelet cross-spectrum indicate the relative lag between components. Horizontal arrows pointing to the right show in-phase relationships or positive correlation, while arrows pointing to the left are out of phase and their correlation is negative (Fu et al., 2012). Causality between the two time series can be implied in regions with large common power and consistent phase relationships (Torrence & Webster, 1998).

2.7 Lag correlations

When a system has a delayed response to a forcing, it is useful to calculate correlation coefficients which indicate the strength of association between two variables at different time shifts (Helsel & Hirsch, 1992). Here, lag correlations were performed between precipitation and groundwater level where precipitation is the independent (causal) variable and groundwater level is the dependent (responsive) variable. Linear correlation coefficients between these cumulative departures are computed using a two-tailed significance t-test at the 95% confidence level. Criteria to conduct lag correlations are that both variable records have the same length along with the same starting and ending dates. The maximum forward and backwards lags between two time series can be specified in HydroClimATe, which is useful if there is an *a priori* expectation that a lag cannot be greater or less than a certain amount (Dickinson et al., 2014). Here, HydroClimATe is used to determine the lag of maximum correlation.

When examining the relation between precipitation and groundwater, all correlations are positive, thus only forward lags are considered in this study. This is supported by the assumption that increased (decreased) precipitation always leads to increased (decreased) groundwater levels. Final lag correlation results include the maximum lag correlation coefficient (unitless) for correlations that are statistically significant at a 95% confidence level.

2.8 Computation of a Groundwater Sustainability Index

Sustainability Indices can be useful to quantify objective groundwater management strategy outcomes, particularly across regional scales and when local groundwater budget data is not readily available. Previous studies have used performance indicators to evaluate surface water systems and their application to groundwater is expanding to address water availability concerns (Ferguson &

Gleeson, 2012; Hirata et al., 2007; Mays, 2013; Peters et al., 2005; Van Camp et al., 2010; Vörösmarty et al., 2000; Vrba et al., 2006; Wada et al., 2010). Here, a groundwater sustainability index (GSI) is computed using performance indicators and groundwater level records applying methods from Thomas (2019), where REL refers to reliability, RES refers to resilience and VUL refers to vulnerability. In this study, a point-wise approach is employed to provide an index-per-piezometer, rather than a system wide classification which would require the analysis of numerous groundwater records per aquifer, currently outside of the scope of this work.

2.8.1 Performance Indicators

Typically, in hydrology performance indicators are applied using weighted, multi-objective approaches to characterize stochastic performance metrics of water resource systems (Thomas et al., 2017). Performance metrics are classically used when the relation between demand and storage is given (Hashimoto et al., 1982; Loucks et al., 1981). Here, a weighted statistical indices scheme is applied (Loucks, 1997; Mays, 2013) to the groundwater level after removing a monthly climatology. While satisfactory and unsatisfactory conditions are subjective, a threshold is applied as a function of the normalized groundwater level time series; where a positive groundwater index is satisfactory, and a negative index is unsatisfactory. Following the method proposed by Thomas et al. (2017), a 3-month condition is applied to the groundwater index by conducting a performance metric analysis on a 3-month smoothed average.

2.8.2 Reliability

Reliability is closely linked to aquifer storage and following Loucks (1997) and Mays (2013) reliability is quantified as:

$$\mathrm{REL} = \frac{\text{number of satisfactory conditions}}{\text{total number of conditions}} \tag{1}$$

Where reliability is defined by how often a system fails (Hashimoto et al., 1982). When applied to coastal aquifer basins, reliability represents the likelihood that aquifer storage falls below a certain threshold.

2.8.3 Resilience

Resilience reflects changes in storage that may be influenced by precipitation and recharge relationships. Following Loucks (1997) and Mays (2013), resilience is quantified as:

$$\mathrm{RES} = \frac{\text{number of times a satisfactory condition follows an unsatisfactory condition}}{\text{total number of unsatisfactory conditions}} \qquad (2)$$

Resilience is an indicator for how quickly a system returns to a satisfactory state after an unsatisfactory state (Hashimoto et al., 1982). As monthly climatology is removed from the groundwater times series, seasonality is therefore removed. Resilience is an important indicator for how an aquifer might return to normal or satisfactory conditions after prolonged droughts or over abstraction.

2.8.4 Vulnerability

Vulnerability is defined as a probabilistic measure that accounts for the extent and magnitude of failure (Hashimoto et al., 1982), where failure represents an unsatisfactory condition. Accounting for both the magnitude of the event $s_j = GDI_j$ and the probability of the severity of the magnitude (e_j), during the study period, *F*, is necessary where:

$$\mathrm{VUL} = \sum_{j \in F} s_j \, e_j \qquad (3)$$

This computation can emphasize the influence of extreme events in groundwater storage, such as drought conditions which may be detected in the time series.

2.8.5 Sustainability Index

Finally, a sustainability index (SI), which is a function of the performance indicators (Mays 2013), may be calculated given:

$$\mathrm{SI} = \mathrm{REL} \times \mathrm{RES} \times (1 - \mathrm{VUL}) \qquad (4)$$

3 RESULTS

3.1 Visualization of piezometric level time series

Several inferences can be gained through the visualization of piezometric data. Here, the evolution of 30 years of piezometric level time series are plotted as a heat map (Figures 6 and 7), illustrating variability, heterogeneity across aquifers throughout the water year, and the spread of droughts. Blue cells represent higher groundwater levels while red cells represent the recording of lower groundwater levels.

Groundwater observation points in northern California, at site CA GW 01 display a consistent yet distinct wet and dry season (Figure 6). CA GW 02 clearly illustrates the drought starting in 2015, whereas CA GW 03 captures the anomalously wet year in 1998-99. Site CA GW 04 maintains consistent groundwater levels throughout the record until 2015. The gradual decline in groundwater level is captured at sites CA GW 05 and 08 from 2005 onward. CA GW 06 and 07 are plotted independently due to the selected date range and show episodes of low groundwater level and years of heavy precipitation around 1998 and 2006. The time series of CA GW 07 preserves the most normal and expected piezometric response to annual and multi-annual hydrologic cycles.

PT GW 01 and 02, located in the same aquifer in northern Portugal behave similarly, although PT GW 01 appears to be more sensitive to drying trends from 2002 through 2012 (Figure 7). PT GW 03 and 04 also contain similar patterns of interannual variability, following an expected response to hydrological cycles. Anomalously low groundwater levels in 1994-95 are well preserved in the records at sites PT 05, 06 and 07 in the Algarve, and coincide with a strong drought (Figure 3). Piezometric levels are consistently low at PT GW 08, aside from specific precipitation events in 1990, 2003 and 2010.

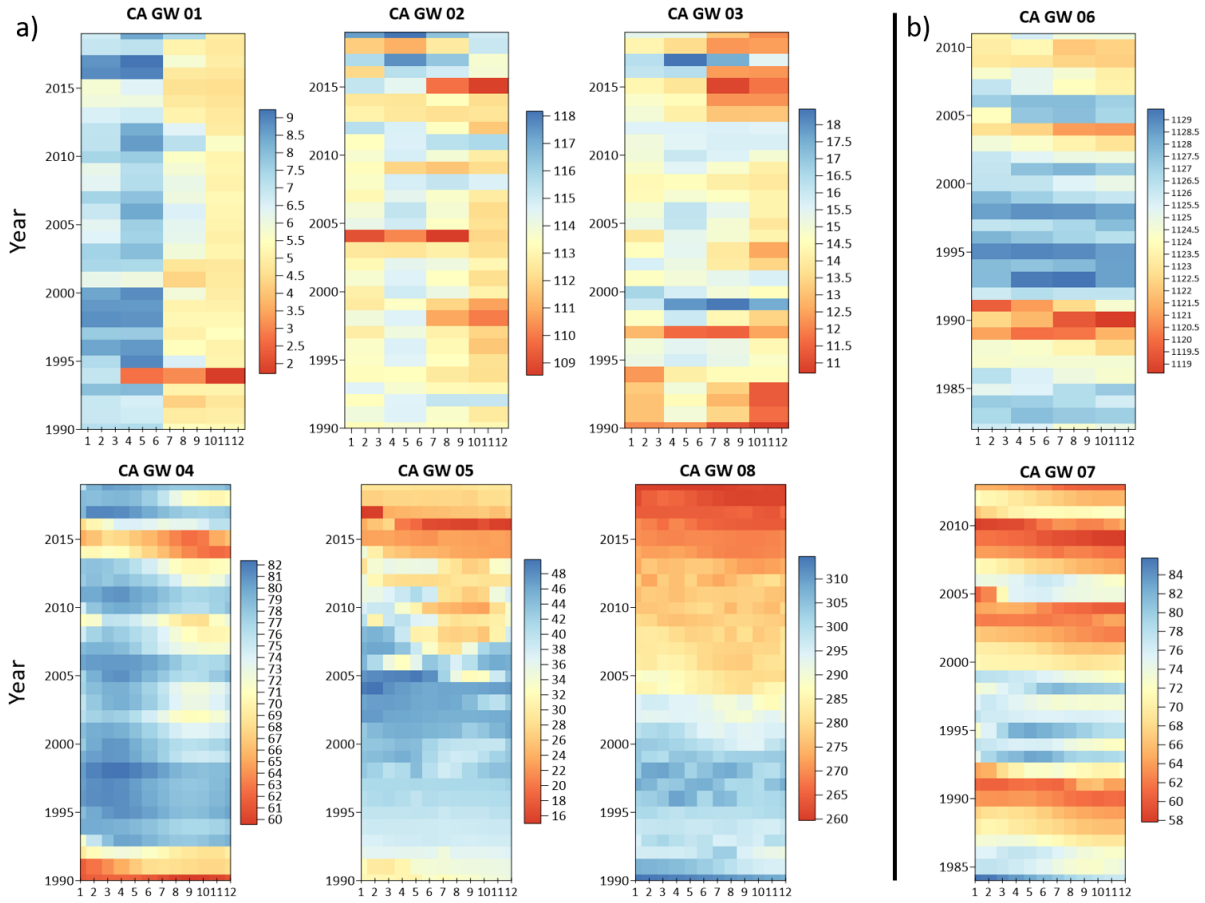

Figure 6. 30-year time series spanning a) 1990-2019 and b) 1982-2011 at CA GW 06 and 1984-2013 at CA GW 07 of piezometric level evolution from selected groundwater observation points within the California Coastal Basins aquifers system.

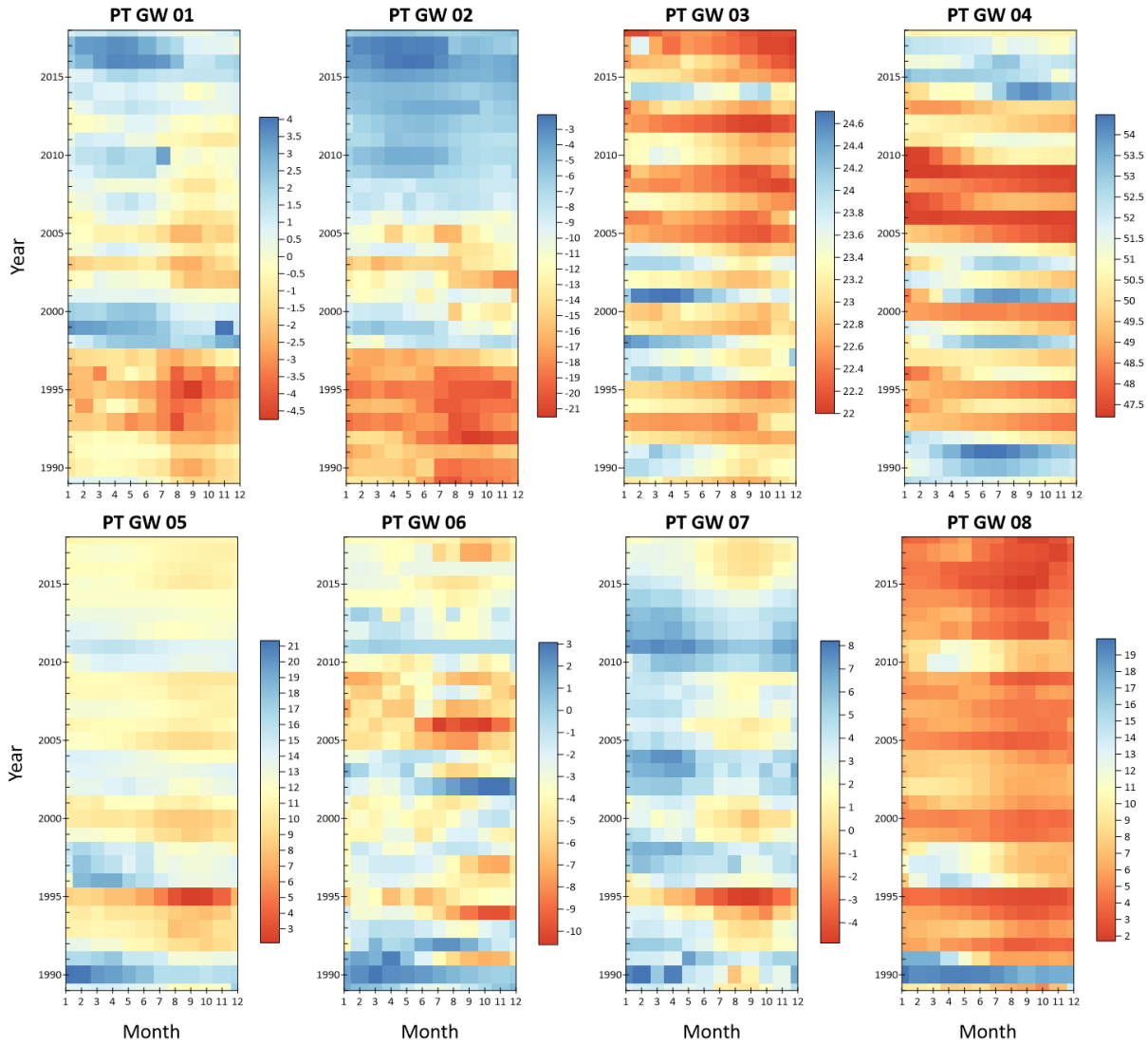

Figure 7. 30-year time series (spanning 1989-2018) of piezometric level evolution from selected groundwater observation points in Portugal's coastal aquifer system.

3.2 Percent variance of climate variability signals in groundwater levels

Results of the SSA show that all groundwater level time series contain statistically significant oscillations, which are potentially related to the PDO, ENSO, and PNA in California and NAO, EA and SCAND in Portugal. These oscillations are determined by the window length of the SSA. The window length must be wide enough to contain the oscillatory component of interest, as it sets the dimension of the lag autocorrelation matrix to be constructed and diagonalized by SSA (Dickinson et al., 2014; Vautard et al., 1992). Variability (% variance) of individual groundwater level reconstructed components (RCs) are plotted in Figures 8 and 9.

In California, the largest amount of groundwater level variance (36-77%) as shown in Table 6, at sites 04, 05, 07 and 08 have signals consistent with PDO periodicities (15-30 year cycles). Although PDO-like signals account for the largest amount of variance, it was only detected at these four sites. Granted, the PDO's 30-year frequency is equal to the record length analyzed, therefore statistically significant 30-year signals may not be fully identified due to the limited length of the data records. The second largest amount of variance in groundwater (11-66%) is consistent with PNA periodicities (<1-4 year cycles). PNA oscillations incorporate both a seasonal (0.5-year) and annual (1-year) signal, which may be accountable for the significant percent variance across all groundwater records in California. The next largest amount of variance in groundwater time series (4-63%) have modes of variability consistent with ENSO (2-7 year) cycles.

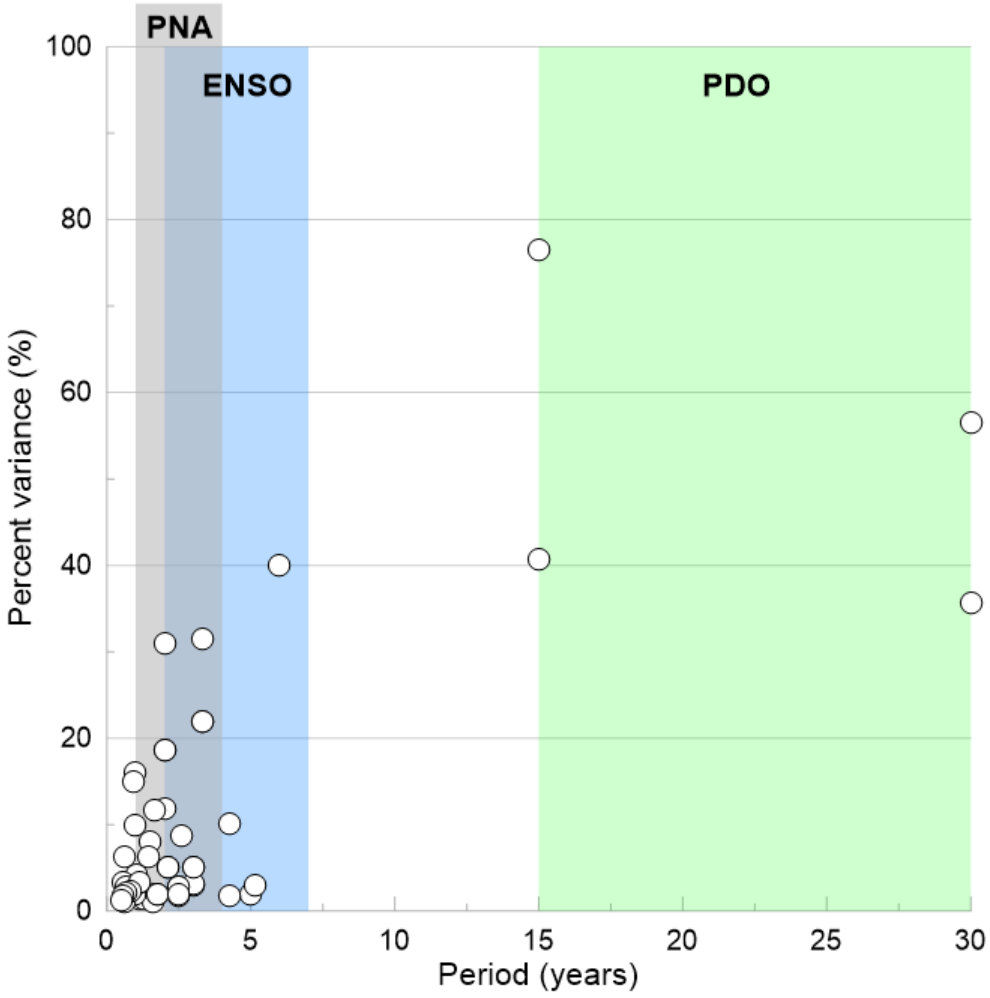

Figure 8. Percent variance (%) and period (years) of individual groundwater reconstructed components (RCs) in the California Coastal Basins aquifers.

Table 6. Statistically significant composite reconstructed components (RCs) for the California Coastal Basin aquifers system that fall within the period of the three climate variability modes of interest (PDO, ENSO, and PNA). A dashed line indicates no significant RC for the specified climate variability mode.

Site ID	PDO			ENSO			PNA		
	RCs	Average Period (years)	Percent Variance (%)	RCs	Average Period (years)	Percent Variance (%)	RCs	Average Period (years)	Percent Variance (%)
CA GW 01	-	-	-	3,7	3.88	12	3,4,5,8,9	1.26	27
CA GW 02	-	-	-	1,2	2.67	41	1,2,3,4,5	1.76	66
CA GW 03	-	-	-	1,2	2	31	1,2,7	1.53	38
CA GW 04	1	30	36	2,3,6,7	4.38	46	4,5,6,7,8,9,10	1.74	22
CA GW 05	1	30	57	5,6,7	3.10	7	3,4,5,6,8,9,10	1.47	20
CA GW 06	-	-	-	1	5	63	2,3,4,5	0.87	35
CA GW 07	1	15	41	3,4,5	3.26	18	4,5,6,7,8,9,10	1.77	13
CA GW 08	1,2	15	77	5,8,9	3.09	4	3,4,6,7,8,9,10	1.59	11

In Portugal, the largest amount of variance in groundwater level (17-63%) have signals consistent with NAO periodicities (6-10 year cycles), yet it is spatially variable across the country (Figure 9). The highest percent variance of RCs consistent with the NAO frequency were present at sites PT GW 01 and 02 (61-63%), PT GW 05 (54%) and PT GW 07 at (54%), as shown in Table 7. However, the NAO signal is most evident in southern Portugal, accounting for 45-54% (50.75% on average) of groundwater variability. NAO's longer 10-year frequency was pertinent at sites PT GW 01 and 02 and the 7.5-10 year frequency was dominant in the aquifers of the Algarve (PT GW 05, 06, 07 and 08), while the 6-year frequency only appeared at PT GW 03 and 04. The second largest amount of variance in groundwater level (8-54%) has modes of variability consistent with EA/SCAND (2-6 year cycles). The EA/SCAND-like patterns were most evident at sites PT GW 03 and 04 accounting for 46-54% variance and were inconsequential for the other aquifers. As the EA and SCAND patterns are often indistinguishable, they are grouped for the purposes of the SSA. Their joint impact on variance is 33.25% on average in the north and 13.25% on average in the south.

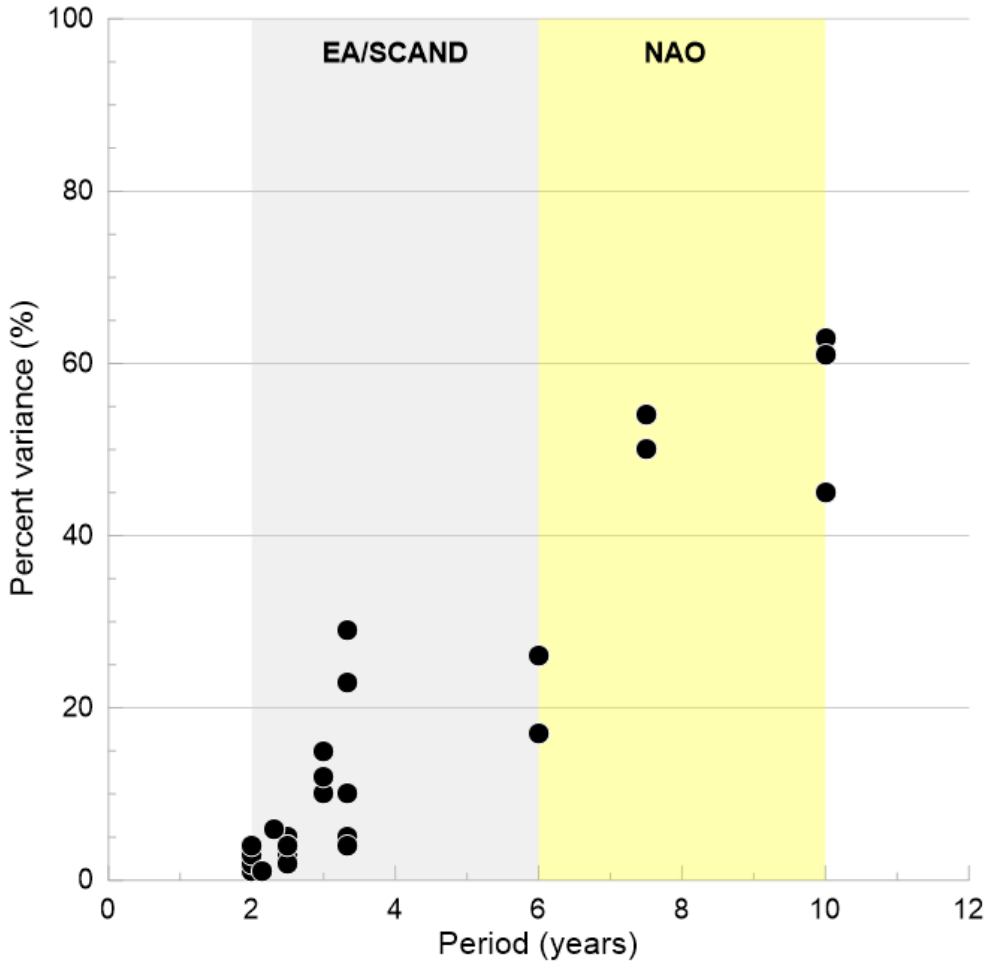

Figure 9. Percent variance (%) and period (years) of groundwater reconstructed components (RCs) in Portugal's coastal aquifer system.

Table 7. Statistically significant composite reconstructed components (RCs) for Portugal's coastal aquifer system that fall within the period of the three climate variability modes of interest (NAO, EA, and SCAND).

	NAO			EA/SCAND		
Site ID	RCs	Average Period (years)	Percent Variance (%)	RCs	Average Period (years)	Percent Variance (%)
PT GW 01	1,2	10	63	5,6,7,8	2.63	14
PT GW 02	1,2	10	61	3,4,5,8	2.63	19
PT GW 03	2	6	17	2,3,4	4.22	46
PT GW 04	2	6	26	2,3,4,5,6	3.46	54
PT GW 05	1,2	7.5	54	6,7,8	2.61	12
PT GW 06	1,2	10	45	3,4,7	2.67	19
PT GW 07	1,2	7.5	54	6,7,8	2.66	8
PT GW 08	1,2	7.5	50	3,7	2.92	14

3.3 A comparison of percent variance of climate variability signals in groundwater levels in California and Portugal

Here, the percent variance of composite groundwater RCs are plotted for both California and Portugal, as shown in Figure 10 in order to make cross-continental, spatial and climatic comparisons of groundwater variability in these Mediterranean climates. The high frequency signals account for the most detectable variability of groundwater level in California and Portugal. These patterns overlap with an average period of 1.5 years for PNA, 3 years for EA/SCAND, 3.4 years for ENSO and 8.1 years for NAO. EA/SCAND and ENSO, which have the most comparable average periodicity between the two regions, drive substantial variability (8-54%) in Portugal and (4-63%) in California. Although high frequency signals are visibly more abundant, the lower frequency patterns (PDO and NAO) account on average for 52.75% and 46.25% of groundwater variability, respectively. Additionally, higher frequency signals may be embedded or coupled with the lower frequency patterns. Results of the SSA presented similar periods (years) between ENSO-like and PNA-like signals, indicating interactions between the two systems. Likewise, in Portugal, NAO-like and EA/SCAND-like signals overlapped indicating an imprint of one system in the other.

Spatially, in Portugal groundwater RCs with the highest variability were predominantly in the north, which aligns with the precipitation regime for the region. In contrast, California groundwater RCs with >50% variability were predominantly in southern and central California. Results of the SSA show that climate variability signals are captured in the response of groundwater level in both California and Portugal.

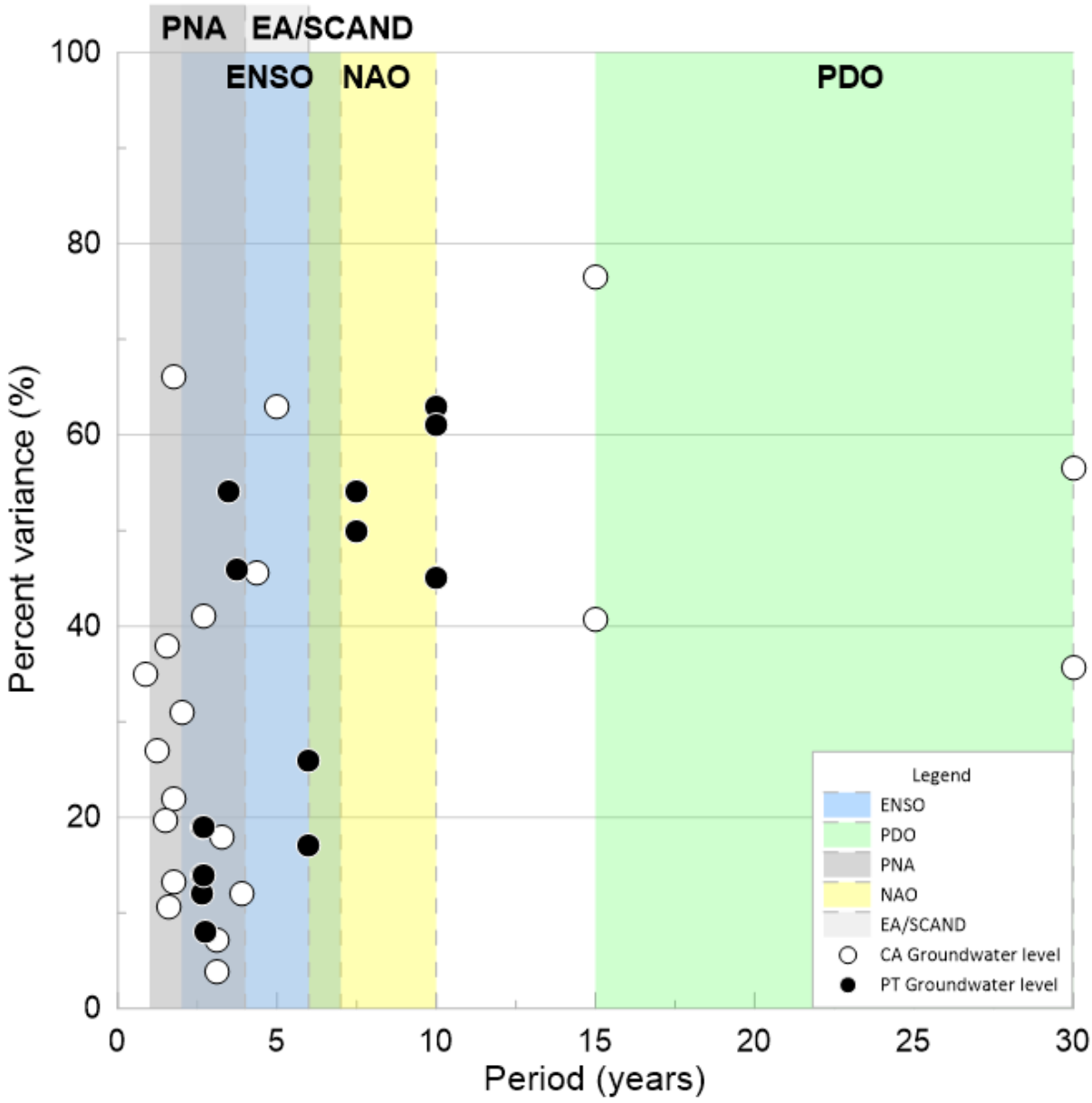

Figure 10. Percent variance (%) and period (years) of composite groundwater reconstructed components (RCs) in California Coastal Basins aquifers and Portugal's coastal aquifer system.

3.4 Continuous wavelet transform of groundwater levels

The normalized wavelet power spectra of groundwater levels are computed using the continuous wavelet transform (CWT) method, as displayed in Figures 11 and 12. Each plot depicts the temporal distribution of the power (variance) of the time series as a function of period (years), over the 30 years of analysis, in a color scale that goes from blue (minimum) to brown (maximum). The 5% significance levels, computed using a Chi-square test against a red noise spectrum as the null hypothesis, are displayed as white contours. Black parabolic lines display the cone of influence

which delimits the regions where the edge effects, due to zero padding, make the results less reliable. The CWT power spectra can illustrate the evolution of significant oscillatory patterns temporally, which visually supplement the SSA results. Anomalous events, such as extreme wet and dry periods are also easily identified on the CWT spectra. Anomalously wet events appear in red, while anomalously dry periods are expressed by a lack of power in white or blue.

In California, anomalous wet precipitation events in 1998 and 2007 are evident in the groundwater records of nearly all sites, excluding site CA GW 06 where the strongest signal falls below the cone of influence, deeming it inconclusive. Groundwater records also display a dramatic division of pre and post 2005 hydroclimatic events (Figure 11). The strongest patches occur in the 4-8 year band in 2008 in central California at site CA GW 04, and 2002-2010 in southern California at site CA GW 07, which may be an indication of the known ENSO events from 2006-2013. Moreover, the significant patch at site CA GW 04 in the 4-8 year band corresponds with the dominant ENSO frequency of 5 years from the SSA. On a smaller scale, a 1-year annual cycle can be observed with consistency throughout sites CA GW 01, 02 and 03 presenting a representation of wet years and potentially a PNA signal.

In Portugal, all records illustrate prolonged statistically significant oscillations in the 4-8 year band (Figure 12). Sites PT GW 05, 06 and 08 show significant power (within the white contour) before 2005, which is accompanied by an expression of the 2004-2005 drought, clearly seen as a blue patch for periods less than 4. PT GW 03 and 04 has two dominant patches in the 4-8 year band both before and after 2004-2005. Aquifers in the Algarve (PT GW 05, 06, 07 and 08) have persistent multi-year patches in the 4-8 year band before 2005-6, with a prolonged lower frequency in the 8-16 year band at PT GW 06 and 07. This low frequency power band is interpreted with caution, as most of the signal falls below the cone of influence. The strongest small-scale patches of known anomalously wet years occur in 1990, 1996, 2000 and 2010.

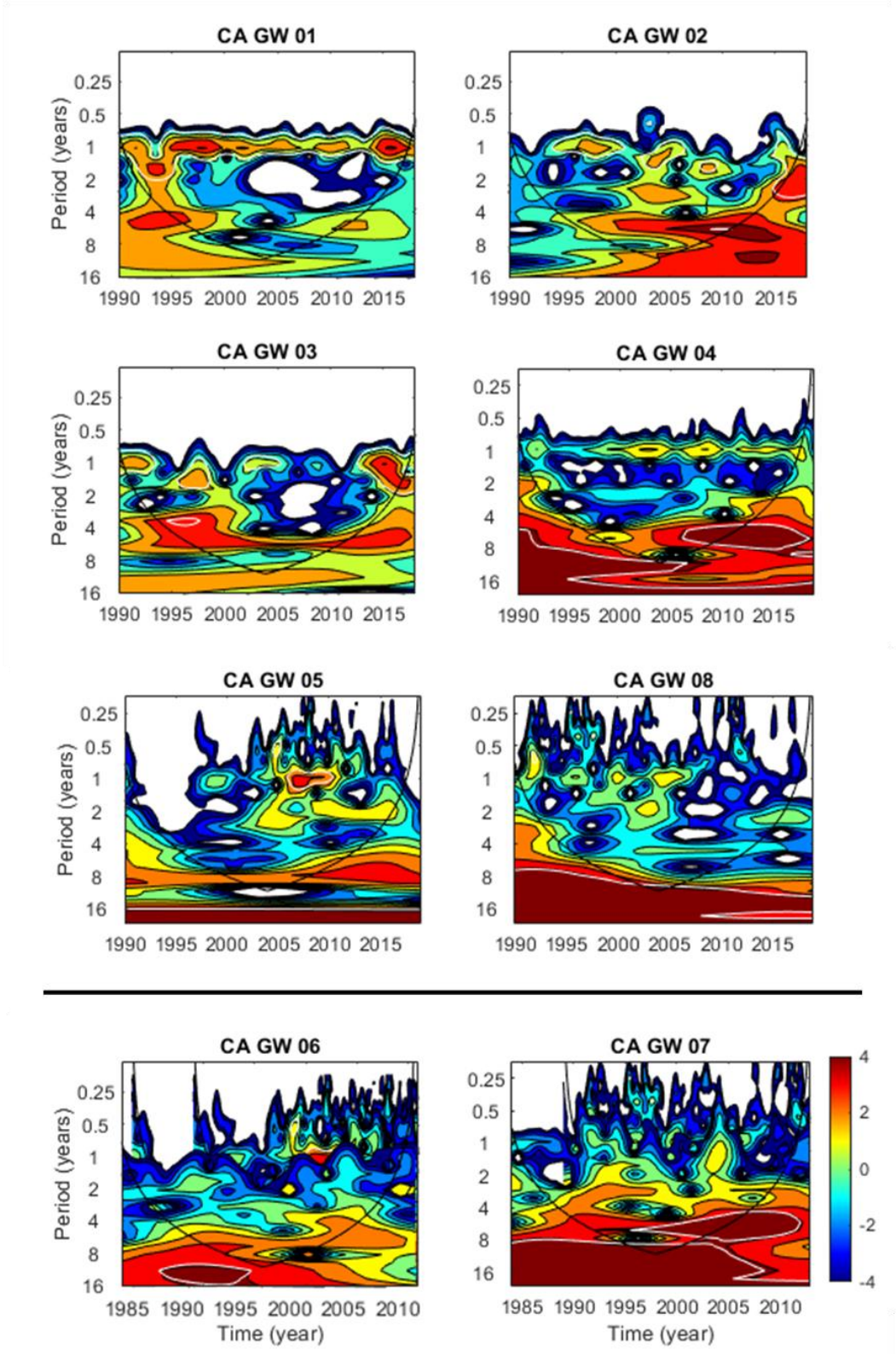

Figure 11. Wavelet power spectra of the California Coastal Basins aquifers system computed using a Morlet wavelet and normalized by 1/O2. The white contours enclose regions that are of greater than 95% confidence levels. The black lines delimit the cone of influence, where zero padding has reduced the variance. CA GW 06 and 07 are plotted separately due to the different time range.

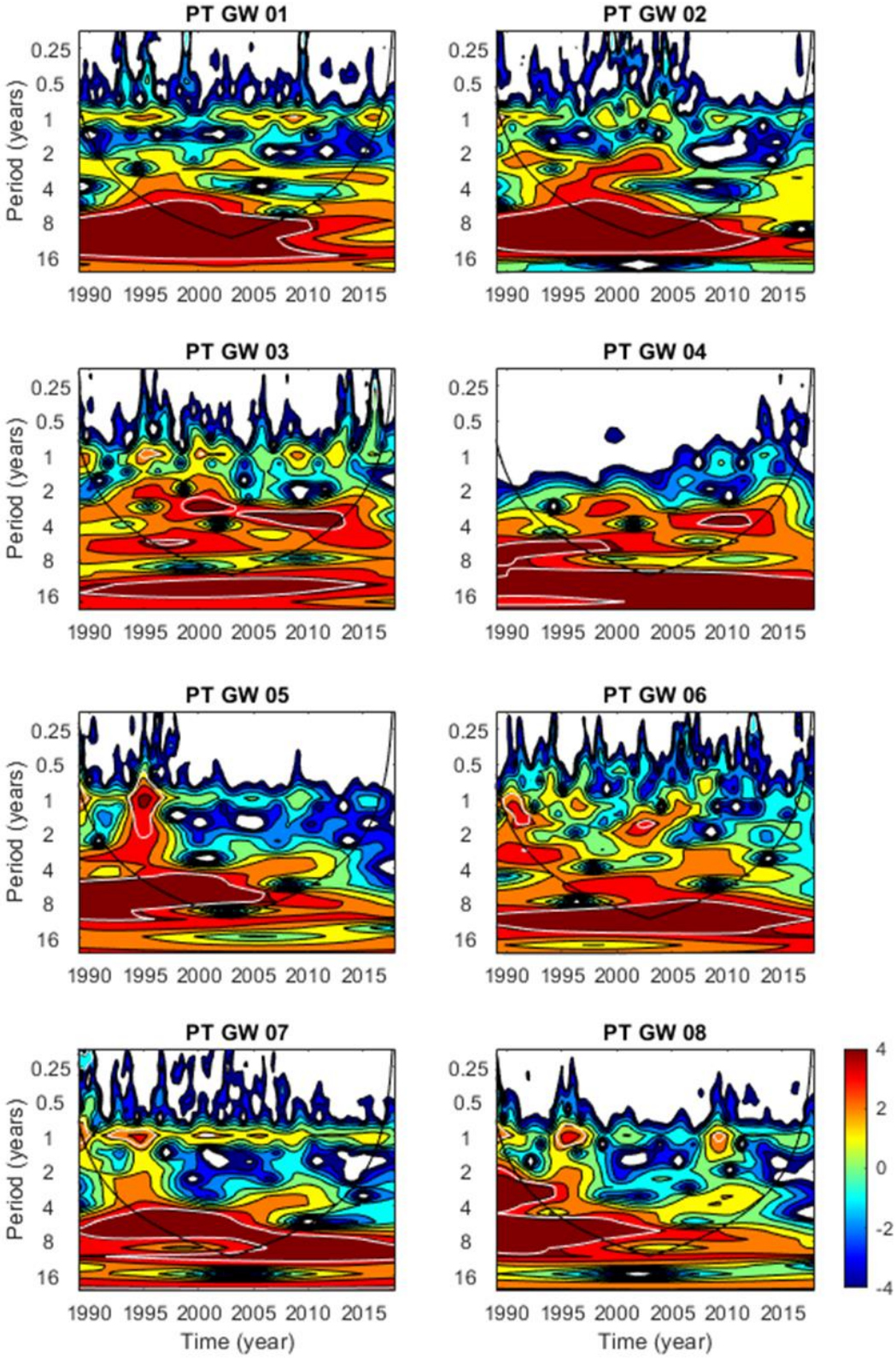

Figure 12. Wavelet power spectra of groundwater level records of coastal aquifers in Portugal computed using a Morlet wavelet and normalized by 1/O2. The white contours enclose regions that are of greater than 95% confidence levels. The black lines delimit the cone of influence, where zero padding has reduced the variance.

3.5 Coherence between climate indices and groundwater levels

In order to relate extreme hydroclimatic events and climate variability indices, yellow vertical lines marking major droughts in California (1987-1992, 2001-2002, 2007-2009, and 2012-2016) (USGS Water Science Center, 2020) and Portugal (1992, 1995, 2004-2005, and 2017) (IPMA, 2020) (Figure 3) have been superimposed onto the WTC plots (Figure 13-18). Sustained drought in California, lasting 5-6 years are coded in orange which signify periods where >50% of the state was in at least “extreme drought”, as defined by the U.S. Drought Monitor scale (United States Drought Monitor Drought Classification, 2020). These lines of episodic drought segment the WTC plots into windows with discrete coherence patterns. Figure 13 through 18 are organized to display the impact of each climate pattern (each column) at each site (each row) sequentially from north to south. Coupling between different climate patterns are identified by the synchronization of coherence patches across patterns at specific periods. Groundwater levels are analyzed in the northern and southern regions of California and Portugal to provide a spatially diverse set of hydrogeologic conditions.

Despite localized hydrogeological differences, every piezometer in California expresses coherence with the ENSO signal, although significant patches of both PDO and PNA are present (Figures 13 and 14). ENSO’s strongest patches occur in the 2-4 year band, consistent with the SSA periodicities. The high coherence with ENSO in the 4-8 year band at sites CA GW 01 and 03 (Figure 13) is visibly coupled with the high coherence of PDO. These two sites present a clear example of coupling between ENSO and PDO within these periods. Additionally, low frequency climate signals such as PDO are more apparent in groundwater observation points located in northern and central California, while high frequency variability patterns are more evident in southern California. These findings align with the spatial distribution of the climate pattern paths, PDO impacting northern California and the Pacific Northwest and the latitudinal shift of the primary storm track during El Niño, increasing above average precipitation in southern California. All groundwater records in California capture an extreme precipitation event linked to El Niño during the 1997-1998 water year which resulted in record rainfall. This anomalously wet year is most obvious at site CA GW 07 throughout the 0.25-4 year band. Scientific and journalistic sources recorded precipitation values in Los Angeles, in southern California that were double (707 mm) of that from the previous annual average (NOAA, 2019). The 2015-2016 El Niño, although it was also one of the strongest storm events may not be detectable due to

its proximity to the cone of influence on the right limit of the time series WTC plot. Additionally, extreme precipitation events may flow as run-off over the land surface when the infiltration capacity is quickly exceeded. Such rainfall may never recharge the groundwater and thus may not be captured in the groundwater level record. Impacts of the 2007-2009 drought are apparent in several PDO and groundwater coherence records, particularly CA GW 02, 03 and 04 where a tapered statistically significant patch in the 4-8 year time band gradually expands around 2010, indicating the rise in groundwater level and graduation from a drought period. Most of the significant patches predominantly occur outside, or on the edge of these drought lines.

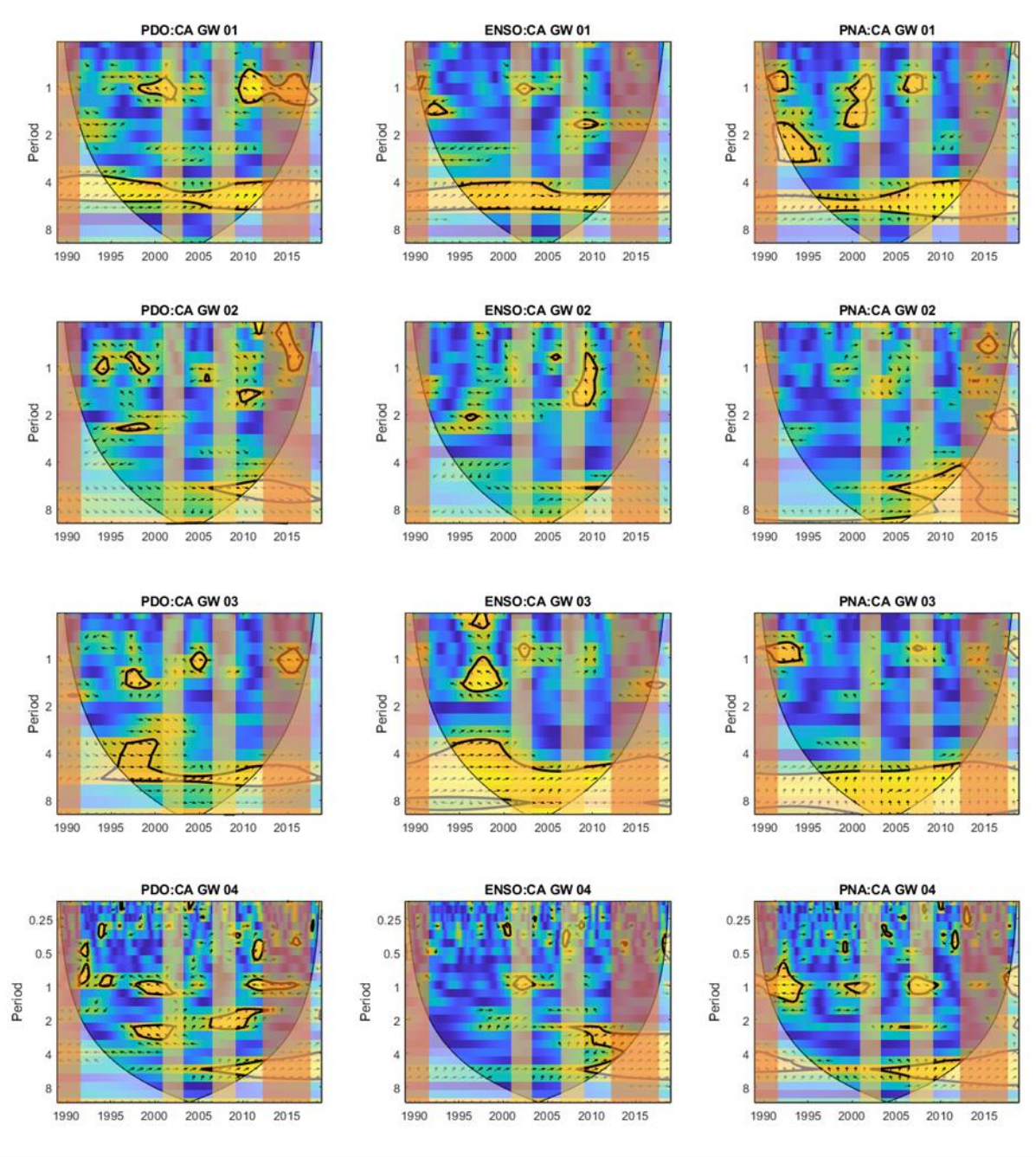

Figure 13. Wavelet coherence of groundwater time series in the California Coastal Basins aquifers system. The thick black lines are the 5% significance level and faded "or less intense" colors indicate the cone of influence. Horizontal right-pointing (left-pointing) arrows indicate the in phase (anti-phase) relationships. Vertical yellow and orange lines indicate the major and prolonged droughts, respectively (United States Drought Monitor Drought Classification, 2020).

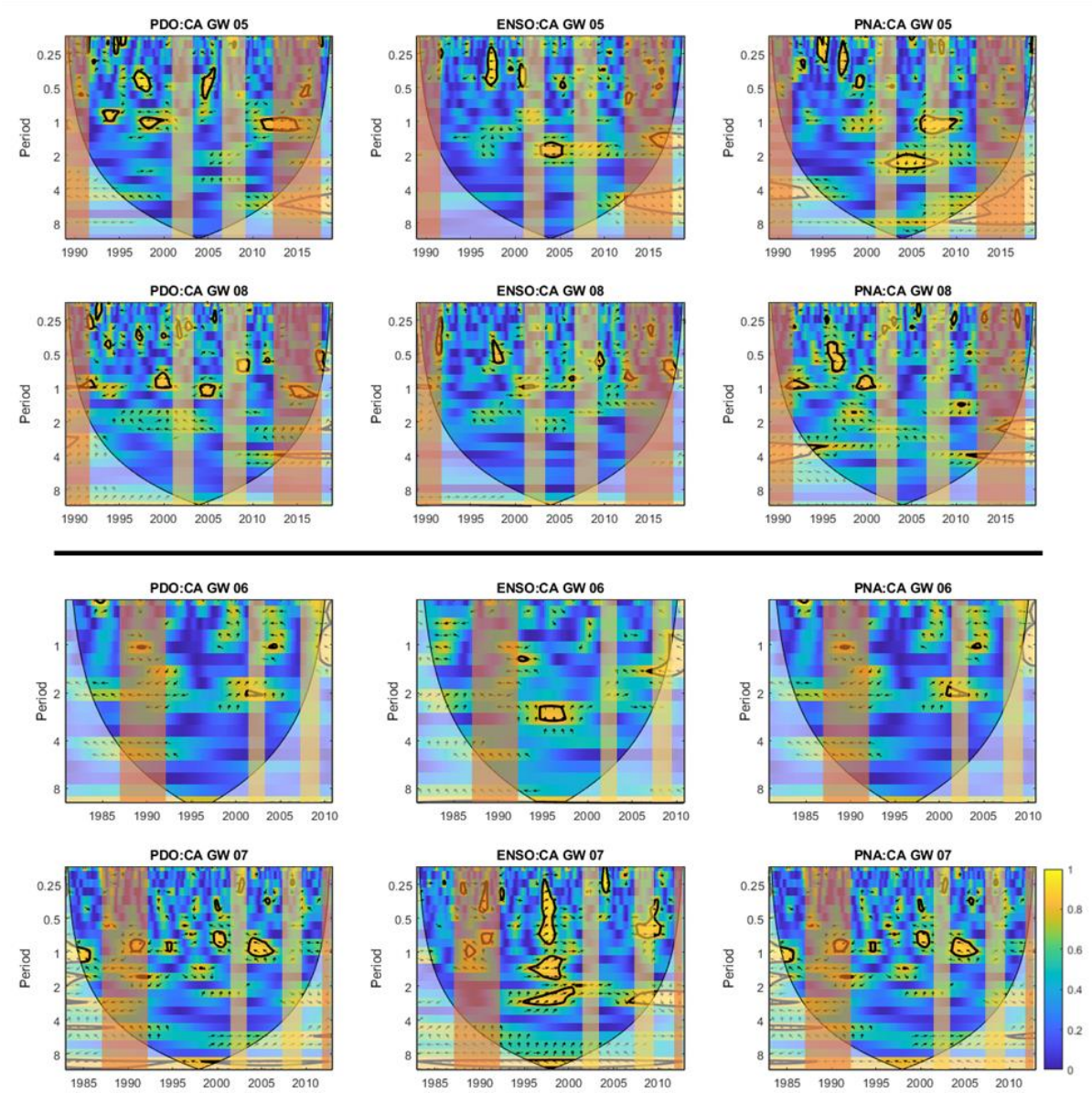

Figure 14. Wavelet coherence of groundwater time series in the California Coastal Basins aquifers system (continuation from Figure 13). Note that CA GW 06 and 07 have a different date range.

The NAO has a strong coherence with groundwater levels across the entire country of Portugal, with specific periods in the north (1-2 years) and the south (2-4 years and 4-8 years) (Figures 15 and 16). The EA's 2-4 year periodicity and the SCAND 4-8 year period have the most significant coherence throughout. Coherence patches of NAO with longer periods, exceeding 4 years are always in an anti-phase, thus NAO- is negatively correlated with groundwater level. As detailed in the introductory chapter, NAO- results in above average precipitation in southern Europe.

All groundwater records in the northern sector of Portugal exhibit a significant NAO patch with an in-phase relationship at sites PT GW 01 and 02 and an anti-phase relationship at PT GW 03 and 04 before 2002, at periods of 1-2 years, consistent with a NAO event occurring around 2000 (Figure 15). Significant synchronized patches appear to be linked to EA and SCAND around 2000 (in the 2-4 year time band) indicating interactions between these three modes. The groundwater level intensity at sites PT GW 01 and 02 associated with the SCAND pattern rapidly declines after the 2004-2005 drought event. The dominant pattern at PT GW 03 and 04 is SCAND which is consistent with the SSA RCs variability with the EA/SCAND frequency which persists from 1996-2012.

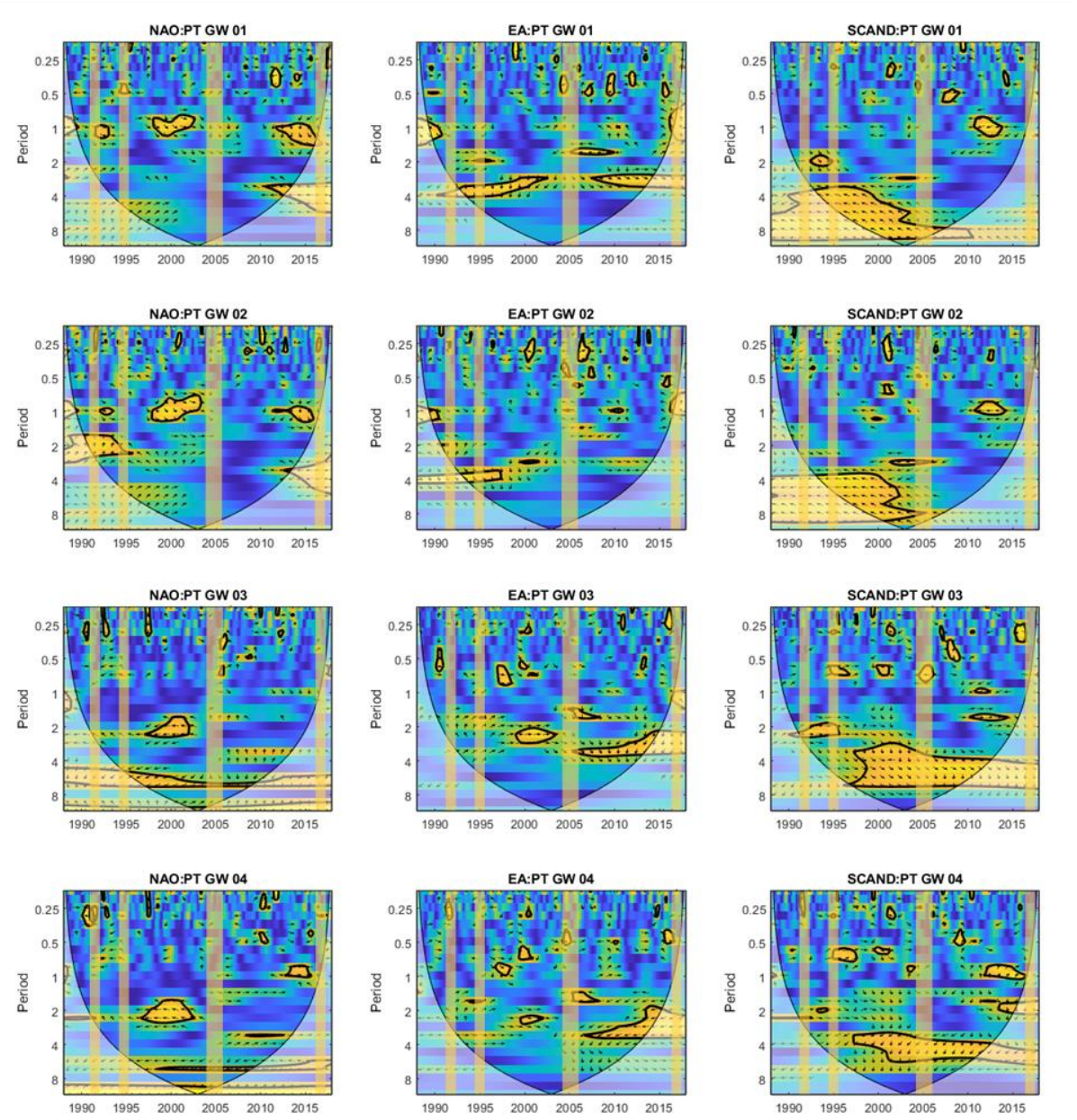

Figure 15. Wavelet coherence of time series in Portugal's coastal aquifers. The thick black lines are the 5% significance level and faded "or less intense" colors indicate the cone of influence. Horizontal right-pointing (left-pointing) arrows indicate the in phase (anti-phase) relationships. Vertical yellow lines indicate the years in which Portugal had the largest droughts (IPMA, 2020).

In the Algarve (Figure 16), coherence with the NAO appears in distinct patches in the 4-8 year band at PT GW 06 and 07 around 1996-2002, and in the 1-year band around 2014 across all records. At sites PT 03, 04, 06 and 07, all NAO patches in the 2-year and 4-8 year band are negatively correlated with groundwater levels, providing

evidence that NAO- drives an increase in groundwater level. Significant coherence with the EA is most evident after 2006, at periods of 2-4 years and the SCAND's strongest frequency is between 4-8 years. Overall, in Portugal the Scandinavian pattern occupies the largest significant patches of coherence, which often persist for over a decade in the groundwater record. While SCAND does have the broadest influence in Portugal, it is difficult to distinguish the SCAND frequency from that of the EA and NAO.

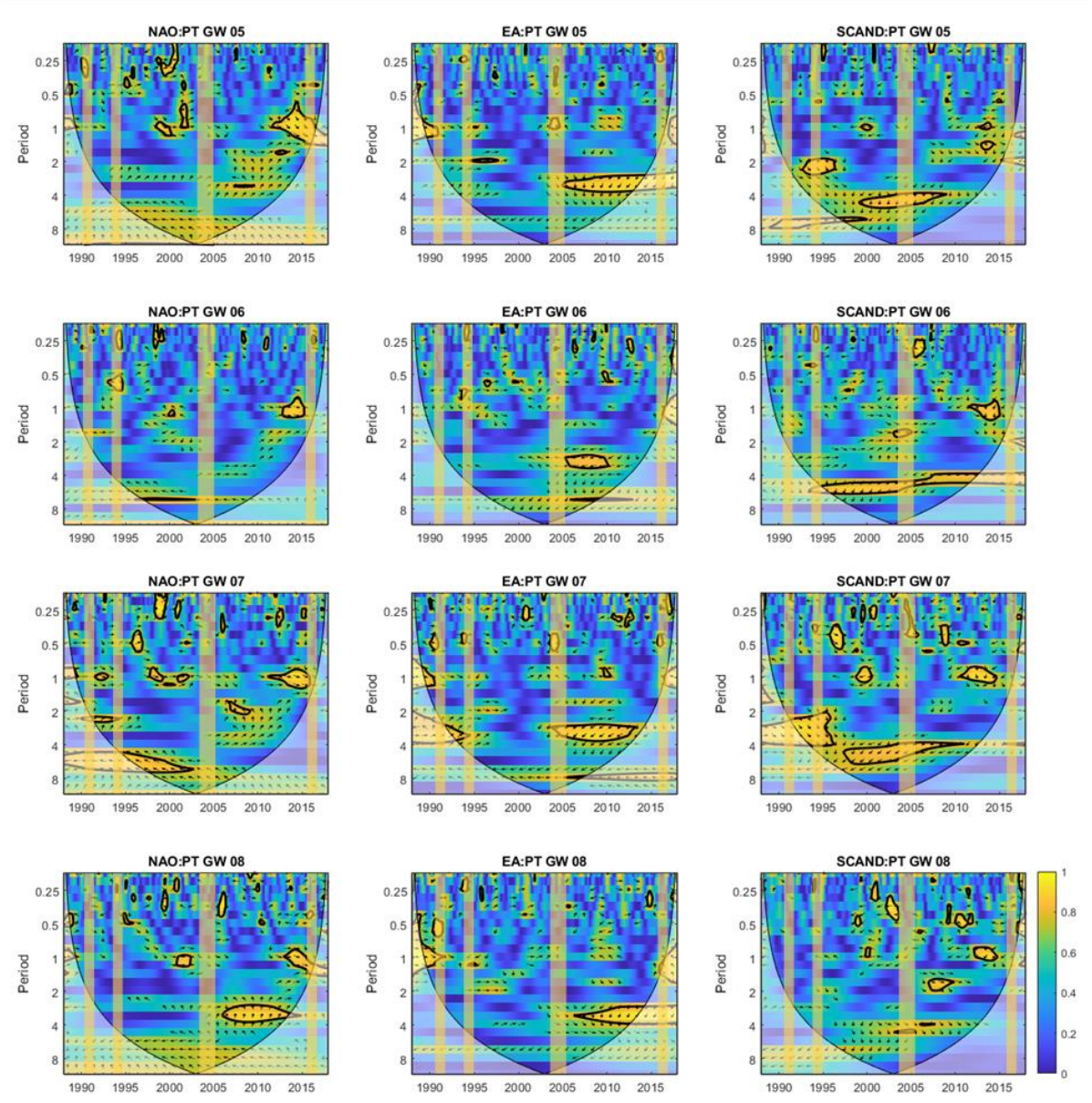

Figure 16. Wavelet coherence of time series in Portugal's coastal aquifers (continuation from Figure 15).

3.6 Lag correlations

Here, lag correlations were performed between precipitation and groundwater level to explore the temporal relationship between these two hydrological variables. Aquifer composition, lithology, depth, climate variability, and human interference are all factors that may influence the rate of direct recharge to the aquifer. The southern sector of both regions exhibits the strongest cross correlations at CA GW 05 (0.73), 06 (0.66) and 08 (0.70) and PT GW 05 (0.71), 06 (0.52), 07 (0.84) and 08 (0.60) (Table 8). SSA and wavelet results also identified the connection between El Niño (ENSO+) and NAO- increasing precipitation in the south, further supporting the significant recharge response in southern California and the Algarve. The sandy limestone composition and faulting in aquifers of the Algarve, enabling rapid recharge may also contribute to the strong correlation with precipitation. It is important to note that the lack of co-location between the precipitation records for Portugal (gridded reanalysis data) and the groundwater observation point can provide another potential explanation for lower correlations values.

Low or insignificant correlations in northern California may be attributed to an embedded human signal, as the use of wells CA GW 01, 02 and 03 are primarily for residential supply or for irrigation, and 04 is influenced by MAR. The correlation at site CA GW 03 (0.47) could relate to the shallow depth of 25 meters allowing this aquifer to be more responsive to precipitation events. The high correlation coefficient at PT GW 03 (0.67) in Portugal may be explained by the porosity, productivity, and multi-layered nature of this aquifer, in addition to the absence of human interference.

Table 8. Summary statistics of lag correlation coefficients (unitless) of precipitation and groundwater level correlations. N/A = Not statistically significant for lag correlations.

Site ID	Correlation coefficient of the max positive lag	Site ID	Correlation coefficient of the max positive lag
CA GW 01	0.33	PT GW 01	N/A
CA GW 02	N/A	PT GW 02	N/A
CA GW 03	0.47	PT GW 03	0.67
CA GW 04	N/A	PT GW 04	N/A
CA GW 05	0.73	PT GW 05	0.71
CA GW 06	0.66	PT GW 06	0.52
CA GW 07	N/A	PT GW 07	0.84
CA GW 08	0.70	PT GW 08	0.60

3.7 Groundwater Sustainability Index

The development of a sustainability index is intended to supplement previous knowledge explored in the statistical and analytical methods. Results of the REL, RES, VUL and GSI are illustrated in Figure 17 and Figure 18.

3.7.1 Reliability

The northernmost groundwater observation point at CA GW 01 exhibited the highest reliability out of the normalized RES calculations. Reliability is linked to aquifer storage; therefore, it is unsurprising that the northernmost aquifer would have the highest reliability. Three sites in southern California (CA GW 06, 07 and 08) are also classified as mildly reliable, within the mid-range (0.4-0.6) of reliability. Aquifers located in northern and central California, on the periphery of the San Francisco Bay Area (CA GW 02, 03 and 04) and southern California (CA GW 05) were the least reliable. Similarly, to California, Portugal's northernmost sites at PT GW 01, 02, 03 and 04 were the most reliable. PT GW 06 and 07 were within the mid-range of reliability whereas, the two piezometers with the lowest reliability are PT GW 05 and PT GW 08.

3.7.2 Resilience

Characteristically, resilience reflects changes in storage that may be influenced by relations between recharge and precipitation (Thomas, 2019). Essentially, resilience is a system's ability to withstand and bounce back from a state of stress. Southern California aquifers (CA GW 05, 06, 07 and 08) are unequivocally less resilient. Given

the precipitation regime, this may influence recharge rates and storage. CA GW 04 again was the least resilient. Although the resilience indicator computes a relatively low resilience for this well, the water levels at CA GW 04 actively recover after droughts due to groundwater management activities by Santa Clara Valley Water District, including nearby MAR facilities (SCVWD, 2020). These groundwater management activities greatly increase the resilience of the water levels at CA GW 04. The two northernmost sites were the most resilient which fits with the precipitation and recharge characteristics. Portugal's northern most piezometers, and PT GW 05 and 08 were the least resilient. On the south coast, PT GW 06 and 07 were most resilient. Due to the precipitation regime in both sectors the rank for resilience was expected to be reversed in Portugal.

3.7.3 Vulnerability

The least vulnerable aquifer basins are in northern California (Figure 17). The most vulnerable aquifers are located at sites CA GW 04, 05, 06, 07 and 08 in the south. In Portugal, the least vulnerable aquifers are all located in the Algarve, and PT GW 01, 03 and 08 also had low vulnerability (Figure 18). Due to the short rainy season and recurrent drought periods in southern Portugal, it is unexpected that vulnerability was so low in this region.

3.7.4 Sustainability Index

A Groundwater Sustainability Index integrates REL, RES and VUL. Here, normalized performance indicators are used to determine the overall sustainability of each groundwater observation point within each aquifer system. These calculations highlight the relevance of extreme events such as droughts, and an aquifer's ability to withstand drought events, since the single variable used in this computation is groundwater level time series. External factors such as land use practices, abstraction, population density (all human signals) is still relevant but do not explain the classification within each performance indicator.

Generally, the GSI across California follows a clear north to south gradient in rank (Figure 17). The northernmost observation point (CA GW 01) is the most sustainable, CA GW 02 has medium sustainability, and CA GW 03 has a low SI. All sites in central and southern California attained very low sustainability. Aquifers of

central and southern California appear to be more “at risk” to drought than those in the north.

The northernmost aquifer system in California, in the Eureka basin (CA GW 01) has very high reliability, very high resilience, and very low vulnerability. Its overall sustainability is high. CA GW 02, located in the north San Francisco Basin has low reliability, high resilience, and has very low vulnerability. The overall sustainability of this system is medium. The Half Moon Bay aquifer, proximal to the Pacific Ocean where CA GW 03 is located has low reliability, medium resilience, low vulnerability. Its overall sustainability is low. Site CA GW 04, located within the Santa Clara Valley Basin has very low reliability, very low resilience, and high vulnerability. The sustainability of this system overall is very low. Given that this GW 04 well has a strong human signal, both from abstraction and water conservation initiatives, this GSI needs to be interpreted with caution. An expansion on the limitations of a strictly index approach is provided in the discussion. CA GW 05, located in southern California has low reliability, very low resilience, and high vulnerability. Its overall sustainability is very low. Site CA GW 06 has medium reliability, low resilience, and high vulnerability. Its overall sustainability is very low. The Los Angeles basin is dominated by faulting and dense urban development reduces the potential for direct rechange. Site CA GW 07 has medium reliability, very low resilience, and high vulnerability. Its overall sustainability is very low. CA GW 08 has high reliability, very low resilience and is the most vulnerable. Its overall sustainability is very low.

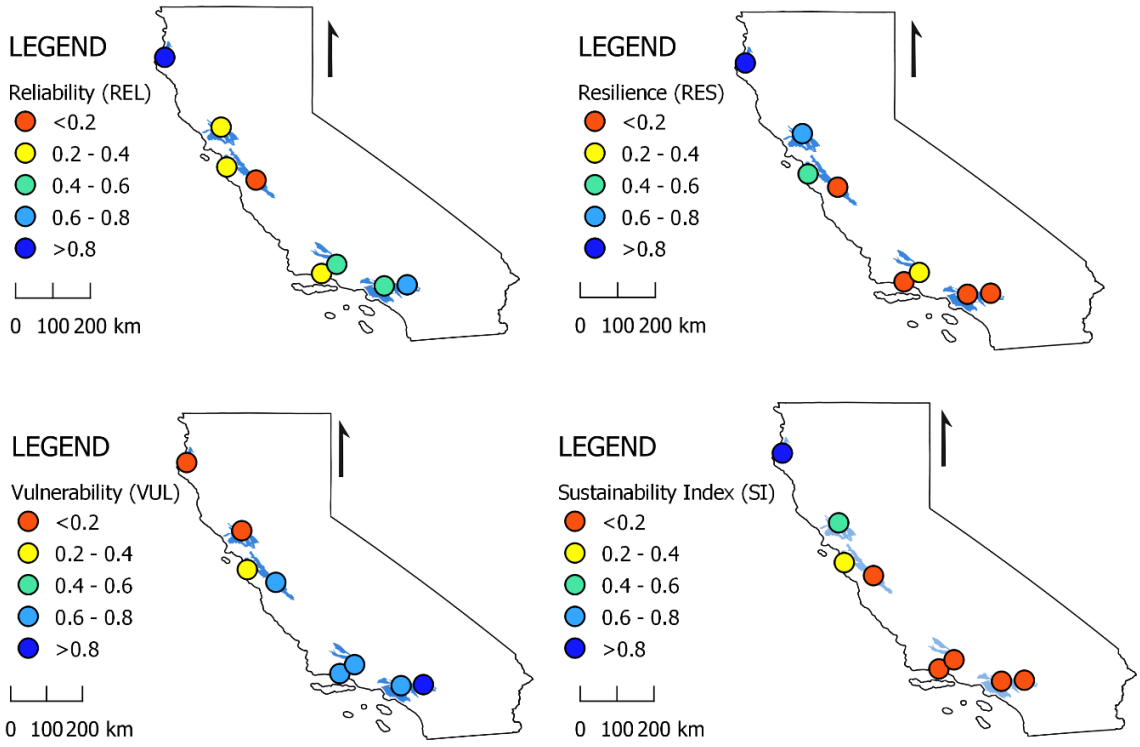

Figure 17. Results of normalized REL, RES, VUL and GSI for the 8 groundwater observation points in the California Coastal Basins aquifers.

In Portugal, the spatial distribution of the GSI is more variable (Figure 18). Directly opposed to results in California, a single aquifer system in southern Portugal (sites PT GW 06 and 07) is the most stable in terms of sustainability, while the remaining six aquifers have very low sustainability.

The northernmost aquifer system in Aveiro (O2) (PT GW 01 and 02) has high reliability, low to very low resilience and very high (02) to low (01) vulnerability. Its overall sustainability is low which seems inconsistent with the productivity of the aquifer system, the precipitation regime in the region and the general characteristics of the aquifer. The highly productive, Leirosa-Monte Real aquifer (O10) (PT GW 03 and 04) has high reliability, low to very low resilience and low to medium vulnerability. Its overall sustainability is low to very low which is unexpected due the fact that it is well preserved, having not suffered from over abstraction in the last decades (Ribeiro & Cunha Da, 2010). The multi-layered Quarteira aquifer system (M7) (PT GW 05) has low reliability, very low resilience, and very low vulnerability, and thus very low in terms of sustainability. The Campina de Faro aquifer (M12) (PT GW 06 and 07) has medium reliability, very high to medium resilience and very low vulnerability. Its overall level of

sustainability matched that of its resilience, very high (06) and medium (07). Lastly, the São João da Venda-Quelfes (M10) (PT GW 08) aquifer behaves similarly to the M7 system, but has very low reliability, low resilience, and low vulnerability, and thus very low in terms of sustainability.

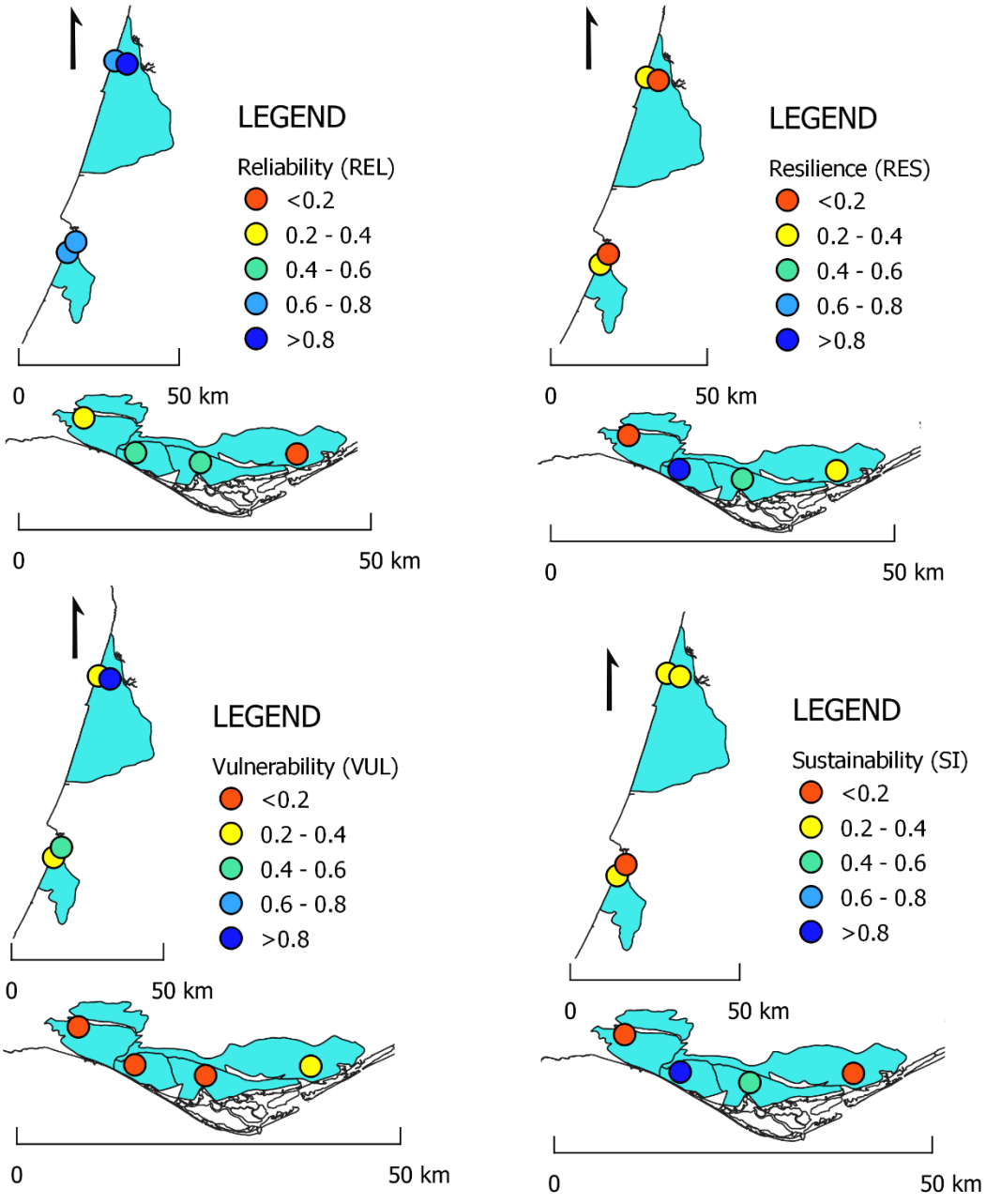

Figure 18. Results of normalized REL, RES, VUL and GSI for the 8 groundwater wells in Portugal's coastal aquifers.

3.7.5 Comparing GSI, Basin Prioritization, and a Water Exploitation Index

To add rigor to the GSI classification in California and Portugal, GSI results are next compared to basin prioritization from SGMA and exploitation classifications from RBMP (Table 9). In California, Basin Prioritization is a technical process that utilizes the best available data and information to classify basins into one of four categories high-, medium-, low-, or very low-priority (California Department of Water Resources, 2020a). The eight components to determine prioritization are identified in the California Water Code Section 10933(b), which include (1) The population overlying the basin or subbasin. (2) The rate of current and projected growth of the population overlying the basin or subbasin. (3) The number of public supply wells that draw from the basin or subbasin. (4) The total number of wells that draw from the basin or subbasin. (5) The irrigated acreage overlying the basin or subbasin. (6) The degree to which persons overlying the basin or subbasin rely on groundwater as their primary source of water. (7) Any documented impacts on the groundwater within the basin or subbasin, including overdraft, subsidence, saline intrusion, and other water quality degradation. (8) Any other information determined to be relevant by the department, including adverse impacts on local habitat and local streamflow.

In Portugal, a Water Exploitation Index (WEI+) illustrates the percentage of water use against renewable freshwater resources in a time and place (EEA, 2018). The WEI+ for river basin districts (1990-2015) provides an overview of water stress conditions including data on hydroclimatic variables, water abstraction, water use, flow estimations and economic data. An annual average (Winter, Spring, Summer, and Autumn) of WEI+ (%) in 2015 is computed for the two basins relevant to this study, Vouga, Mondego and Lis (RH4) and Algarve Basins (RH8). The higher the WEI+ (%), the more exploited or stressed the basin system. For example, in the summer months of 2015, when rainfall is minimal to nonexistent RH4 had a WEI+ of 14.44% and RH8 had a WEI+ of 91.99%. The annual average provides an overview of WEI+ for the year, but seasonal stressors fluctuate dramatically.

Table 9. Classification of basins under the SGMA's Basin Prioritization and RBMP's Water Exploitation Index plus (WEI+) and the GSI for individual groundwater observation points in California and Portugal.

Site ID	Basin Name	SGMA Basin Priority	GSI Class
CA SGMA Basins			
CA GW 01	Eel River Valley	Medium	Very High
CA GW 02	Napa-Sonoma Valley	High	Medium
CA GW 03	Half Moon Bay Terrace	Very Low	Low
CA GW 04	Gilroy-Hollister-Llagas Valley	High	Very Low
CA GW 05	Foothill	N/A	Very Low
CA GW 06	Cuyama Valley	High	Very Low
CA GW 07	San Gabriel Valley	Very Low	Very Low
CA GW 08	Upper Santa Ana Valley	N/A	Very Low
PT RBMP Basins			
Site ID	**Basin Name**	**WEI+ (%)**	**GSI Class**
PT GW 01	Vouga, Mondego and Lis	8.86	Low
PT GW 02	Vouga, Mondego and Lis	8.86	Low
PT GW 03	Vouga, Mondego and Lis	8.86	Low
PT GW 04	Vouga, Mondego and Lis	8.86	Very Low
PT GW 05	Algarve Basins	47.98	Very Low
PT GW 06	Algarve Basins	47.98	Very High
PT GW 07	Algarve Basins	47.98	Medium
PT GW 08	Algarve Basins	47.98	Very Low

Comparing indices with different priorities (performance indicators), such as sustainability and exploitive use in this case can help identify aquifer systems which may need immediate policy, conservation or mitigation interventions, and others that may be self-sustaining for a longer period of time. In this way, indices can be complementary and should be used in tandem to identify and prioritize management measures. For example, when a basin is classified as a high priority and has a low GSI, that could alert basin managers that the system, which is of high importance but is heavily threatened, requires immediate conservation measures enacted. However, basing policy and/or groundwater management measures on a single index may have limitations by presenting bias or an incomplete understanding of the overall condition of the basin.

When pairing SGMA and GSI, two aquifers are flagged as high priority and high risk due to their very low levels of sustainability (Table 9). These are CA GW 04 and CA GW 06. CA GW 02 warrants attention as well due to its high priority and medium levels of sustainability. Using WEI+ and GSI in conjunction helps to identify two aquifers with a WEI+ at nearly 50% and very low sustainability in Portugal which are

PT GW 05 and 08. These two sites within the Algarve Basins system could be reprioritized within the RBMP. PT GW 07 is also flagged due to its WEI+ and medium level of sustainability. These findings could be reported back to water resource managers to establish specific REL, RES and VUL mitigation measures for these high priority aquifers.

4 DISCUSSION

4.1 Hydroclimatic teleconnections

The teleconnections analyzed in this study account for a significant amount of groundwater level variability in both California and Portugal. The largest amount of variability is attributed to lower frequency patterns, PDO in California and NAO in Portugal, which account on average for 52.75% and 46.25% of groundwater variability, respectively. These results are consistent with findings from Gurdak et al. (2007), Kuss (2011) and Velasco et al. (2017), where longer-term climate variations in California aquifers account for greater amounts of variance in hydrologic time series than high frequency (shorter-term) climate variations. In Portugal, the dominance of NAO variability is also reinforced by Neves et al. (2019b) who found that NAO is the primary driver of hydrological variability in the country. Other authors studying the relationship between the NAO, groundwater variability and river flow had similar findings to the SSA results presented earlier, that NAO has stronger influence in the south of Portugal (Gámiz-Fortis et al., 2002).

A concentration of ENSO-like signals in southern California is supported by previous studies that show a strong influence of ENSO on winter precipitation anomalies of the southern U.S. (Kiladis & Diaz, 1989; Kurtzman & Scanlon, 2007; Ropelewski & Halpert, 1986). Therefore, it was expected that the ENSO signal would contain the second largest percent of variability in California, yet it fell below PNA by a 1.25% margin on average. Due to its status as the most important interannual climate pattern globally (Palmer & Anderson, 1994) and its influence on coastal California, the slightly lower percent of variability is unexpected. This may be associated with the embedding of the PNA signal in the ENSO frequency during coupling events. As presented in Figure 8, the periodicities of the PNA and ENSO overlap, thus it is inherently difficult to attribute a hydroclimatic signal to either ESNO of PNA when they have overlapping periodicities. Less detection of the higher frequency ENSO signal in the groundwater levels, as compared to the PDO signal, may also be attributed to the relative greater damping of the higher frequencies in the relatively thick vadose zones of the study area (Corona et al., 2018).

In Portugal, the joint impact of higher frequency signals (EA and SCAND) on variance is 33.25% on average in the north and 13.25% on average in the south, which is similar to findings from Neves et al. (2019b). However due to their overlapping periodicities, it is important to acknowledge that EA and SCAND are difficult to

distinguish. The overlap in the periodicities of the two climate variability modes in both study areas (ENSO and PNA in California and EA and SCAND in Portugal) highlights an important limitation of using SSA to identify influence from specific modes of climate variability on groundwater level. Due to this, additional methods, such as the wavelet transform, wavelet coherence and lag correlations are leveraged to enrich this research.

The continuous wavelet transform (CWT) spectra support findings from the SSA and add a new layer of evidence that climate variability signals can be captured in groundwater level fluctuations. Anomalous events such as the heavy precipitation years of 1998, and 2007 coincide with known ENSO events in California, and the occurrence and impact of drought appear in groundwater level records in Portugal from 2004-05. Dominant frequencies (or periods) on the CWT plots generally coincide with periodicities from the SSA. While the CWT effectively visualizes the evolution of significant meteorological events in groundwater level records, the interactions between climate phenomena are not thoroughly explored until the coherence between groundwater level and climate patterns are computed via a wavelet coherence.

4.2 Coherence between climate indices and groundwater levels and drought

The wavelet coherence is effective at identifying common time-localized oscillatory behaviors in two time series. Interpretation of this method is advanced when drought events are highlighted since this helps relate climate mode coupling and drought occurrence.

Previous studies suggest that a positive PDO phase can intensify El Niño, driving a more robust pattern of wetter winters in the southern U. S. (Brown & Comrie, 2004; Gershunov & Barnett, 1998). The reverse occurs for the negative phase. In this study the coherence plots show that in northern and central California, a strong PDO+ coherence with a 4-8 period precede drought events at all four sites (CA GW 01, 02, 03 and 04). Small yet significant patches of PDO- coherence occur between drought bars in southern California around a 1-year period in 2000 and 2005, which align with the PDO- ENSO- coupling events illustrated in Figure 3. Thus, coherence between PDO and groundwater level behaves as expected, with lower (higher) precipitation in northern (southern) California during positive (negative) PDO therefore contributing to and in most cases preceding periods of drought in both regions. The implications of El Niño (ENSO+) on drought occurrence are also evident across the state of California.

In northern California and at CA GW 07, El Niño coherence with a 4-8 year period persists throughout major drought events. The synchronization of PDO+ and El Niño also become most evident in northern California, marking interactions between both patterns and drought events. While ENSO's significant patches are in the 2-4 year frequency, the 4-8 year synchronizations appear when PDO and ENSO are coupled. The PNA loosely follows the phasing of ENSO and often occurs before or even during periods of drought.

The phase and impact of NAO in northern Portugal around the year 2000 is rather conspicuous in the WTC plot. Significant patches of coherence with a 1-year period are in-phase (NAO+) at PT GW 02 and 03, whilst a similar patch with a 2-year period is anti-phase (NAO-). A NAO+ signal would be expected to appear in all northern sites, particularly since NAO+ drives above average precipitation in northern Europe. Figure 3 also confirms that NAO was in a positive phase in 2000. This variability could be attributed to the influenceability of shorter period signals or the hydrogeographic composition of the aquifer. In the Algarve, the impacts of NAO- are most evident at PT GW 07 in the 4-8 year period. A significant NAO event occurs before the 2004-2005 drought episode, and coupling between NAO+ and EA- are centered in the middle of the drought episode (Figure 3). EA and SCAND coherence patterns are tapered near droughts events. This behavior is most obvious in the 2-4 year period in southern Portugal, although it occurs in all records. Additionally, the groundwater level intensity at sites PT GW 01 and 02 associated with the SCAND pattern rapidly declines after the 2004-2005 drought event. This corresponds with the coupled NAO-EA+SCAND+ phases in 2001 and 2003 as discovered by Neves et al., (2019b).

The impact of climate variability coupling is evidenced throughout both aquifers systems in California and Portugal although drought incidence and behavior seem to be different in California, where sustained droughts can last up to 6 years.

4.3 Groundwater Sustainability

Packaging both climate variability science and sustainable groundwater management information can offer a well calibrated set of methods to inform groundwater policy or groundwater management practices. Previous sections detailed how coupled climate modes drive groundwater fluctuations, constructively or destructively, and that these events often coincide with episodes of drought. How

might this relate to outcomes of a sustainability index? Firstly, a sustainability index uses in-situ groundwater observation data to calculate groundwater sustainability performance indicators. REL, RES and VUL performance indicators relate to groundwater variability, storage capacity and recovery after abnormal conditions occur, particularly drought. The resilience parameter is of particular importance as resilience represents the likelihood of a return to above normal conditions after excessive groundwater use or a long-term groundwater drought (Thomas, 2019), which occurred in both California and Portugal throughout the 30-year span of this study. The resilience indicator is also heavily influential in setting the overall sustainability of an aquifer system. When developing an GSI, metrics can be customized to suit the questions or concerns within a basin, for example, in California, under the SGMA, a GSA may be focused on groundwater storage changes and could compute Equation (1), only. Weighting may also be incorporated into Equation (4) to increase or decrease the influence of a performance metric over others when evaluating groundwater changes (May 2013). Customization was not performed here, although it would be recommended to water resource managers. In the case study of the Central Valley in California, Thomas (2019) developed a GSI in conjunction with known SGMA knowledge. Here the GSI was paired with methods to determine the presence and extent of climate variability patterns in groundwater level fluctuations, which were then compared to basin prioritization and exploitation indices. It is important to note that a stand-alone GSI could be misleading if it does not integrate or leverage local water management efforts.

The most significant output from the GSI is a clear indication of how well (or poor) a specific aquifer can withstand drought conditions. Of course, land use practices, water conservation measures and a potentially hidden human signal should also be considered when interpreting the results, as these information only enrich and compliment the GSI. For example, CA GW 02, located in Napa Valley known within the U.S. for “Calistoga spring water” and globally for Napa’s extensive wine vineyards may be less resilient than what was computed (high resilience) due to consistent pressure on the Napa basin. Napa is also classified as a high priority basin within the SGMA and attained medium sustainability from the GSI, warranting additional conservation interventions. Additionally, CA GW 04 is in the Llagas Subbasin of the Santa Clara Valley, has a history of considerable agricultural activities, including groundwater pumping to support irrigated agriculture. It is also a high priority basin,

which has undergone considerable policy and conservation efforts. Recent water conservation measures including managed aquifer recharge, following the peak of the 2014-2015 drought should make this system more resilient. This aquifer also experienced repeated coupling events between PDO, ENSO and PNA preceding episodic and extended drought periods. The Los Angeles basin, where CA GW 06 is located, is one of high priority for SGMA with a very low sustainability. This system has experienced a reduction in direct recharge due to urban development and has a history of sea water intrusion, yet recent mitigation measures have been put in place to slow or cease sea water intrusion.

Due to the overall precipitation regime of northern Portugal, higher reliability and higher resilience in the northern aquifers is expected, yet all four observation points had low or very low resilience. It could be that these systems are less tolerant to drought conditions. Low levels of exploitation in the northern aquifers (Table 9) could signal that while these systems have a limited human signal, they are quite vulnerable to natural stressors such as drought. Although, aquifers with the most significant and well-preserved coupling signals from the WTC and the CWT occur at sites PT GW 01, 02, 03 and 07. The potential inability to return to a normal condition following coupling and drought events, could be the factor to deem these northern aquifers less resilient. Conversely, the Campina de Faro aquifer (M12) where sites PT GW 06 and 07 are located were indexed with high to medium resilience. Tourism and intense agricultural pressure characterise this area, thus the resilience of this system may be lower due to these external stressors. The WEI+ and the GSI flag Campina de Faro and São João da Venda-Quelfes as heavily exploited systems with very low sustainability, drawing special attention to these two aquifers within the Algarve basins.

4.4 Groundwater variability and climate forcing in two coastal aquifer systems with prevailing Mediterranean climates

An investigation of coastal groundwater response to climate variability coupling in two West Coast aquifer systems were selected due to their similarities within a prevailing Mediterranean climate zone and the overall vulnerability of groundwater systems in these climates globally. Findings from this research present both distinct similarities and differences between the two systems.

Coastal aquifers in both California and Portugal are unequivocally impacted by modes of climate variability. Lower frequency patterns (NAO with 8-years and PDO

with 22-years on average) were the dominant driver of variability in groundwater level. Two patterns had comparable periodicities (EA/SCAND with a 3-year period and ENSO with a 3.4-year period) and drove up to 54% and 63% of groundwater variability, respectively. Longer term patterns also influence the shorter term (high frequency) patterns during coupling events. In the SSA, overlapping frequencies occurred for both patterns in California and Portugal, potentially masking one signal and strongly expressing another. Coupling events were evidenced in the WCT, aligning with some mode interactions presented in Figure 3. Specific coupling arrangements (phase combinations) are associated with extreme events, such as anomalously wet conditions (PDO+ ENSO+) or drought (NAO+ EA-).

Progressive groundwater sustainability measures are also underway in both regions through the SGMA and the RBMP. The GSI highlights aquifers which are vulnerable to drought, and when paired with complimentary indices aquifer management and mitigation can be prioritized and enacted.

Some noticeable differences between California and Portugal are also presented throughout this work. Firstly, the highest percent of groundwater level variability was opposing in California and Portugal. In the SSA, RCs with the highest variability were predominantly in northern Portugal, while California groundwater RCs with >50% variability were predominantly in southern and central California. This could be attributed to a mix of the precipitation regime, the coupling of climate patterns and the spatial implications of these coupling events. Recall that the positive phases of PDO and ENSO increase precipitation in southern California, and these signals were also captured in the WCT.

According to findings from the GSI, the two aquifers in northern Portugal were more vulnerable, while aquifers in southern California expressed higher vulnerability. Higher vulnerability to drought in southern aquifer systems was expected in both regions. This difference is complex as it could relate to the hydrogeologic composition of the aquifers including flow regimes and direct recharge, where aquifers in the south of Portugal may be replenished by northern (upstream) flows. Another consideration is that the results of the GSI may not be fully representative of conditions of aquifers in northern Portugal. A sampling of two aquifers with adjacent piezometers present very localized conditions and are not representative of all coastal aquifers of northern Portugal. The vulnerability to drought largely depends on the hydrogeology of the aquifer system and hydrogeologic properties which are restricted to a localized area.

Hydrogeologic characteristics can vary widely across different aquifers, especially in northern Portugal where aquifer typologies vary more than in the Algarve. Aquifers of the Algarve are predominantly karst-porous aquifers with rich connections, which supports the likelihood of replenishment from northern flows moving seaward.

One obvious distinction, however, is that drought incidence and behavior seem to be different in California, where sustained droughts can last up to 6 years. The recent 5-year drought in California spanning 2012-2017 occurred and persisted due to a mix of hydro-climatological events, such as record dry conditions, three below normal rainfall seasons, low snowpack, and one of the strongest recorded El Niño's. California is also more heavily dependent on groundwater for domestic supply, whereas Portugal relies more on surface water reservoirs. The differences in drought extent, since the occurrence is similar between California and Portugal could be attributed to water management, extreme drying conditions, and climate variability.

4.5 Limitations of the study

This work aims to expand the knowledge regarding piezometric response to coupled modes of climate variability. To analyze recent impacts of climate variability patterns, both groundwater level times series and climate mode data were selected for a 30-year time frame as close to the present as possible. Some records spanning 1982 to 2019 display natural and obvious hydrological cycles. Others behave in an abnormal and conspicuous manner, possibly due to the sampling rate, the use of the well or general land use practices in the surrounding area or the geologic composition of the aquifer. Additionally, while the five aquifer systems in Portugal, and eight in California were selected for their hydrogeographic variety, analyzing one or two piezometers per aquifer system may not provide enough data for a comprehensive understanding of groundwater level variability across the entire system. To achieve this, future studies could analyze several piezometers per aquifer. Nonetheless, groundwater records were selected and analyzed for their contemporariness, relevance as a coastal aquifer system, and potential to display significant signals of climate variably patterns. As with most research, data quality and access can be a limiting factor, yet this study presents novel findings regarding climate variability response comparatively in California and Portugal, regardless of the pristineness of the data itself.

5 CONCLUSION

The application of SSA to identify and evaluate quasi-periodic signals in groundwater level time series indicates that PDO, ENSO, PNA, NAO, EA, SCAND have significant influence on groundwater fluctuations across coastal aquifer systems in California and Portugal. Lower frequency oscillations have a greater influence on hydrologic patterns, with PDO and NAO accounting for the largest amount of variability. While the imprint of high frequency signals is also evident, the lower frequency signals tend to be better preserved in groundwater level fluctuations.

Interrelationships between climate patterns, groundwater level variability and drought occurrence are evidenced through the application of wavelet transform methods. Coupled climate modes coincide with hydrological droughts throughout the 30-year time span of this study, where specific mode combinations (NAO+ EA- and drought, NAO- EA+ SCAND+ and heavy precipitation, PDO+ ENSO+ increased precipitation in southern CA, PDO- ENSO- increased precipitation in northern CA) drive groundwater level anomalies. The strongest covariability between climate patterns and groundwater levels occurs in the following dominant periods: 4-8 years for PDO, 2-4 years for ENSO, 1-2 years for PNA, 5-8 years band for NAO, 2-4 years for EA and 2-8 years for SCAND. Frequencies from EA and SCAND are often coupled with NAO signals.

The sensitivity to drought is further explored through the development of a GSI. Aquifer resilience is the leading performance indicator determining the overall GSI classification. Aquifers with low resilience were in southern California and northern Portugal. However, differences in the spatial distribution of the GSI between Portugal and California are due to the localized and specific hydrogeological characteristics of the aquifers. Comparing the GSI with existing water management indices helps to identify the most at-risk aquifers which may be re-prioritized by coastal water resource managers.

To ensure water security in a future where water resources are continually threatened by increasing drying trends, extended drought occurrences and desertification, a deeper understanding of how climate pattern coupling events influence groundwater variability will help to improve future projections of groundwater availability. This invaluable information can then be applied by pairing hydro-climatological knowledge with a GSI, which can enrich and inform effective sustainable groundwater management policies.

6 REFERENCES

Almeida, C., Mendonca, J., Jesus, M., & Gomes, A. (2000). Sistemas Aquiferos de Portugal Continental. *INAG, Lisbon*, *I–III*. https://doi.org/10.13140/RG.2.1.1012.6160

APA. (2019). *Surface and Groundwater Availability*. https://rea.apambiente.pt/content/surface-and-groundwater-availability?language=en

Barco, J., Hogue, T. S., Girotto, M., Kendall, D. R., & Putti, M. (2010). Climate signal propagation in southern California aquifers. *Water Resources Research*, *46*(11), 1–19. https://doi.org/10.1029/2009WR008376

Barnston, A. G., & Livezey, R. E. (1987). Classification, seasonality and persistence of low-frequency atmospheric circulation patterns. *Monthly Weather Review*, *115*(6), 1083–1126. https://doi.org/10.1175/1520-0493(1987)115<1083:CSAPOL>2.0.CO;2

Bastos, A., Janssens, I. A., Gouveia, C. M., Trigo, R. M., Ciais, P., Chevallier, F., Peñuelas, J., Rödenbeck, C., Piao, S., Friedlingstein, P., & Running, S. W. (2016). European land CO2 sink influenced by NAO and East-Atlantic Pattern coupling. *Nature Communications*, *7*. https://doi.org/10.1038/ncomms10315

Beebee, R. A., & Manga, M. (2004). Variation in the relationship between snowmelt runoff in Oregon and ENSO and PDO. *Journal of the American Water Resources Association*, *40*(4), 1011–1024. https://doi.org/10.1111/j.1752-1688.2004.tb01063.x

Bove, M. C., Elsner, J. B., Landsea, C. W., Niu, X., & O'Brien, J. J. (1998). Effect of El Niño on U.S. Landfalling Hurricanes, Revisited. *Bulletin of the American Meteorological Society*, *79*(11), 2477–2482. https://doi.org/10.1175/1520-0477(1998)079<2477:EOENOO>2.0.CO;2

Brabets, T. P., & Walvoord, M. A. (2009). Trends in streamflow in the Yukon River Basin from 1944 to 2005 and the influence of the Pacific Decadal Oscillation. *Journal of Hydrology*, *371*(1–4), 108–119. https://doi.org/10.1016/j.jhydrol.2009.03.018

Broomhead, D. S., & King, G. P. (1986). Extracting qualitative dynamics from experimental data. *Physica D: Nonlinear Phenomena*, *20*(2–3), 217–236. https://doi.org/10.1016/0167-2789(86)90031-X

Brown, D. P., & Comrie, A. C. (2004). A winter precipitation "dipole" in the western United States associated with multidecadal ENSO variability. *Geophysical Research Letters*, *31*(9), 1–4. https://doi.org/10.1029/2003GL018726

Bueha, C. and, & Nakamurab, H. (2007). Scandinavian pattern and its climatic impact. *Quarterly Journal of the Royal Meteorological Society*, *133*, 2117–2131. https://doi.org/10.1002/qj

California Department of Water Resources. (2020a). *Basin Prioritization*. https://water.ca.gov/Programs/Groundwater-Management/Basin-Prioritization#:~:text=Statewide Map of Current SGMA Basin Prioritization&text=Basin Prioritization is a technical,%2C or very low-priority.

California Department of Water Resources. (2020b). *Sustainable Groundwater Management Act*. https://water.ca.gov/Programs/Groundwater-Management/SGMA-Groundwater-Management

Cayan, D. R., Redmond, K. T., & Riddle, L. G. (1999). ENSO and hydrologic extremes in the western

United States. *Journal of Climate*, *12*(9), 2881–2893. https://doi.org/10.1175/1520-0442(1999)012<2881:EAHEIT>2.0.CO;2

Condesso, & Marques Da Silva. (2008). The Aveiro Quaternary and Cretaceous Aquifers, Portugal. *Natural Groundwater Quality*, 232–262. https://doi.org/10.1002/9781444300345.ch11

Copernicus Climate Change Service (C3S). (2019). *C3S ERA5-Land reanalysis*. Copernicus Climate Change Service. https://cds.climate.copernicus.eu/cdsapp#!/home

Corona, C. R., Gurdak, J. J., Dickinson, J. E., Ferré, T. P. A., & Maurer, E. P. (2018). Climate variability and vadose zone controls on damping of transient recharge. *Journal of Hydrology*, *561*, 1094–1104. https://doi.org/10.1016/j.jhydrol.2017.08.028

Correia, J. M., Bastos, A., Brito, M. C., & Trigo, R. M. (2017). The influence of the main large-scale circulation patterns on wind power production in Portugal. *Renewable Energy*, *102*, 214–223. https://doi.org/10.1016/j.renene.2016.10.002

Dahlman, L. (2009). Climate Variability: Pacific - North American Teleconnection Pattern. *NOAA ClimateWatch Magazine*. https://www.climate.gov/news-features/understanding-climate/climate-variability-pacific-north-american-teleconnection

Dai, A. (2013). Increasing drought under global warming in observations and models. *Nature Climate Change*, *3*(1), 52–58. https://doi.org/10.1038/nclimate1633

Daubechies, I. (1990). The Wavelet Transform, Time-Frequency Localization and Signal Analysis. *IEEE Transactions on Information Theory*, *36*(5), 961–1005. https://doi.org/10.1109/18.57199

De Vita, P., Allocca, V., Manna, F., & Fabbrocino, S. (2012). Coupled decadal variability of the North Atlantic Oscillation, regional rainfall and karst spring discharges in the Campania region (southern Italy). *Hydrology and Earth System Sciences*, *16*(5), 1389–1399. https://doi.org/10.5194/hess-16-1389-2012

Dickinson, J. E., Hanson, R. T., & Predmore, S. K. (2014). HydroClimATe: hydrologic and climatic analysis toolkit. *Techniques and Methods*. https://doi.org/10.3133/tm4a9

Döll, P. (2009). Vulnerability to the impact of climate change on renewable groundwater resources: A global-scale assessment. *Environmental Research Letters*, *4*(3). https://doi.org/10.1088/1748-9326/4/3/035006

EEA. (2018). *Water exploitation index plus (WEI+) for river basin districts (1990-2015)*. https://www.eea.europa.eu/data-and-maps/explore-interactive-maps/water-exploitation-index-for-river-2

Enfield, D. B., Mestas-Nufiez, A. M., & Trinble, P. J. (2001). The Atlantic multidecadal oscillation and its relation to rainfall and river flows in the continental U.S. *Geophysical Research Letters*, *28*(10), 2077–2080.

Famiglietti, J. S. (2014). The global groundwater crisis. *Nature Climate Change*, *4*(11), 945–948. https://doi.org/10.1038/nclimate2425

Feng, S., Hu, Q., & Oglesby, R. J. (2011). Influence of Atlantic sea surface temperatures on persistent drought in North America. *Climate Dynamics*, *37*(3), 569–586. https://doi.org/10.1007/s00382-010-0835-x

Ferguson, G., & Gleeson, T. (2012). Vulnerability of coastal aquifers to groundwater use and climate

change. *Nature Climate Change*, *2*(5), 342–345. https://doi.org/10.1038/nclimate1413

Freckleton, J. R., Martin, P., & Nishikawa, T. (1998). *Geohydrology of Storage Unit III and a Combined Flow Model of the Santa Barbara and Foothill Ground-water Basins, Santa Barbara County, California. U.S. Geological Survey Water-Resources Investigations Report 97-4121*. 85.

Fu, C., James, A. L., & Wachowiak, M. P. (2012). Analyzing the combined influence of solar activity and El Niño on streamflow across southern Canada. *Water Resources Research*, *48*(5). https://doi.org/10.1029/2011WR011507

Gámiz-Fortis, S. R., Pozo-Vázquez, D., Esteban-Parra, M. J., & Castro-Díez, Y. (2002). Spectral characteristics and predictability of the NAO assessed through Singular Spectral Analysis. *Journal of Geophysical Research Atmospheres*, *107*(23), ACL 11-1-ACL 11-15. https://doi.org/10.1029/2001JD001436

García-Herrera, R., Paredes, D., Trigo, R. M., Trigo, I. F., Hernández, E., Barriopedro, D., & Mendes, M. A. (2007). The outstanding 2004/05 drought in the Iberian Peninsula: Associated atmospheric circulation. *Journal of Hydrometeorology*, *8*(3), 483–498. https://doi.org/10.1175/JHM578.1

Gershunou, A., Barnett, T. P., & Cayan, D. R. (1999). North pacific interdecadal oscillation seen as factor in ENSO-related north American climate anomalies. *Eos*, *80*(3). https://doi.org/10.1029/99eo00019

Gershunov, A., & Barnett, T. P. (1998). Interdecadal Modulation of ENSO Teleconnections. *Bulletin of the American Meteorological Society*, *79*(12), 2715–2725.

Ghil, M. (2002). Natural Climate Variability. In *Encyclopedia of Global Environmental Change* (Vol. 1, pp. 544–549).

Ghil, & Mo. (1991). Intraseasonal Oscillations in the Global Atmosphere. Part I: Northern Hemisphere and Tropics. *Journal of the Atmospheric Sciences*, *48(5)*, *752*. https://doi.org/10.1175/1520-0469(1991)048<0752:ioitga>2.0.co;2

Giorgi, F. (2006). Climate change hot-spots. *Geophysical Research Letters*, *33*(8), 1–4. https://doi.org/10.1029/2006GL025734

Gleeson, T., Wada, Y., Bierkens, M. F. P., & Van Beek, L. P. H. (2012). Water balance of global aquifers revealed by groundwater footprint. *Nature*, *488*(7410), 197–200. https://doi.org/10.1038/nature11295

Grinsted, A., Moore, J. C., & Jevrejeva, S. (2004). Application of the cross wavelet transform and wavelet coherence to geophysical time series. *Nonlinear Processes in Geophysics*, *11*(5/6), 515–533. https://doi.org/10.5194/npg-11-515-2004

Gurdak, J. J. (2017). Groundwater: Climate-induced pumping. *Nature Geoscience*, *10*(2), 71–72. https://doi.org/10.1038/ngeo2885

Gurdak, J. J., Hanson, R. T., McMahon, P. B., Bruce, B. W., McCray, J. E., Thyne, G. D., & Reedy, R. C. (2007). Climate Variability Controls on Unsaturated Water and Chemical Movement, High Plains Aquifer, USA. *Vadose Zone Journal*, *6*(3), 533–547. https://doi.org/10.2136/vzj2006.0087

Gutzler, D. S., Kann, D. M., & Thornbrugh, C. (2002). Modulation of ENSO-based long-lead outlooks of Southwestern U.S. winter precipitation by the Pacific Decadal Oscillation. *Weather and Forecasting*, *17*(6), 1163–1172. https://doi.org/10.1175/1520-

0434(2002)017<1163:MOEBLL>2.0.CO;2

Hanson, R. T., Dettinger, M. D., & Newhouse, M. W. (2006). Relations between climatic variability and hydrologic time series from four alluvial basins across the southwestern United States. *Hydrogeology Journal*, *14*(7), 1122–1146. https://doi.org/10.1007/s10040-006-0067-7

Hanson, R. T., Newhouse, M. W., & Dettinger, M. D. (2004). A methodology to asess relations between climatic variability and variations in hydrologic time series in the southwestern United States. *Journal of Hydrology*, *287*(1–4), 252–269. https://doi.org/10.1016/j.jhydrol.2003.10.006

Hashimoto, T., Stedinger, J. R., & Loucks, D. P. (1982). Reliability, Resiliency, and Vulnerability Criteria. *Water Resources Research*, *18*(1), 14–20.

Helsel, D. R., & Hirsch, R. M. (1992). Statistical methods in water resources. *Statistical Methods in Water Resources*. https://doi.org/10.2307/1269385

Higgins, R. W., Silva, V. B. S., Shi, W., & Larson, J. (2007). Relationships between climate variability and fluctuations in daily precipitation over the United States. *Journal of Climate*, *20*(14), 3561–3579. https://doi.org/10.1175/JCLI4196.1

Hirata, R., Suhogusoff, A., & Fernandes, A. (2007). Groundwater resources in the State of São Paulo (Brazil): *Anais Da Academia Brasileira de Ciências*, *79*(1), 141–152. https://doi.org/10.1590/S0001-37652007000100016

Holman, I. P., Rivas-Casado, M., Bloomfield, J. P., & Gurdak, J. J. (2011). Identifying non-stationary groundwater level response to North Atlantic ocean-atmosphere teleconnection patterns using wavelet coherence. *Hydrogeology Journal*, *19*(6), 1269–1278. https://doi.org/10.1007/s10040-011-0755-9

Huang, X., & Ullrich, P. A. (2017). The changing character of twenty-first-century precipitation over the western United States in the variable-resolution CESM. *Journal of Climate*, *30*(18), 7555–7575. https://doi.org/10.1175/JCLI-D-16-0673.1

Hurrell, J W. (1995). Decadal Trends in the North Atlantic Oscillation: Regional Temperatures and Precipitation. *Science*, *269*, 676–679.

Hurrell, J W, Kushnir, Y., & Ottersen, G. (2003). An overview of the North Atlantic Oscillation,. *Climatic Significance and Environmental Impact*, 1–35. https://doi.org/10.1029/GM134

Hurrell, James W., & Van Loon, H. (1997). Decadal variations in climate associated with the North Atlantic oscillation. *Climatic Change*, *36*(3–4), 301–326. https://doi.org/10.1007/978-94-015-8905-5_4

IPCC. (2001). Contribution of Working Group I to the Third Assessment Report of the Intergovernmental Panel on Climate Change [Houghton, J.T. Ding, Y. Griggs, D.J. Noguer, M. Linden, P.J. van der Dai, X. Maskell, K. Johnson, C.A.]. *Cambridge University Press*, 94.

IPMA. (2020). *Instituto Português do Mar a e da Atmosfera [Portuguese Institute ofSea Atmosphere]*. https://www.ipma.pt/

Jerez, S., Trigo, R. M., Vicente-Serrano, S. M., Pozo-VáZquez, D., Lorente-Plazas, R., Lorenzo-Lacruz, J., Santos-Alamillos, F., & MontáVez, J. P. (2013). The impact of the north atlantic oscillation on renewable energy resources in Southwestern Europe. *Journal of Applied Meteorology and Climatology*, *52*(10), 2204–2225. https://doi.org/10.1175/JAMC-D-12-0257.1

Jerez, Sonia, & Trigo, R. M. (2013). Time-scale and extent at which large-scale circulation modes determine the wind and solar potential in the Iberian Peninsula. *Environmental Research Letters*, *8*(4). https://doi.org/10.1088/1748-9326/8/4/044035

Jolly, W. M., Cochrane, M. A., Freeborn, P. H., Holden, Z. A., Brown, T. J., Williamson, G. J., & Bowman, D. M. J. S. (2015). Climate-induced variations in global wildfire danger from 1979 to 2013. *Nature Communications*, *6*(May), 1–11. https://doi.org/10.1038/ncomms8537

Jong, B. T., Ting, M., & Seager, R. (2016). El Niño's impact on California precipitation: Seasonality, regionality, and El Niño intensity. *Environmental Research Letters*, *11*(5). https://doi.org/10.1088/1748-9326/11/5/054021

Kalimeris, A., Ranieri, E., Founda, D., & Norrant, C. (2017). Variability modes of precipitation along a Central Mediterranean area and their relations with ENSO, NAO, and other climatic patterns. *Atmospheric Research*, *198*(March), 56–80. https://doi.org/10.1016/j.atmosres.2017.07.031

Kiladis, G. N., & Diaz, H. F. (1989). Global Climatic Anomalies Associated with Extremes in the Southern Oscillation. *Journal of Climate*, *2*(9), 1069–1090. https://doi.org/10.1175/1520-0442(1989)002<1069:gcaawe>2.0.co;2

Kottek, M., Grieser, J., Beck, C., Rudolf, B., & Rubel, F. (2006). World map of the Köppen-Geiger climate classification updated. *Meteorologische Zeitschrift*, *15*(3), 259–263. https://doi.org/10.1127/0941-2948/2006/0130

Kurtzman, D., & Scanlon, B. R. (2007). El Niño-Southern Oscillation and Pacific Decadal Oscillation impacts on precipitation in the southern and central United States: Evaluation of spatial distribution and predictions. *Water Resources Research*, *43*(10), 1–12. https://doi.org/10.1029/2007WR005863

Kuss, A.J.M. (2011). Effects of climate variability on recharge in regional aquifers of the United States. In *San Francisco State University, San Francisco, CA*.

Kuss, Amber Jean M., & Gurdak, J. J. (2014). Groundwater level response in U.S. principal aquifers to ENSO, NAO, PDO, and AMO. *Journal of Hydrology*, *519*(PB), 1939–1952. https://doi.org/10.1016/j.jhydrol.2014.09.069

Lapp, S. L., St. Jacques, J. M., Sauchyn, D. J., & Vanstone, J. R. (2013). Forcing of hydroclimatic variability in the northwestern Great Plains since AD 1406. *Quaternary International*, *310*, 47–61. https://doi.org/10.1016/j.quaint.2012.09.011

Liu, Y., Stanturf, J., & Goodrick, S. (2010). Trends in global wildfire potential in a changing climate. *Forest Ecology and Management*, *259*(4), 685–697. https://doi.org/10.1016/j.foreco.2009.09.002

Loucks, D. P. (1997). Quantification des tendances de la durabilité des systèmes. *Hydrological Sciences Journal*, *42*(4), 513–530. https://doi.org/10.1080/02626669709492051

Loucks, D. P., Stedinger, J. R., & Haith, D. (1981). Water resource systems planning and analysis: Solutions manual. *Prentice-Hall, Englewood Cliffs, N.J*.

Manna, F., Walton, K. M., Cherry, J. A., & Parker, B. L. (2019). Five-century record of climate and groundwater recharge variability in southern California. *Scientific Reports*, *9*(1), 1–8. https://doi.org/10.1038/s41598-019-54560-w

Mantua, N., & Hare, S. (2002). *The Pacific Decadal Oscillation* (p. 35). Journal of Oceanography.

https://doi.org/10.1023/A:1015820616384

Mantua, N. J., Hare, S. R., Zhang, Y., Wallace, J. M., & Francis, R. C. (1997). A Pacific Interdecadal Climate Oscillation with Impacts on Salmon Production. *Bulletin of the American Meteorological Society*, *78*(6), 1069–1079. https://doi.org/10.1175/1520-0477(1997)078<1069:APICOW>2.0.CO;2

Maupin, M. A., & Barber, N. L. (2005). Estimated withdrawals from principal aquifers in the United States, 2000. In *US Geological Survey Circular* (Issue 1279). https://doi.org/10.3133/cir1279

Mays, L. W. (2013). Groundwater Resources Sustainability: Past, Present, and Future. *Water Resources Management*, *27*(13), 4409–4424. https://doi.org/10.1007/s11269-013-0436-7

McCabe, G. J., Palecki, M. A., & Betancourt, J. L. (2004). Pacific and Atlantic Ocean influences on multidecadal drought frequency in the United States. *Proceedings of the National Academy of Sciences of the United States of America*, *101*(12), 4136–4141. https://doi.org/10.1073/pnas.0306738101

Miranda, P., Coelho, F.E.S., Tomé, A.R., Valente, M. A. (2002). 20th century Portuguese climate and climate scenarios. *Climate Change in Portugal. Scenarios, Impacts and Adaptation Measures.*, SIAMproject, pp. 23–83.

Navarra, A., & Tubiana, L. (eds. . (2013). Regional Assessment of Climate Change in the Mediterranean: Volume 3: Case Studies. In *Advances in Global Change Research*. http://www.springer.com/series/5588

Neves, M. C., Costa, L., Hugman, R., & Monteiro, J. P. (2019a). The impact of atmospheric teleconnections on the coastal aquifers of Ria Formosa (Algarve, Portugal). *Hydrogeology Journal*, *27*(8), 2775–2787. https://doi.org/10.1007/s10040-019-02052-6

Neves, M. C., Jerez, S., & Trigo, R. M. (2019b). The response of piezometric levels in Portugal to NAO, EA, and SCAND climate patterns. *Journal of Hydrology*, *568*, 1105–1117. https://doi.org/10.1016/j.jhydrol.2018.11.054

NOAA. (2012). *Northern Hemisphere Teleconnection Patterns: Scandinavia (SCAND)*. NOAA Climate Prediction Center. https://www.cpc.ncep.noaa.gov/data/teledoc/scand.shtml

NOAA. (2019). *National Oceanic and Atmospheric Administration, Climate Prediction Center website*. http://www.cpc.ncep.noaa.gov

NOAA. (2020a). *California Nevada River Forecast Center*. https://www.cnrfc.noaa.gov/awipsProducts/RNOWRKCLI.php

NOAA. (2020b). *Climate Monitoring - Teleconnections*. National Centers for Environmental Information. https://www.ncdc.noaa.gov/teleconnections/

NOAA. (2020c). *Global Historical Climatology Network (GHCN). National Climate Data Center*. https://www.ncdc.noaa.gov/data-access/land-based-station-data/land-based-datasets/global-historical-climatology-network-ghcn

NOAA. (2020d). *Multivariate ENSO Index Version 2 (MEI.v2)*. Physical Sciences Labratory. https://psl.noaa.gov/enso/mei/

Norman, S. P., & Taylor, A. H. (2003). Tropical and north Pacific teleconnections influence fire regimes in pine-dominated forests of north-eastern California, USA. *Journal of Biogeography*, *30*(7), 1081–

1092. https://doi.org/10.1046/j.1365-2699.2003.00889.x

O'Brien, J. P., O'Brien, T. A., Patricola, C. M., & Wang, S. Y. S. (2019). Metrics for understanding large-scale controls of multivariate temperature and precipitation variability. *Climate Dynamics*, *53*(7–8), 3805–3823. https://doi.org/10.1007/s00382-019-04749-6

Palmer, T. N., & Anderson, D. L. T. (1994). The prospects for seasonal forecasting-A review paper. *Quarterly Journal of the Royal Meteorological Society*, *120*(518), 755–793. https://doi.org/10.1256/qj.03.130

Paulinski, S. R., Nishikawa, T., Cromwell, G., Boyce, S. E., & Stanko, Z. P. (2018). Santa Barbara and Foothill groundwater basins Geohydrology and optimal water resources management—Developed using density dependent solute transport and optimization models. *Scientific Investigations Report*, *July*, 402. https://doi.org/10.3133/sir20185059

Peters, E., Van Lanen, H. A. J., Torfs, P. J. J. F., & Bier, G. (2005). Drought in groundwater - Drought distribution and performance indicators. *Journal of Hydrology*, *306*(1–4), 302–317. https://doi.org/10.1016/j.jhydrol.2004.09.014

Planert, M., & Williams, J. S. (1995). Ground Water Atlas of the United States: Segment 1 California, Nevada. *Hydrologic Investigations Atlas 730-B*, 30.

Poveda, G., Rojas, W., Quinones, M. L., Velez, I. D., Mantilla, R. I., Ruiz, D., Zuluaga, J. S., & Rua, G. L. (2001). Coupling between Annual and ENSO Timescales in the Malaria: Climate Association in Colombia. *Environmental Health Perspectives*, *109*(5), 489. https://doi.org/10.2307/3454707

Reichard, E. G., Land, M., Crawford, S. M., Johnson, T., Everett, R. R., Kulshan, T. V., Ponti, D. J., Halford, K. J., Johnson, T. A., Paybins, K. S., & Nishikawa, T. (2003). Geohydrology, Geochemistry, and Ground-Water Simulation-Optimization of the Central and West Coast Basins, Los Angeles County, California. *U.S. Geological Survey Water-Resources Investigations Report 03-4065*, 184.

Ribeiro, L., & Cunha Da, L. V. (2010). Portuguese Groundwater Report. In *Groundwater in the Southern Member States of the European Union* (Issue June, p. 23). http://www.easac.eu/home/reports-and-statements/detail-view/article/groundwater-1.html

Rodionov, S., & Assel, R. (2001). A new look at the Pacific/North American Index. *Geophysical Research Letters*, *28*(8), 1519–1522.

Ropelewski, C. F., & Halpert, M. S. (1986). North American Precipitation and Temperature Patterns Associated with the El Niño/Southern Oscillation (ENSO). *Monthly Weather Review*, *114*, 2352–2362.

Russo, T. A., & Lall, U. (2017). Depletion and response of deep groundwater to climate-induced pumping variability. *Nature Geoscience*, *10*(2), 105–108. https://doi.org/10.1038/ngeo2883

Sang, Y. F. (2013). A review on the applications of wavelet transform in hydrology time series analysis. *Atmospheric Research*, *122*, 8–15. https://doi.org/10.1016/j.atmosres.2012.11.003

SCVWD. (2020). *Santa Clara Valley Water District Annual Groundwater Report 2019*. https://www.valleywater.org/sites/default/files/2020-09/2019_Annual_Groundwater_Report_Web_Version.pdf

SNIRH. (2020). *Sistemas Aquíferos, Sistema Nacional de Informação de Recursos Hídricos [National*

Information System for Water Resources]. https://snirh.apambiente.pt/index.php?idMain=4&idItem=3&idISubtem=link1

Steiger, N. J., Smerdon, J. E., Cook, B. I., Seager, R., Park Williams, A., & Cook, E. R. (2019). Oceanic and radiative forcing of medieval megadroughts in the American Southwest. *Science Advances*, *5*(7), 1–9. https://doi.org/10.1126/sciadv.aax0087

Steirou, E., Gerlitz, L., Apel, H., & Merz, B. (2017). Links between large-scale circulation patterns and streamflow in Central Europe: A review. *Journal of Hydrology*, *549*, 484–500. https://doi.org/10.1016/j.jhydrol.2017.04.003

Stigter, T. Y., Monteiro, J. P., Nunes, L. M., Vieira, J., Cunha, M. C., Ribeiro, L., Nascimento, J., & Lucas, H. (2009). Screening of sustainable groundwater sources for integration into a regional drought-prone water supply system. *Hydrology and Earth System Sciences*, *13*(7), 1185–1199. https://doi.org/10.5194/hess-13-1185-2009

Stigter, T. Y., Nunes, J. P., Pisani, B., Fakir, Y., Hugman, R., Li, Y., Tomé, S., Ribeiro, L., Samper, J., Oliveira, R., Monteiro, J. P., Silva, A., Tavares, P. C. F., Shapouri, M., Cancela da Fonseca, L., & El Himer, H. (2014). Comparative assessment of climate change and its impacts on three coastal aquifers in the Mediterranean. *Regional Environmental Change*, *14*(SUPPL.1), 41–56. https://doi.org/10.1007/s10113-012-0377-3

Stigter, Tibor Yvan. (2005). *Integrated Analysis of Hydrogeochemistry and Assessment of Groundwater Contamination Induced by Agricultural Practices*.

Sutton, R. T., & Hodson, D. L. R. (2005). Ocean science: Atlantic Ocean forcing of North American and European summer climate. *Science*, *309*(5731), 115–118. https://doi.org/10.1126/science.1109496

Taylor, R. G., Scanlon, B., Döll, P., Rodell, M., Van Beek, R., Wada, Y., Longuevergne, L., Leblanc, M., Famiglietti, J. S., Edmunds, M., Konikow, L., Green, T. R., Chen, J., Taniguchi, M., Bierkens, M. F. P., Macdonald, A., Fan, Y., Maxwell, R. M., Yechieli, Y., … Treidel, H. (2013). Ground water and climate change. In *Nature Climate Change*. https://doi.org/10.1038/nclimate1744

Thomas, B. F. (2019). Sustainability indices to evaluate groundwater adaptive management: a case study in California (USA) for the Sustainable Groundwater Management Act. *Hydrogeology Journal*, *27*(1), 239–248. https://doi.org/10.1007/s10040-018-1863-6

Thomas, B. F., Caineta, J., & Nanteza, J. (2017). Global Assessment of Groundwater Sustainability Based On Storage Anomalies. *Geophysical Research Letters*, *44*(22), 11,445-11,455. https://doi.org/10.1002/2017GL076005

Torrence, C., & Compo, G. P. (1998). A Practical Guide to Wavelet Analysis. *Bulletin of the American Meteorological Society*, *79*(1), 61–78. https://doi.org/10.1175/1520-0477(1998)079<0061:APGTWA>2.0.CO;2

Torrence, C., & Webster, P. (1998). The annual cycle of persistence in the El Nino/Southern Oscillation. *Quarterly Journal of the Royal Meteorological Society*, *124*(550), 1985–2004. https://doi.org/10.1256/smsqj.55009

Trigo, R.M., Añel, J., Barriopedro, D., García-Herrera, R., Gimeno, L., Nieto, R., Castillo, R., Allen, M.R. and Massey, N. (2013). The record winter drought of 2011–12 in the Iberian Peninsula. *Bulletin of*

the American Meteorological Society, *94(9)*, S41-S45.

Trigo, R. M., Pozo-Vázquez, D., Osborn, T. J., Castro-Díez, Y., Gámiz-Fortis, S., & Esteban-Parra, M. J. (2004). North Atlantic oscillation influence on precipitation, river flow and water resources in the Iberian Peninsula. *International Journal of Climatology*, *24*(8), 925–944. https://doi.org/10.1002/joc.1048

Trigo, R. M., Valente, M. A., Trigo, I. F., Miranda, P. M. A., Ramos, A. M., Paredes, D., & García-Herrera, R. (2008). The impact of North Atlantic wind and cyclone trends on European precipitation and significant wave height in the Atlantic. *Annals of the New York Academy of Sciences*, *1146*, 212–234. https://doi.org/10.1196/annals.1446.014

UN-Water. (2006). Coping with water scarcity. *UN-Water Thematic Initiatives*, *22*(3), 12. https://doi.org/10.1007/978-1-4020-9579-5

United States Drought Monitor Drought Classification. (2020). In *The National Drought Mitigation Center*. https://droughtmonitor.unl.edu/About/AbouttheData/DroughtClassification.aspx

USGS. (2015). *National Water Information System. U.S. Geological Survey*. http://waterdata.usgs.gov/nwis

USGS Water Science Center. (2020). *USGS*. https://ca.water.usgs.gov/california-drought/california-drought-comparisons.html

Van Camp, M., Radfar, M., & Walraevens, K. (2010). Assessment of groundwater storage depletion by overexploitation using simple indicators in an irrigated closed aquifer basin in Iran. *Agricultural Water Management*, *97*(11), 1876–1886. https://doi.org/10.1016/j.agwat.2010.02.006

Van Loon, A. F., Gleeson, T., Clark, J., Van Dijk, A. I. J. M., Stahl, K., Hannaford, J., Di Baldassarre, G., Teuling, A. J., Tallaksen, L. M., Uijlenhoet, R., Hannah, D. M., Sheffield, J., Svoboda, M., Verbeiren, B., Wagener, T., Rangecroft, S., Wanders, N., & Van Lanen, H. A. J. (2016). Drought in the Anthropocene. *Nature Geoscience*, *9*(2), 89–91. https://doi.org/10.1038/ngeo2646

Vautard, R., Yiou, P., & Ghil, M. (1992). Singular-spectrum analysis: A toolkit for short, noisy chaotic signals. *Physica D: Nonlinear Phenomena*, *58*(1–4), 95–126. https://doi.org/10.1016/0167-2789(92)90103-T

Velasco, E. M., Gurdak, J. J., Dickinson, J. E., Ferré, T. P. A., & Corona, C. R. (2017). Interannual to multidecadal climate forcings on groundwater resources of the U.S. West Coast. *Journal of Hydrology: Regional Studies*, *11*, 250–265. https://doi.org/10.1016/j.ejrh.2015.11.018

Vicente-Serrano, S. M., López-Moreno, J. I., Gimeno, L., Nieto, R., Morán-Tejeda, E., Lorenzo-Lacruz, J., Beguería, S., & Azorin-Molina, C. (2011). A multiscalar global evaluation of the impact of ENSO on droughts. *Journal of Geophysical Research Atmospheres*, *116*(20), 1–23. https://doi.org/10.1029/2011JD016039

Vörösmarty, C. J., Green, P., Salisbury, J., & Lammers, R. B. (2000). Global water resources: Vulnerability from climate change and population growth. *Science*, *289*(5477), 284–288. https://doi.org/10.1126/science.289.5477.284

Vrba, J., Hirata, R., Girman, J., Haie, N., Lipponen, A., Neupane, B., Shah, T., & Wallin, B. (2006). Groundwater resources sustainability indicators. *IAHS-AISH Publication*, *302*, 3–9.

Wada, Y., Van Beek, L. P. H., Van Kempen, C. M., Reckman, J. W. T. M., Vasak, S., & Bierkens, M. F.

P. (2010). Global depletion of groundwater resources. *Geophysical Research Letters*, *37*(20), 1–5. https://doi.org/10.1029/2010GL044571

Wallace, J. M., & Gutzler, D. S. (1981). Teleconnections in the Geopotential Height Field during the Northern Hemisphere Winter. *Monthly Weather Review*, *109*, 784–812.

Wolter, K., & Timlin, M. S. (1993). Monitoring ENSO in COADS with a Seasonally Adjusted Principal Component Index. *Proceedings of the 17th Climate Diagnostics Workshop*, 52–57.

Wolter, K., & Timlin, M. S. (1998). Measuring the strength of ENSO events: How does 1997/98 rank? *Weather*, *53*(9), 315–324.

Wolter, K., & Timlin, M. S. (2011). El Niño/Southern Oscillation behaviour since 1871 as diagnosed in an extended multivariate ENSO index (MEI.ext). *International Journal of Climatology*, *31*(7), 1074–1087. https://doi.org/10.1002/joc.2336

Yuan Zhang, Wallace, J. M., & Battisti, D. S. (1997). ENSO-like interdecadal variability: 1900-93. *Journal of Climate*, *10*(5), 1004–1020. https://doi.org/10.1175/1520-0442(1997)010<1004:eliv>2.0.co;2

Ground water level hydrographs

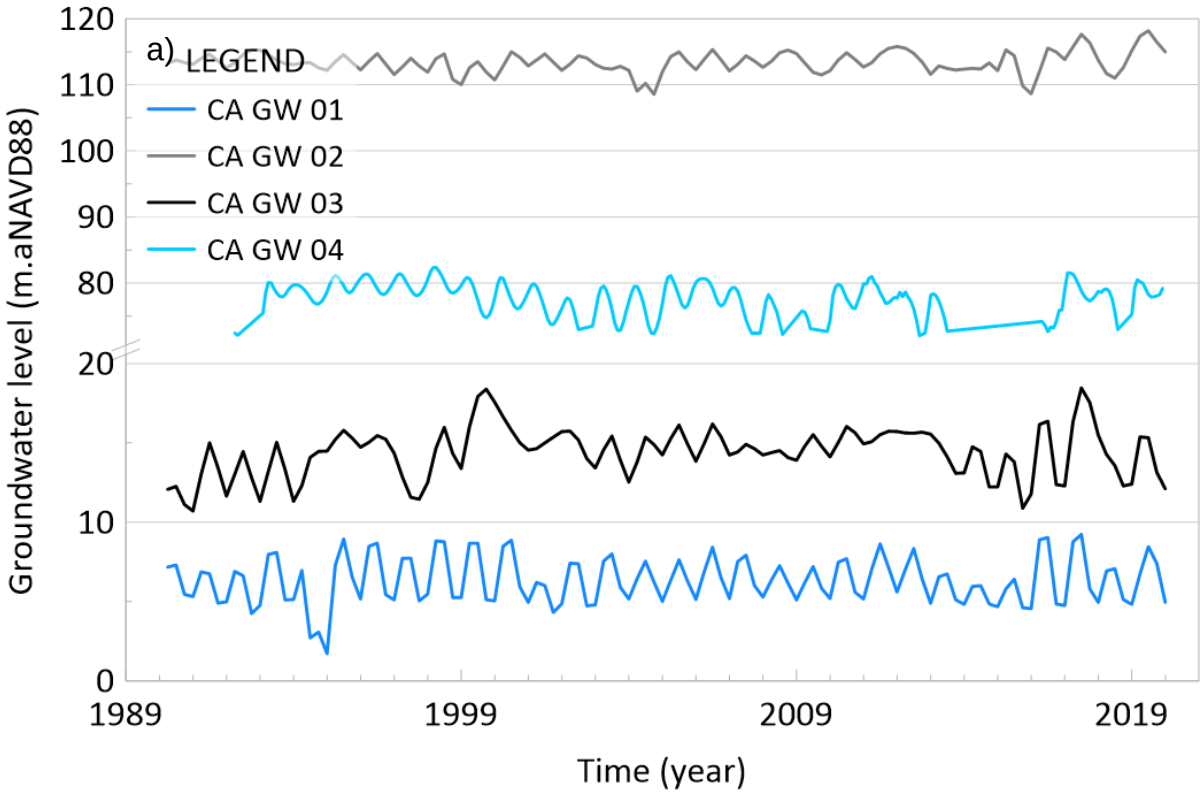

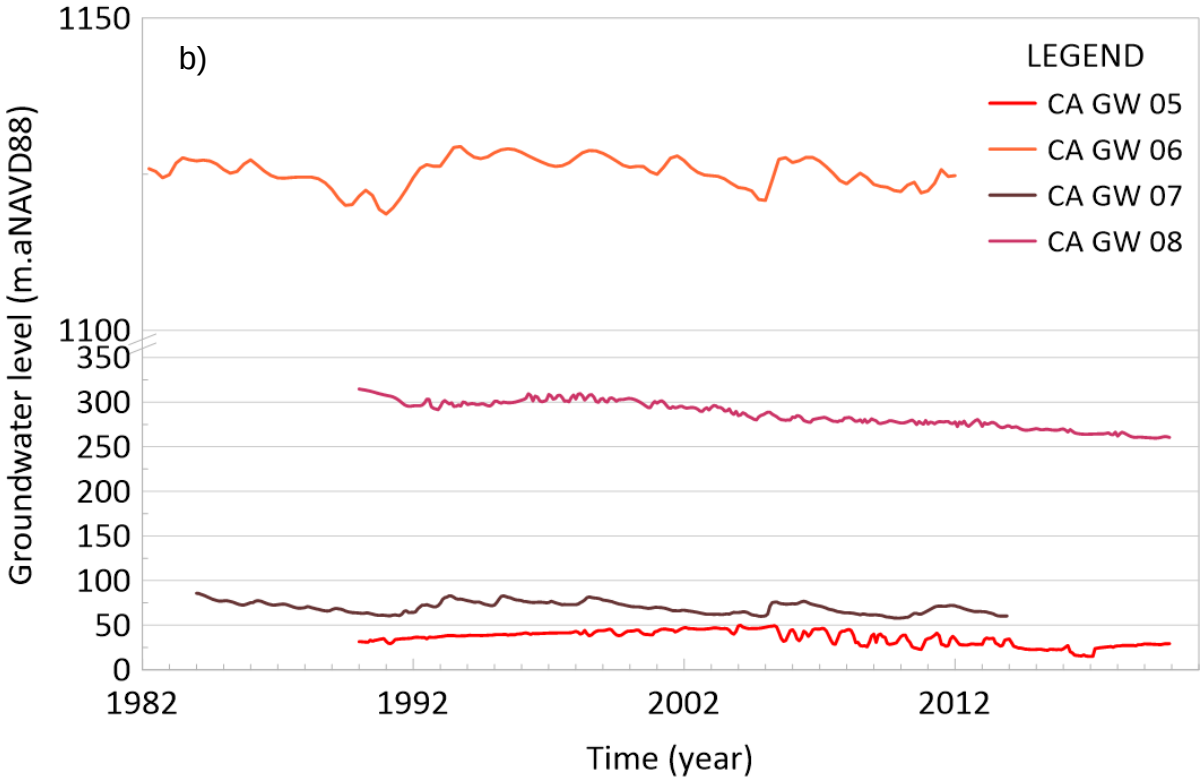

Appendix I. Groundwater level time series of eight observation points within the California Coastal Basins aquifers system. a) Observation points in northern California are coded in cooler colors, and b) warm colors represent records in southern California.

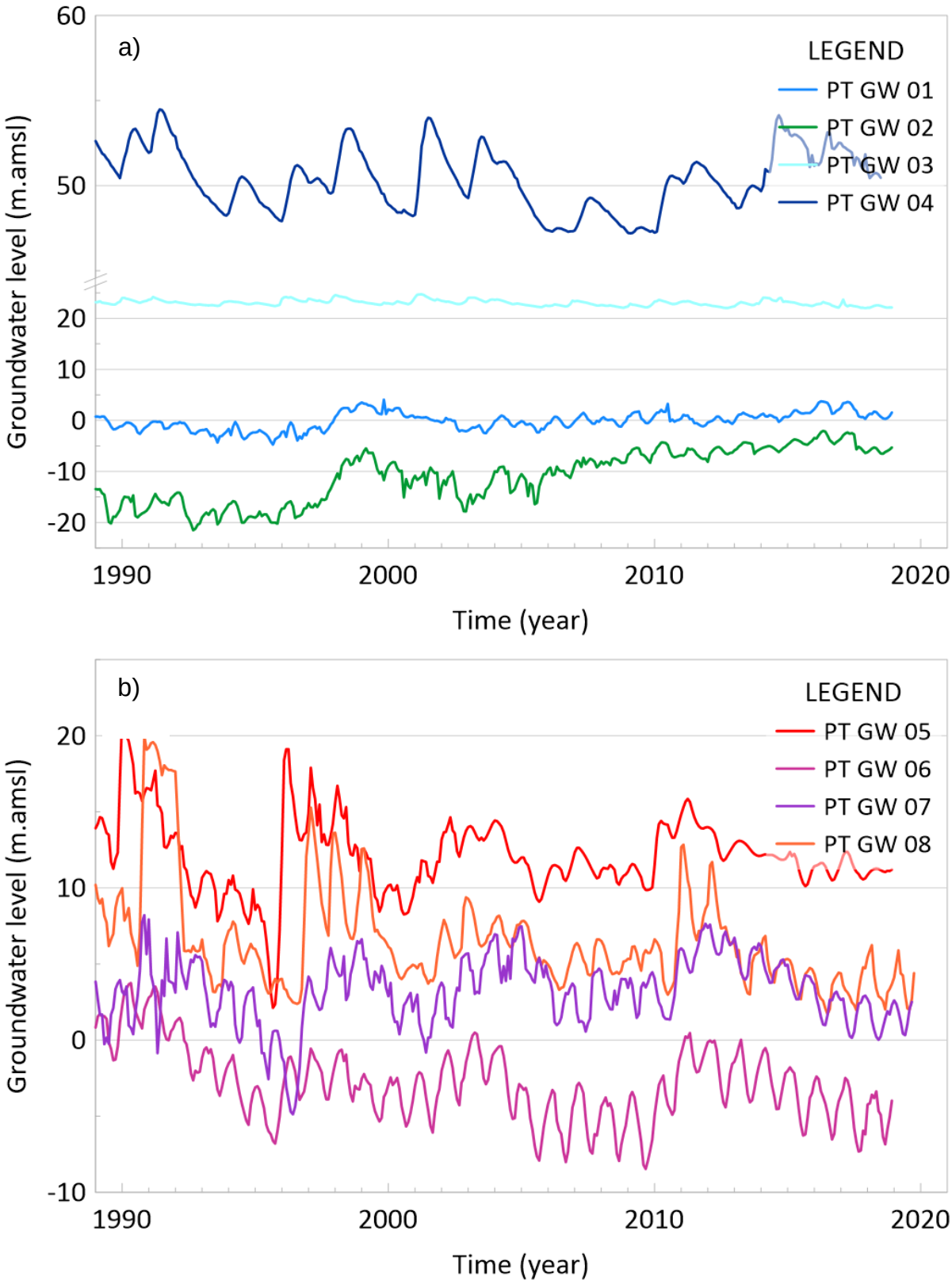

Appendix II. Groundwater level time series of eight observation points within Portugal's coastal aquifers system. a) Observation points in northern Portugal are coded in cooler colors, and b) warm colors represent records in southern Portugal.

Precipitation records

(a) Site ID	Location	Site Number	Latitude	Longitude
CA PR 01	Eureka	USW00024213	40.8097°	-124.1602°
CA PR 02	Napa	USC00046074	38.2777	-122.2647
CA PR 03	Half Moon Bay	USC00043714	37.4725°	-122.4433°
CA PR 04	Gilroy	USC00043417	37.003°	-121.5608°
CA PR 05	Santa Barbara	USC00047902	34.4167°	-119.6844°
CA PR 06	Ojai	USC00046399	34.4477°	-119.2275°
CA PR 07	San Gabriel	USC00047785	34.0842°	-118.1003°
CA PR 08	Redlands	USC00047306	34.037°	-117.1948°

(b) Site ID	Starting Year	Ending Year	Length of Record (years)	Data coverage
CA PR 01	1990	2019	30	100%
CA PR 02	1990	2019	30	94%
CA PR 03	1990	2019	30	96%
CA PR 04	1990	2019	30	58%
CA PR 05	1990	2019	30	97%
CA PR 06	1982	2011	30	97%
CA PR 07	1984	2013	30	93%
CA PR 08	1990	2019	30	95%

Appendix IV. Descriptive attributes for a) the location and b) the precipitation record and hydrology of precipitation stations in the California Coastal Basins aquifer. The Site ID identifies the aquifer name (CA), the site type (PR for precipitation), and the location (01–08 from northwest to southeast).

(a) Site ID	Site Number	Latitude	Longitude
PT PR 01	ERA5_Land_162A/9	-8.7118256	40.753993
PT PR 02	ERA5 Land 174/2	-8.6676507	40.742662
PT PR 03	ERA5 Land 249/4	-8.8843293	40.055807
PT PR 04	ERA5 Land 261/117	-8.854263	40.094272
PT PR 05	ERA5_Land_605/303	-8.1342549	37.12038
PT PR 06	ERA5 Land 606/647	-8.0515888	37.064728
PT PR 07	ERA5 Land 611/230	-7.9481014	37.048967
PT PR 08	ERA5_Land_607/484	-7.7941745	37.06265

(b) Site ID	Starting Year	Ending Year	Length of Record (years)	Data coverage
PT PR 01	1989	2018	30	¬9 km
PT PR 02	1989	2018	30	¬9 km
PT PR 03	1989	2018	30	¬9 km
PT PR 04	1989	2018	30	¬9 km
PT PR 05	1989	2018	30	¬9 km
PT PR 06	1989	2018	30	¬9 km
PT PR 07	1989	2018	30	¬9 km
PT PR 08	1989	2018	30	¬9 km

Appendix V. Descriptive attributes for a) the location and b) the precipitation record and hydrology of precipitation stations in Portugal's coastal aquifer system. The Site ID identifies the aquifer name (PT), the site type (PR for precipitation), and the location (01–08 from northwest to southeast).

Linear regression summary statistics and lag correlations

Site ID	Corr. coeff.	r sqrd	Effective sample size	t statistic	t lower	t upper	Max lag	p-value
CA GW 01	0.33	0.11	81	3.12	-1.99	1.99	0.33	0.00
CA GW 02	-0.05	0.00	36	-0.30	-2.03	2.03	0.43	0.77
CA GW 03	0.47	0.22	29	2.78	-2.05	2.05	0.47	0.01
CA GW 04	0.44	0.19	7	1.09	-2.36	2.36	0.44	0.32
CA GW 05	0.73	0.53	11	3.17	-2.20	2.20	0.73	0.01
CA GW 06	0.66	0.43	9	2.32	-2.26	2.26	0.66	0.05
CA GW 07	0.38	0.14	6	0.82	-2.45	2.45	0.39	0.44
CA GW 08	0.54	0.30	18	2.59	-2.10	2.10	0.70	0.02
PT GW 01	0.21	0.04	19	0.89	-2.09	2.09	0.21	0.39
PT GW 02	0.12	0.01	20	0.50	-2.09	2.09	0.12	0.62
PT GW 03	0.67	0.45	20	3.82	-2.09	2.09	0.67	0.00
PT GW 04	0.35	0.12	8	0.92	-2.31	2.31	0.35	0.39
PT GW 05	0.71	0.50	17	3.91	-2.11	2.11	0.71	0.00
PT GW 06	0.52	0.27	26	2.99	-2.06	2.06	0.52	0.01
PT GW 07	0.84	0.71	25	7.48	-2.06	2.06	0.84	<.00001
PT GW 08	0.60	0.36	17	2.89	-2.11	2.11	0.60	0.01